UNIVERSITÀ DI PISA

SCUOLA DI DOTTORATO IN INGEGNERIA "LEONARDO DA VINCI"

CORSO DI DOTTORATO DI RICERCA IN
TELERILEVAMENTO

PhD Thesis

DESIGN OF RF SYSTEMS AT HF AND VHF FOR COMMUNICATIONS, RADAR AND BIOMEDICAL APPLICATIONS: MINIATURIZATION OF RADIATING ELEMENTS AND SYNTHESIS OF TUNING AND MATCHING NETWORKS

Tutor:

Prof. Agostino MONORCHIO

_____

Prof. Guido BIFFI GENTILI

_____

Candidate:

Nunzia FONTANA

_____

CICLO XXV – ANNO 2011
SSD ING-INF/02

ABSTRACT

Electrically small antennas have received an increasing interest especially for both radar and medical applications. In this dissertation, several approaches for antennas miniaturization have been studied and proposed for Over the Horizon (OTH) phased array radars. In the last case, the need to reduce the size of the antenna is dictated by the wavelengths in the HF frequency range. To this aim, most of this dissertation is focused on a new methodology for reaching both wideband and small sizes characteristics of the antenna for radar purposes. Additionally, several matching networks have been studied in order to reduce the mutual coupling between the radiating elements in the array. As a side work, by exploiting the miniaturization of the antennas, Radio Frequency coils for Magnetic Resonance Imaging application have been analyzed. A new approach has been presented in order to study the behaviour of these antennas in realistic environments.

To Amerigo and my family.

ACKNOWLEDGMENTS

Special thanks are due to Prof. Monorchio for his precious guidance and support over these three years. Many thanks to Prof. Biffi Gentili for giving me important feedbacks. I would like to acknowledge Dr. Alessandro Corucci, for his invaluable advice. Many thanks to Prof. Hao, from Queen Mary University College of London, who gave me the opportunity of working at School of Electronic Engineering and Computer Science.

INDEX

LIST OF ACRONYMS

A.C.: *Alternating Current*

AFS: *Antenna Framework Simulator*

CAD: *Computer Aided Drafting*

D.C.: *Direct Current*

E.M., e.m.: *Electromagnetic*

FD: *Frequency Domain*

FDTD: *Finite Differences Transient Domain*

FEM: *Finite Element Method*

GUI: *Graphic User Interface*

HF: *High Frequency*

IEEE: *Institute of Electrical and Electronic Engineering*

MoM: *Method of Moment*

MRI: *Magnetic Resonance Imaging*

NMR: *Nuclear Magnetic Resonance*

OTH: *Over The Horizon*

PEC: *Perfect Electric Conductor*

SAL: *Small Antenna Limit*

SAR: *Specific Absorption Rate*

SNR: *Signal to Noise Ratio*

TD: *Time Domain*

VHF: *Very High Frequency*

VSWR: *Voltage Standing Wave Ratio*

INTRODUCTION

In the last times, electrically small antennas are receiving an increasing interest for both medical and military applications.

For instance, in the HF band communications and radar applications, the use of wideband antennas is necessary in order to deal with the variability of the ionosphere and therefore to cover large areas for security purposes, but at the same time a size reduction of these antennas is required. In particular, some radar systems like the Over The Horizon (OTH) radar operate in the 5-30 MHz frequency range in order to detect and track targets over wide areas by exploiting the long range sky-wave propagation of HF electromagnetic waves through the ionosphere. Antennas for the last applications typically consist of long wires conductors and many existing wideband wire antennas for OTH radar purposes are very large in size.

For medical applications, antennas for Magnetic Resonance Imaging (MRI) for instance are narrowband and small compared to the wavelength in order to reach low spatial variability of the magnetic field distribution in a specific region of interest. They appear as coils resonating at different frequencies in the VHF frequency range.

The miniaturization of radiating elements can be accomplished through different techniques: by loading the antenna with lumped elements; by the optimisation of the antenna geometry; by the use of grounded pins. All the proposed approaches make the antenna resonant by increasing the total wire length in a specific volume.

At first, the subject of this dissertation deals with the study of a design methodology for broadband miniaturized antennas with application in the HF band (5-30MHz) radar phased arrays. In the case of radar application, the study of the stand alone broadband antenna has been investigated by taking into account mutual coupling mechanisms that arise when operating in presence of many radiating elements within a phased array. The scanning performance of the array is generally determined by the element spacing, which is limited by the element size, being this latter very large at these frequencies. Moreover the mutual couplings also depend on the shape of the array, the radiation pattern of the single element, on the frequency and on the pointing direction of the beam.

The use of a ground plane combined with the concepts concerning the biconical antennas and meandered antennas have been investigated in order to reduce the size of the

single antenna, maintaining its broadband characteristics. The use of shorting pins has been investigated for improving the matching performances at lower frequencies, where the mutual couplings phenomena are stronger. A miniaturized version of the last configuration was studied in order to make the antenna electrically small and thus to maintain the radiation pattern performances, which were disrupted by the pin introduction.

Moreover the study of narrowband and broadband impedance matching networks has been widely investigated in order to further enhance the matching performance, which has to be well-matched especially at lower frequencies of the HF band.

As a side work, the concepts related to the miniaturized antennas have been applied to the Radio Frequency coils, for Magnetic Resonance Imaging applications.

The MRI system operates in the whole VHF band and up to now the lower part of the VHF band has been the most used (e. g. around 64MHz). The trend of the future MRI systems is the use of higher frequencies of the VHF band (e. g. around 300MHz). The numerical simulation is very important especially when the operating frequencies of RF coils increase (e.g. 300MHz), because their size becomes comparable to the wavelengths and the traditional equivalent circuit models are no more accurate.

RF surface coils have been studied in order to estimate all the parameters in realistic environments (e.g. in the presence of a numerical model of the human body) with numerical electromagnetic solvers. For lower operating frequencies, these antennas are electrically small structures that are able to resonate only through the use of lumped elements along the structure. For a complete analysis in realistic configurations, an electromagnetic equivalent model has been proposed in order to reduce the computational burden of the numerical analysis.

The work is organized in the following way. In chapter 1 some broadband antenna solutions have been presented. We focused on the main concepts that we used as reference in the antenna designed for radar application. Then, the definition of electrically small antennas has been presented. Furthermore the techniques used for the antenna miniaturization have been treated.

In chapter 2 some configurations of antennas for OTH radar applications have been presented. The issues related to the mutual coupling in phased array have been described. Finally the effect of the introduction of a shorting pin on the original antenna has been discussed.

In chapter 3 the importance of the use of an impedance matching network in a HF band radar array has been described. The design techniques of narrowband and broadband matching networks have been reported from the analytical point of view. Furthermore, the combination with optimization algorithms for the broadband matching of the antenna previously studied has been investigated.

In chapter 4 the analysis of RF surface coils for MRI has been presented. A new equivalent numerical model of the coils has been studied and validated. The proposed equivalent model has been used for complex environments, e.g. to account for the presence of a numerical human body implanted with a pacemaker system.

1 BROADBAND ANTENNA MINIATURIZATION

Wideband antennas are useful for different applications. Such applications require several features such as wide scan, security, high speed communication and high reliability in a compact size. The element size is a critical parameter in determining the scan angle in an array radar antenna. Especially in the range of the HF (3-30MHz), the sizes of the antennas, which have to self-resonate at these frequencies, are very large due to the wavelengths (100-10m). Small size is preferred for the single antenna, in order to reduce mutual couplings between the elements and to reduce the overall size of the array.

1.1 Broadband antennas

The IEEE standard [1] defines the bandwidth of an antenna as "the range of frequencies within which the performance of the antenna, with respect to some characteristics, conforms to a specific standard". The last definition is quite large and related to different parameters of the performance of the antenna. Because it is not possible to give a unique definition of bandwidth, it is important to give some criteria for a complete design of an antenna system. In this dissertation, the bandwidth is defined for impedance and radiation pattern separately. For instance, the bandwidth is defined by the behaviour of the input impedance and the VSWR and by a good independence of the radiation pattern of the antenna according to the frequency.

The bandwidth B_p can be denoted as a percentage of the center frequency as follows:

$$B_p = \frac{f_U - f_L}{f_C} \times 100\% \tag{1.1}$$

where

$$f_c = \frac{f_L + f_U}{2} \tag{1.2}$$

and f_U and f_L are the upper and lower frequencies of operation for which satisfactory performance is obtained.

In the following paragraphs, some typical broadband antennas, known in literature are presented.

1.1.1 Biconical antenna

In 1943, Schelkunoff proposed a biconical antenna as shown in Figure 1.1 (a). The biconical antenna concept is based on the fact that thicker wire provides wider impedance bandwidth than that for a thin wire dipole antenna. This concept can be extended to further increase bandwidth if the conductors are flared to form the biconical structure. The biconical antenna can be analyzed as transmission line if the biconical antenna is flared out to infinity. The infinite biconical antenna, as shown in Figure 1.1 (a), acts as a guide for a spherical wave.

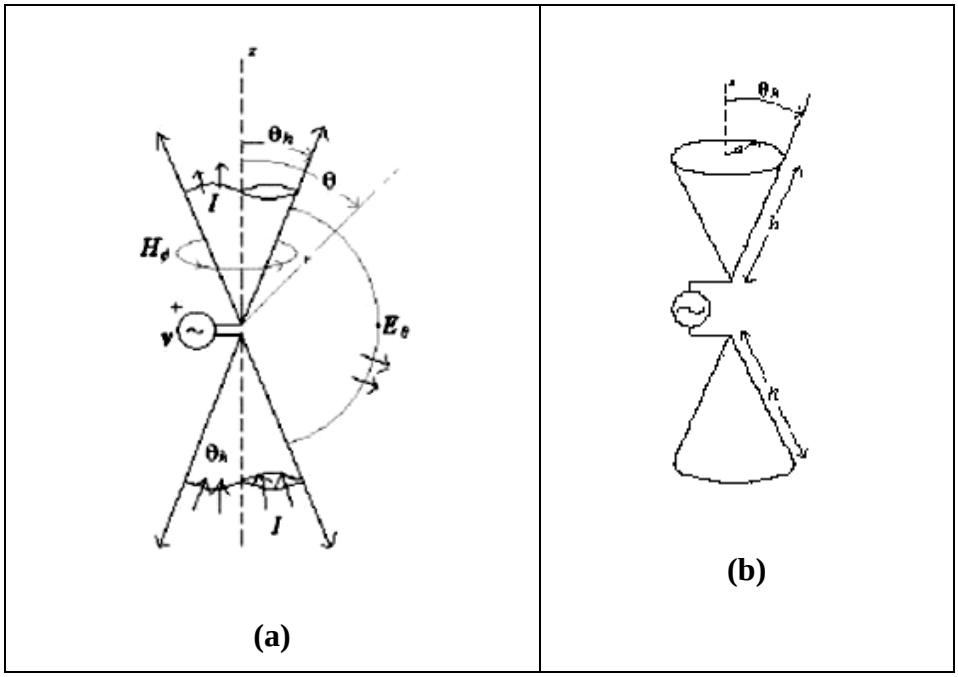

Figure 1.1 – Biconical antenna: (a) infinite version; (b) finite version.

It was proved that there is only a TEM mode in the infinite biconical antenna. The input impedance of the infinite biconical antenna can be computed from the ratio of terminal voltage and current. The terminal voltage and current can be computed by integrating E_ϑ and H_φ respectively:

$$V(r) = \int_0^{2\pi} E_\vartheta r d\vartheta = 2\eta H_0 e^{-jkr} \ln\left[\cot\left(\frac{\alpha}{2}\right)\right] \tag{1.3}$$

$$I(r) = \int_0^{2\pi} H_\varphi r \sin\vartheta d\phi = 2\pi H_0 e^{-jkr} \tag{1.4}$$

The characteristic impedance at any point r, from (1.3) and (1.4), is

$$Z_{in} = \frac{\eta}{\pi} \ln\left[\cot\left(\frac{\alpha}{2}\right)\right] \tag{1.5}$$

Since this is not a function of distance r, the antenna input impedance must also be equal the characteristic impedance. Thus, (1.5) gives the input impedance:

$$Z_{in} = Z_c \cong 120 \ln\left[\cot\left(\frac{\alpha}{2}\right)\right] \tag{1.6}$$

where $\eta/\pi \approx 120$ was used.

The input impedance of the infinite biconical antenna is real valued because there is only a pure travelling wave. In other words, the infinite structure has no discontinuities and does not cause reflections that, in turn, set up standing waves, which generate a reactive component in the impedance. The polarization of the biconical antenna is vertical.

The practical form in the biconical antenna family is the finite biconical antenna shown in Figure 1.1 (b) and formed by finite sections of the two infinite cones. The discontinuity at the ends of the cones causes higher order modes, which introduce a reactive component and increase the standing wave ratio. However, experimental results by G. H. Brown revealed that for large angle θ_h (see Figure 1.1 (b)) the reactive component is reduced and the bandwidth is wider [2]. As well as presenting good wide-band features, this antenna has got good performances in terms of radiation pattern, which is omni-directional on the horizontal plane, and symmetrical on the vertical plane. Further, the shape of the radiation pattern is almost independent of the frequency.

A variation of the finite biconical antenna (shown in Figure 1.2), realized with wires, which it is the solution that we used in this dissertation, was widely studied by varying the number of wires, and compared with a real prototype [3].

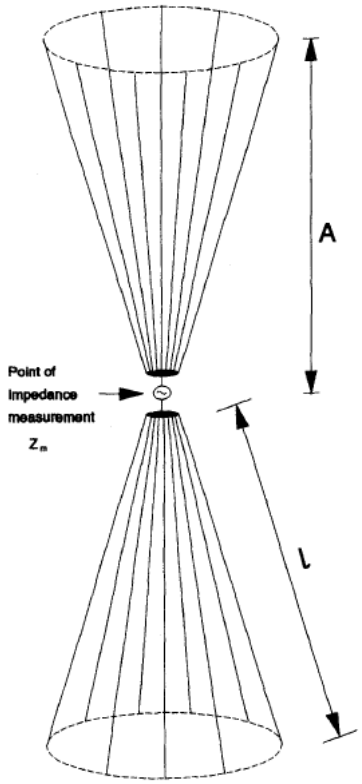

Figure 1.2 – Skeletal wires biconical antenna.

A further variation of the finite biconical antenna, called the discone antenna, was developed by Kandoian in 1945 [5]; see Figure 1.3. A disc-shaped ground plane is used instead of a cone on top of the finite biconical antenna. There are many useful applications for the discone antenna.

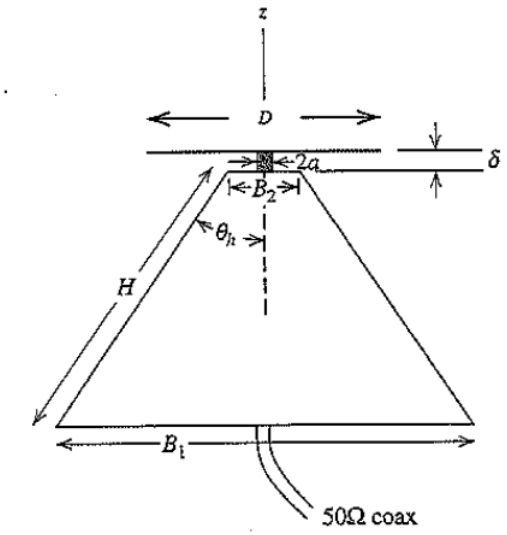

Figure 1.3 – Discone antenna.

The polarization of the antenna is vertical. The radiation pattern on the horizontal plane is omni-directional. On the vertical plane for low frequencies, while the antenna is electrically small, the radiation pattern is similar to that short dipole one. Otherwise, with the increasing of the frequency the electric length of the ground plane increases and the effect of the ground on the radiation pattern is predominant, because it is confined in the lower half-plane.

Typical dimensions of the discone antenna are:

$$H = 0.7\lambda,\ B = 0.6\lambda,\ D = 0.4\lambda,\ \vartheta_h = 25°,\ \delta << D \tag{1.7}$$

The discone antenna can be also realized with conductive wires.

1.1.2 Folded dipole

The folded dipole antenna is widely used in practice both because of its easy realization and for the characteristics of its input impedance. The input impedance of the folded dipole is larger than that of a half-wave dipole and it has a wider bandwidth. The geometry is presented in Figure 1.4. The geometry is obtained by combining two dipoles of equal lengths, and feeding them in the center. Usually, the radius of the wires is chosen equal for the two dipoles. The folding produces two parallel currents having the same amplitude but opposite directions.

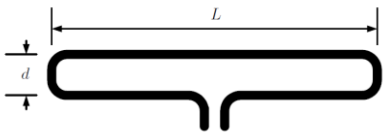

Figure 1.4 – Folded dipole.

The analysis of the folded dipole can be done by interpreting the feed of the dipole as the combination of two modes (Figure 1.4): a symmetrical mode with two identical voltages and an asymmetric mode, which has two voltages of opposite phase.

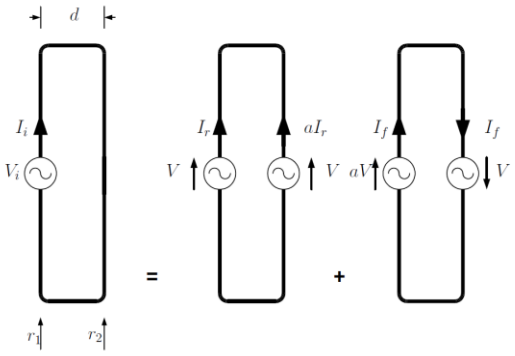

Figure 1.5 – Equivalent model of a folded dipole.

The equivalent impedance of the symmetrical mode is given by the following expression:

$$Z_r = \frac{V}{(1+a)I_r} \tag{1.8}$$

where *a* is the *step-up ratio*, which relates the radii of the two wires of the folded dipole and it is given by the following formulation:

$$a = \frac{\cosh^{-1}\left(\frac{\nu^2 - \mu^2 + 1}{2\nu}\right)}{\cosh^{-1}\left(\frac{\nu^2 + \mu^2 - 1}{2\nu\mu}\right)} \tag{1.9}$$

where μ and υ relate the radii of the conductors and their distances:

$$\nu = \frac{d}{r_1}, \mu = \frac{r_2}{r_1} \tag{1.10}$$

The asymmetrically mode can be seen as a transmission line of length L, equal to the length of the conductors and thus its impedance is given by:

$$Z_f = \frac{(1+a)V}{2I_f} = jZ_0 \tan \beta L/2 \tag{1.11}$$

where Z_0 is the characteristic impedance of the transmission line. Thus the total input impedance of the folded dipole can be obtained by combining Z_f and Zr:

$$Z_i = \frac{(1+a)V}{I_r + I_f} = \frac{2\left(1+a^2\right)Z_r Z_f}{\left(1+a^2\right)Z_r + 2Z_f} \tag{1.12}$$

If L=λ/2, the input impedance of a half-wavelength dipole is:

$$Z_i = 4Z_{dipole} \tag{1.13}$$

Because the input impedance of a half-wavelength dipole is equal to 70Ω, the input impedance of a half-wavelength folded dipole is equal to 280Ω.

In the present dissertation we used the folded dipole in a new configuration of the antenna, in order to reduce the size of the antenna.

1.2 Antennas miniaturization

The broadband antenna configurations well-known in literature, previously presented, allowed us to study a new configuration of antenna in the HF and VHF band. This antenna configuration comes from the concepts related to the biconical antenna, which itself has good broadband performances. The main issue with the last proposed topologies is that, in order to design a self-resonating biconical antenna in the range 5-30MHz (HF band), a very large size antenna should be used. The proposed solution had to be optimized and miniaturized.

The miniaturization of a radiating element consists on rendering the antenna electrically small and resonant at the same time. An antenna is electrically small antenna if its sizes are small compared to the wavelength and the *Small Antenna Limit (SAL)* is satisfied:

$$a = \frac{1}{k} = \frac{\lambda}{2\pi} \tag{1.14}$$

where *a* is the radius of a sphere which completely fit the antenna and *k* is the wave number. The corresponding frequency *f* to the wavelength which respects (1.14) is the maximum operating frequency of the electrically small antenna.

As Wheeler studied [6], the electrical performance limitations include the decreasing radiation resistance, efficiency and bandwidth that occur with decreasing resonant frequency.

"An electrically small wire antenna of any specific volume can be made resonant by increasing the total wire length" [7]. "The practical constraint is the limitation on how much wire, of a given finite diameter, can be made to fit within the volume".

The miniaturization of a radiating element could be realized by using the following techniques [7]:

1) Antenna loaded with lumped elements;

2) Antenna loaded with high dielectric constant dielectrics;
3) Antenna on a ground plane and short circuits (shorting pins and vias);
4) Optimization of the antenna geometry;
5) Use of special materials (metamaterials).

In some cases it is very useful the use of lumped elements for loading the antennas. The last technique is often used for the design of resonating structure like Radio Frequencies coils [25], for Magnetic Resonance Imaging (MRI). It happens especially for electrically small structure, where it can be possible to represent the antenna as a lumped circuit. In the last case, it's easy to estimate the values of a capacitance or an inductance which have to compensate the reactance of the input impedance of the antenna and make it resonant at a specific frequency.

In other cases, the lumped element can be distributed along the conductors of the antenna in order to reach for instance, good performance on the bandwidth. The main issue with the last solution is that, a broadband antenna is self-resonating at different frequencies, so it is quite difficult to dimension the values of the lumped element in order to reach the performances, but it could be realized by using specific optimization algorithms [4].

In this dissertation for the project of the antenna for radar applications, we wanted to avoid this first technique and make the antenna self-resonating, miniaturizing it just by working on its shape. For this reason, first we used a ground plane, in order to reduce of one half the size of the original antenna (coming from the biconical antenna concept), and then we used an optimization of the shape antenna, exploiting the concepts on the meandered antennas. Finally, further investigations have been done in order to enhance the bandwidth of the antenna, and some shorting pins, having different folded shape have been used. The investigation made with the shorting pins has been described in the following chapter. The concepts related to the meandered antennas and to the benefits of a ground plane, have been described in the following paragraphs.

1.2.1 Antenna on a ground plane

The scattering phenomena that occur from radiating elements on a perfect electric conductor (PEC) infinite ground plane can be properly studied by using the image theorem.

The last system is equivalent to consider two radiating elements, placed like in Figure 1.6, without the ground plane. The fields of the first system in the upper region of the space can be calculate like the fields radiated by the equivalent system, where the second radiating element is the image of the first one. In particular, the field radiated in a generic point *P* in the region of far field (parallel-rays approximation), can be calculated as the sum of the field radiated by the original antenna in the upper region and, the field radiated by the image antenna.

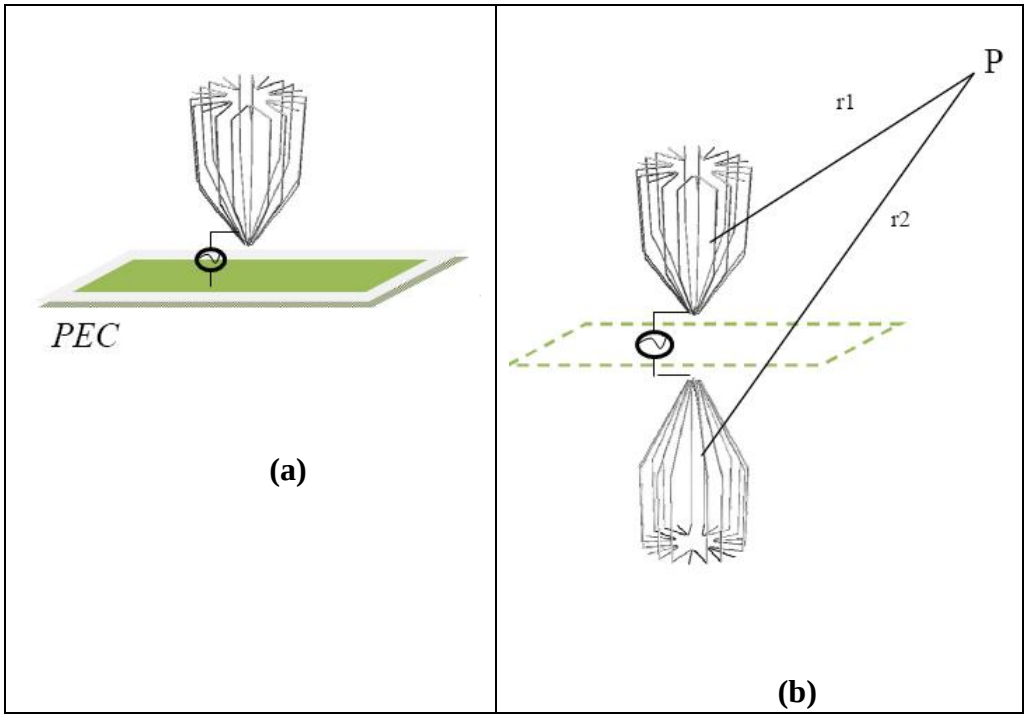

Figure 1.6 – Antenna on a PEC ground plane: (a) original system; (b) equivalent system by applying the images theorem.

In order to take into account the effect of the presence of a ground plane on the input impedance and on the radiation pattern of the antenna, the case of a monopole on a PEC ground plane has been considered.

By applying the image theorem, a monopole on a Perfect infinitely ground plane is like a half dipole of length L, fed in correspondence of its center (as shown in Figure 1.7).

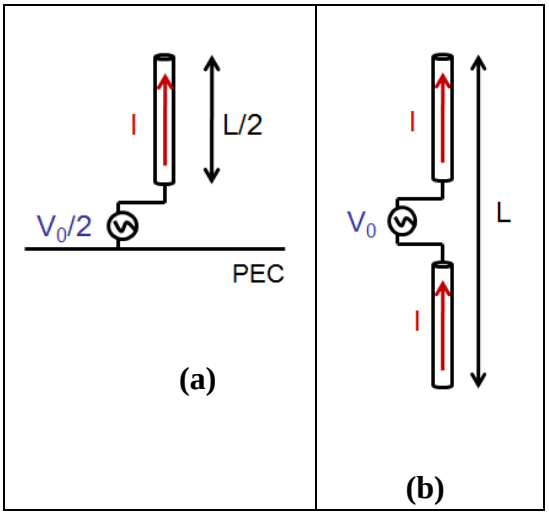

Figure 1.7 – Monopole on a PEC ground plane: (a) monopole; (b) dipole.

The current on the monopole is equal to the current on the equivalent dipole; however the voltage on the monopole is the half of the voltage on the dipole, so the input impedance of the monopole on the ground plane is [16]:

$$Z_{mono} = \frac{V_{mono}}{I_{mono}} = \frac{\frac{1}{2}V_{dipole}}{I_{dipole}} = \frac{1}{2}Z_{dipole} \tag{1.15}$$

Because the fields are present just in the upper half-plane, the power radiated by the monopole on the ground plane is the half of the power radiated by the equivalent dipole, so the radiating resistance of the monopole is:

$$R_{r,mono} = \frac{P_{mono}}{\frac{1}{2}\left|I_{mono}\right|^2} = \frac{\frac{1}{2}P_{dipole}}{\frac{1}{2}\left|I_{dipole}\right|^2} = \frac{1}{2}R_{r,dipole} \tag{1.16}$$

The radiation pattern of the monopole on the PEC ground plane is one half the radiation pattern of its equivalent dipole. So, the monopole radiates just in the upper half-plane.

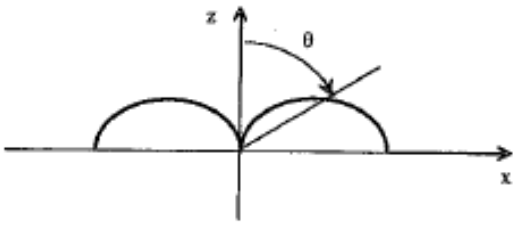

Figure 1.8 – Radiation pattern of a monopole on a PEC ground plane.

The directivity of the monopole is:

$$D_{mono} = 2D_{dipole} \tag{1.17}$$

For instance, if the monopole on a ground plane is like one half of a λ/2 dipole (λ/4 length, typical of stylus or marconian antenna) its directivity is:

$$D_{mono,\lambda/4} = 2(1.64) = 3.28 = 5.16dB \tag{1.18}$$

Its input impedance is:

$$Z_{A,\lambda/4} = \frac{1}{2}(72 + j42.5)\Omega = 36 + j21.3\Omega \tag{1.19}$$

1.2.2 Antenna with shorting pins

In literature other solutions for size reduction of antennas are present. In some cases the use of a ground plane is avoided and the low profile configurations are obtained by using shorting pins. Figure 1.9 shows an antenna solution which is a simple modified configuration of a biconical antenna, and it is a balance between simplicity, performance, size and while providing the omni-directional and broadband characteristics of a biconical antenna [9].

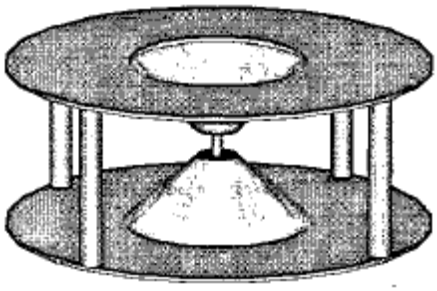

Figure 1.9 – Shorted biconical antenna for UWB applications.

Two disks have been used in order to allow a reduction of the electric height of the antenna; avoiding the great variation of the radiation pattern with the frequency. The same

effect comes from the use of four shorting pins, which also allow a tuning of the antenna. For our purposes we used the second concept, based on the use of folded pin shorting the antenna to a ground plane, in order to enhance the impedance matching performances.

Recent studies [10] have been used the same concepts. First, they compared different size of a ground plane, noting that larger size of a ground plane drastically reduces the lowest operating frequency. Further, the introduction of capacitive loading with shorting pins causes additional reduction of the operating frequency.

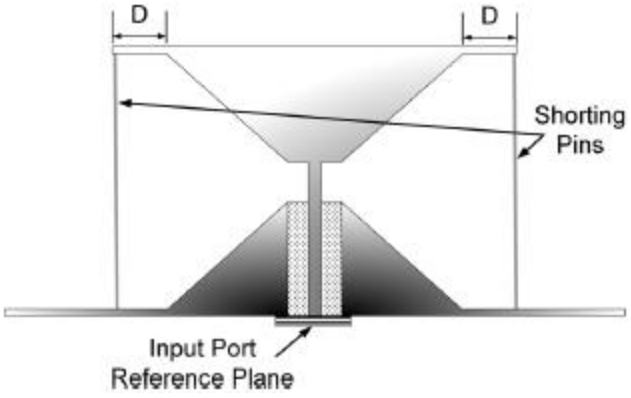

Figure 1.10 – Shorted biconical antenna on a ground plane for UWB applications.

Shorting pins loaded with lumped elements on mono-conical antenna on a ground plane have been studied for VHF frequency range [11], in order to reach again a reduction of the size and enhancing the broadband performances of the conical antenna.

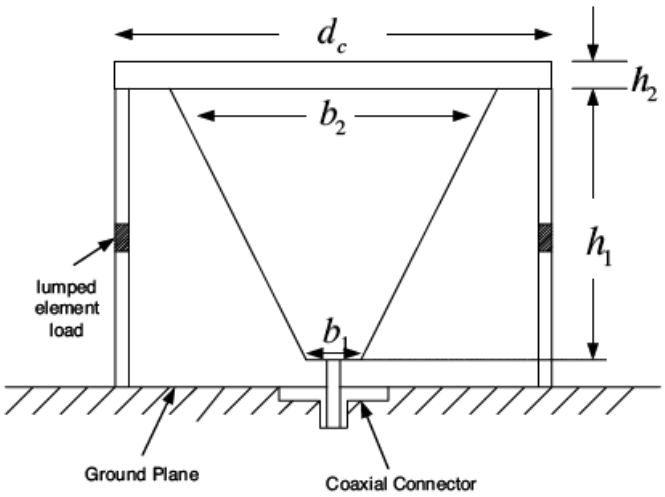

Figure 1.11 – Shorted mono-conical antenna on a ground plane for UWB applications.

All the presented literature concern with antenna loaded with capacitive shorting pins, in which the antenna is fed and the pins are passive devices.

Other solutions have been studied, concerning with shorting pins fed. One of them it is presented by Choo [18], who optimized an inductive fed pin to reach self-resonance, good efficiency and bandwidth, without the use of matching networks or lumped loads. In the last solution the inductive pins are fed.

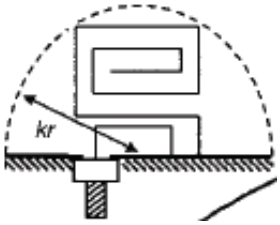

Figure 1.12 – Inductive coupled fed pins.

Other configuration present in literature [17], have folded pins fed and coupled with naval structure (like mast or flue) and they present lumped element loads along the wires.

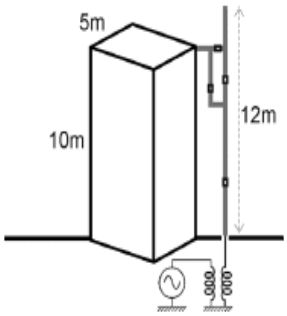

Figure 1.13 – Capacitive coupled fed pins.

In this dissertation we used a combination of the solutions presented in literature and we wanted to avoid the use of lumped loads along the conductors of the antenna.

1.2.3 Meandered antennas

The meandered antennas are a class of wires antennas consisting of multiple folded sections obtained folding the wire antenna on itself and joining these sections together [8]. The main issue is to reduce the size of the antenna at a specific resonance frequency. The

resonance frequency and the performances of the antenna depend on the number of folded sections and on the distance *w* between the folded sections (see Figure 1.14).

In general, *w* is smaller than the overall size of the antenna, so the radiation effect produced by these segments can be negligible.

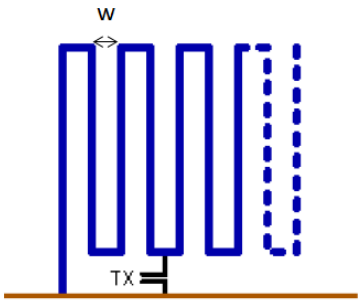

Figure 1.14 – Meandered antenna.

The quantity β (<1) is defined as the reduction factor of a meander antenna. If a conventional monopole of length *L* and a meander monopole of length *I* have the same resonant frequency, therefore the reduction factor is $\beta = I/L$. This factor depends primarily on the number of sections per wavelength (N) and the width of the rectangular loops (W).

The reduction factor gives the information about the number of folded sections of a meandered monopole (i.e. *I*) necessary to reach the same resonance frequency of a conventional monopole of length *L*. This technique allows reducing the size of the antenna, because in the same volume/surface the path of the currents can be extended.

Theoretically, it can be possible to create multiple folds in order to further reduce the size of the antenna. However, some coupling effects between the folded sections could cause undesired discharges. Further investigations demonstrate that increasing the number of folds can reduce the operating bandwidth of the antenna.

These concepts have been applied to the antenna for radar applications purposes, as described in the following chapter.

2 ANTENNAS FOR OVER THE HORIZON (OTH) RADAR

This dissertation is mainly focused on the study and the design of radiating elements suitable for Over The Horizon (OTH) radars. This kind of radars operates in the 5-30 MHz frequency range to detect and track targets over wide areas by exploiting the long range skywave propagation of HF e.m. waves through the ionosphere. This technology is used for surveillance over wide areas, as well as for monitoring the sea surface state and subsequently the wind direction and intensity, for ocean remote sensing purposes.

The antennas used for this application are phased arrays of many radiating elements. The receiving array is designed as a simple repetition of active dipoles, whose dimensions are not a critical parameter due to the possibility of miniaturization without affecting the overall performance. On the contrary, the transmission array must be composed of broadband radiating elements. Because of the large number of radiating elements in the array, one of the most critical aspects of this study concern the reduction of the size of each antenna. The analysis we focussed on is therefore related to the challenging design of a miniaturized broad-band single radiating element suitable for being used in the transmitting array of HF OTH radars.

2.1 Arrays configurations for OTH radar

In order to test different configurations of the array for OTH radar, the tool Antenna Framework Simulator (AFS) has been implemented. The tool allows designing, visualizing and analyzing several planar array shapes, through dedicated GUIs. The AFS is very flexible.

Some GUIs for designing circular concentric arrays and spiral arrays are showed in Figure 2.1.

The array geometry chosen for OTH application is a circular shape and it consists of 50 radiating elements, like reported in Figure 2.2. The last choice is a compromise between a study made on the reduction of the mutual couplings (well explained in the following paragraph) between the elements and the radiation patterns of the phased array according to the frequency and the pointing direction. The radiation pattern of the phased array for OTH radar has to realize very low Side Lobe Levels.

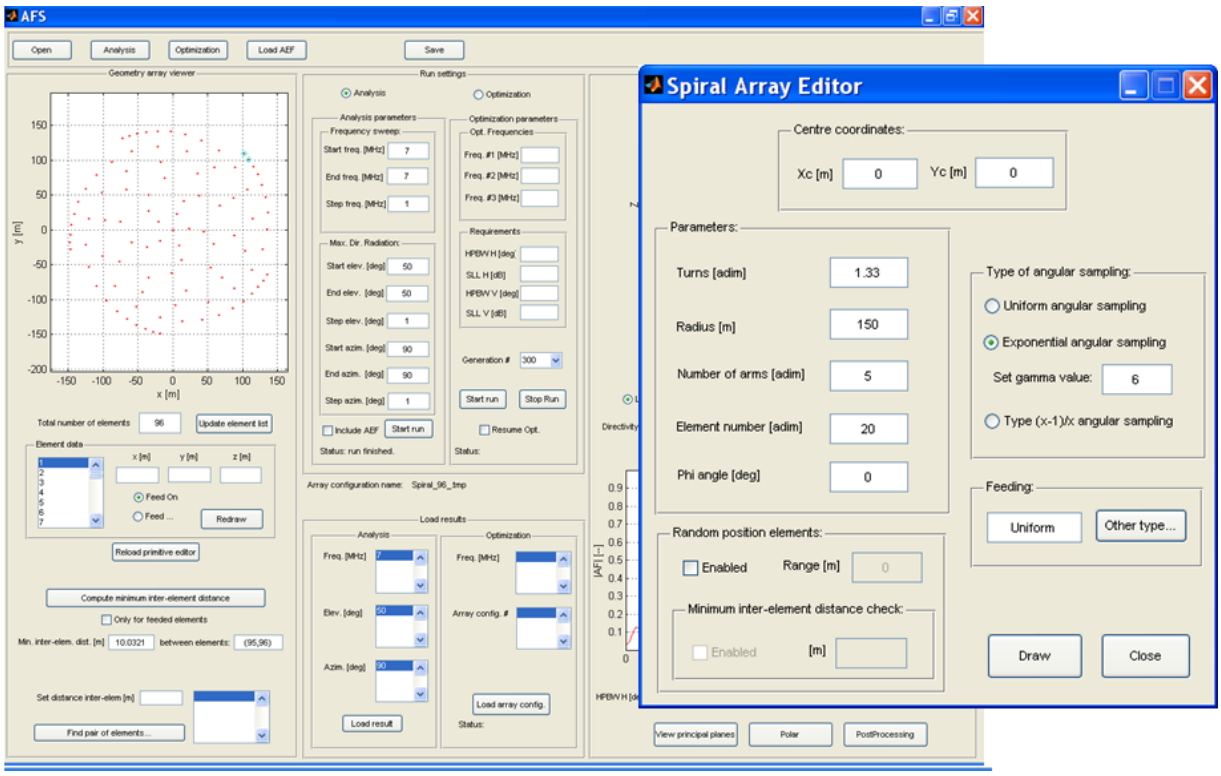

Figure 2.1 – AFS GUI for spiral array design.

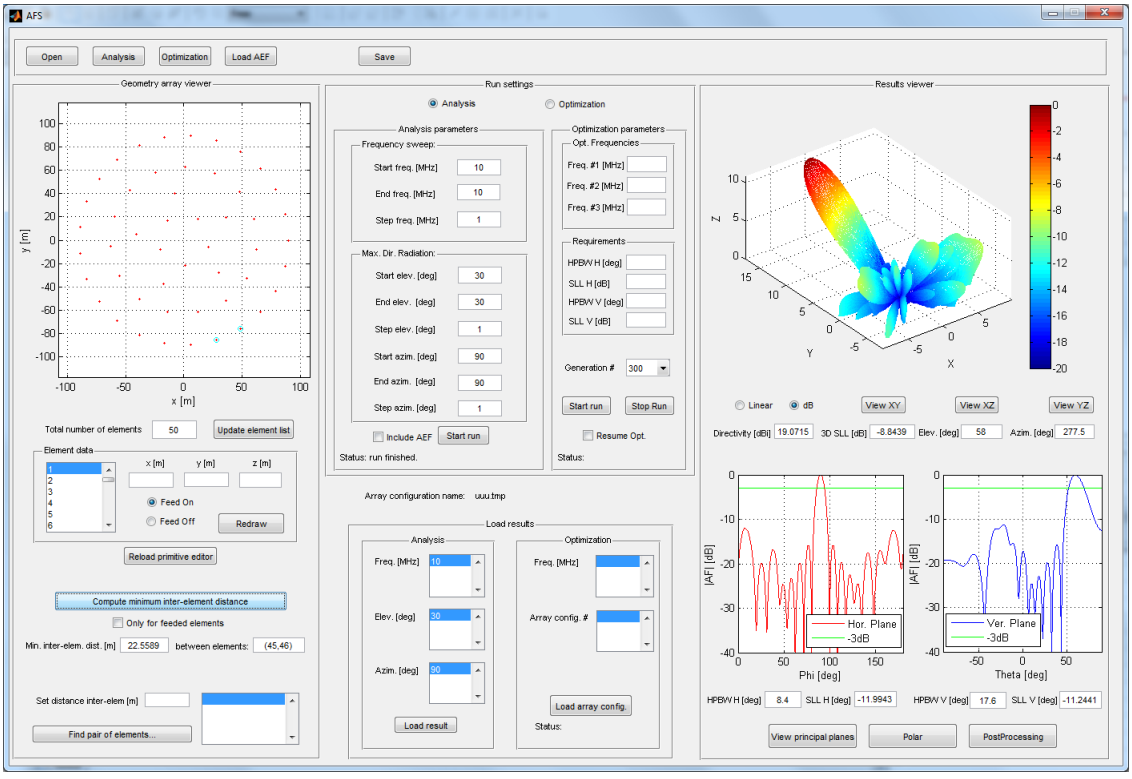

Figure 2.2 – Circular array configuration and radiation performance with the AFS GUI.

2.2 *Stand alone antenna design for OTH array*

As mentioned before, the configuration of the antenna thought for radar purposes has to be compact, but at the same time with broadband performances in the HF band.

We assume that the stand alone antenna has to operate in the range of 7MHz to 30MHz, with input impedance equal to 50Ω and it has to realize a maximum gain equal to 4dBi. The shape of the radiation pattern has to maintain the same shape according to the frequency and it has to be omni-directional on the H plane, and symmetrical on the E plane with a linear polarization.

The first version of the antenna was a combination of a biconical antenna and a meandered antenna placed on a perfect electrical conductor infinite ground plane. It consists of two pieces, the nearest to the ground is similar to a conical antenna and the second one goes straight to a flat top.

The resulting antenna was formed of six folded arms and with one stub on the top (as shown in Figure 2.3). The height of the antenna was equal to 10.5m and the width was 6m and it was made of copper wires having a radius equal to 0.015m.

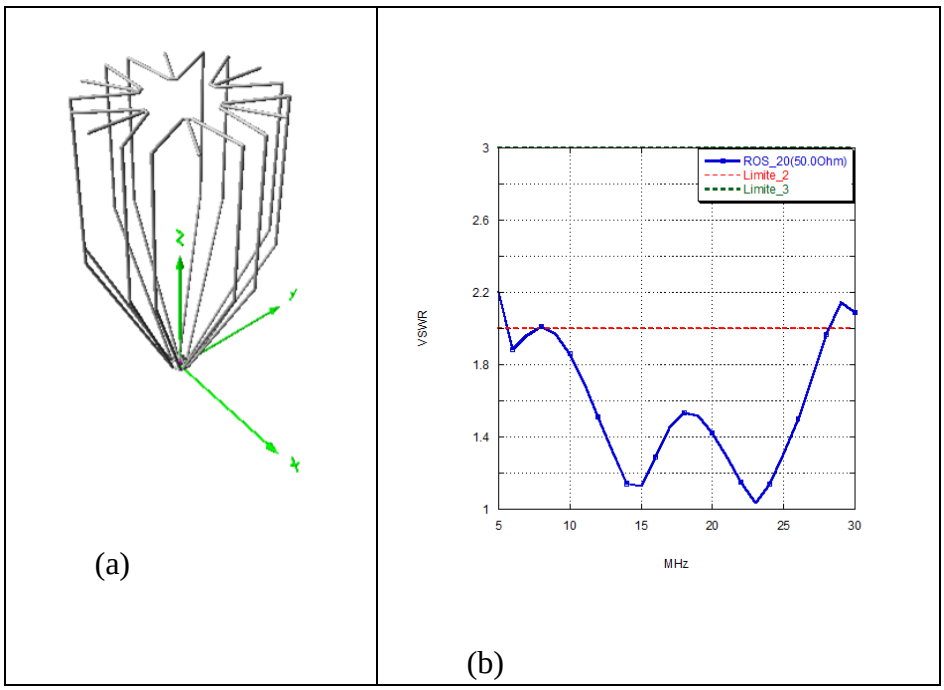

Figure 2.3 – Antenna first design input impedance: (a) VSWR according to the frequency.

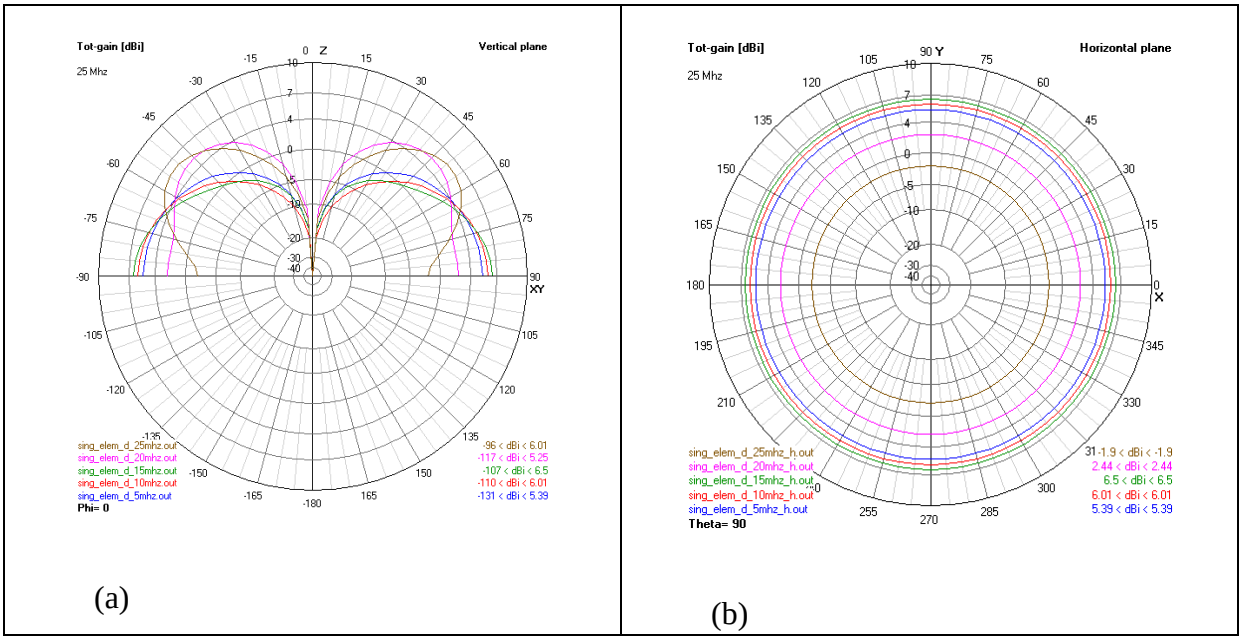

Figure 2.4 – Antenna first design radiation pattern: (a) E plane; (b) H plane.

The antenna performances have been analyzed with a Method of Moment (MoM) solver and it operated like a monopole on a perfect ground plane, with very good performances in terms of matching in the band of interest (Figure 2.3 (b)). At the same time, it presented good performances in terms of radiation pattern, however on the E plane the shape was quite different at higher frequencies than the lower frequencies one Figure 2.4. The antenna radiated with a linear polarization.

Because the proposed configuration was not physically feasible, another solution has been proposed, having the same performances but with a different shape. The new antenna consists of twelve arms joined together on the top Figure 2.5. This new configuration gives to the antenna more structural and mechanical stability than the previous one. The performances in terms of input impedance and radiation pattern of this new antenna are reported in Figure 2.7- Figure 2.8 and they have been evaluated with a MoM solver.

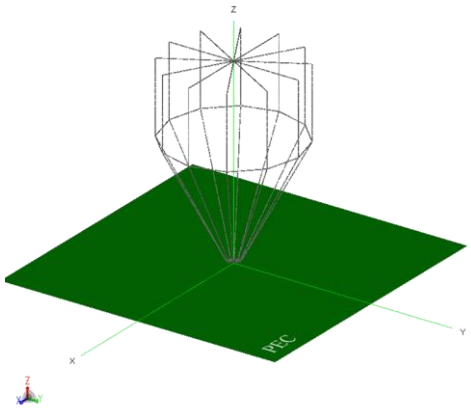

Figure 2.5 – Antenna with the modified design.

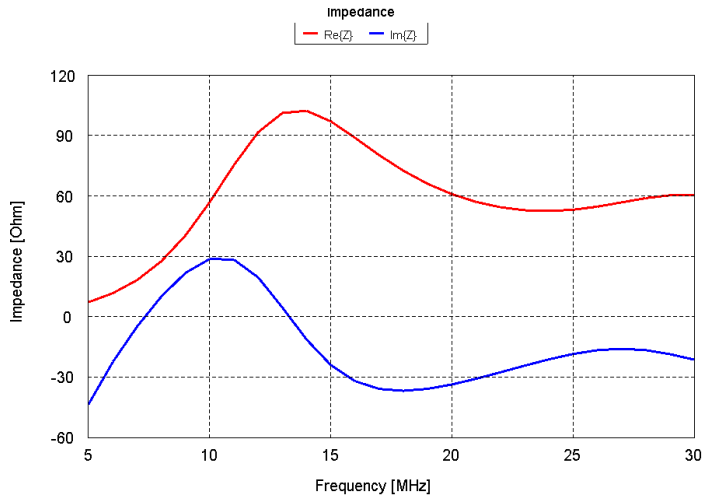

Figure 2.6 – Input impedance of the antenna with the modified design.

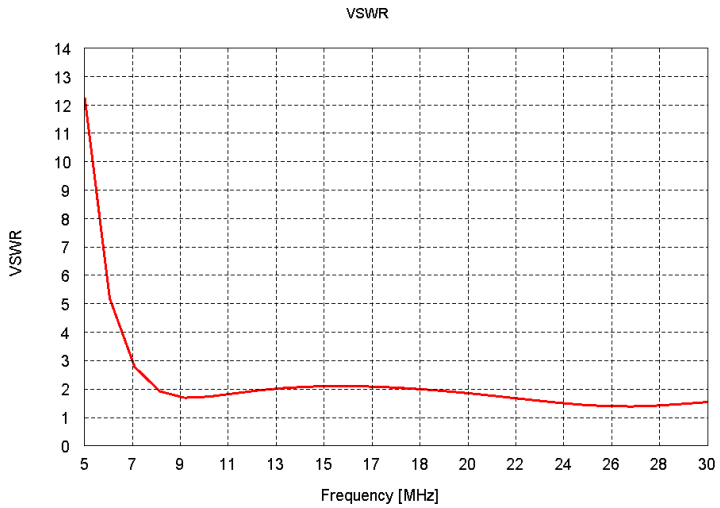

Figure 2.7 – VSWR of the antenna with the modified design.

The antenna has a VSWR less than 3 in the range 7-30MHz. The new antenna is smaller than the previous one, its height is 6.5m and its width is equal to 4.6m. The material of the wires is copper and their radius is equal to 0.015m. It can be notice that the lower operating frequency is higher than the first version antenna one.

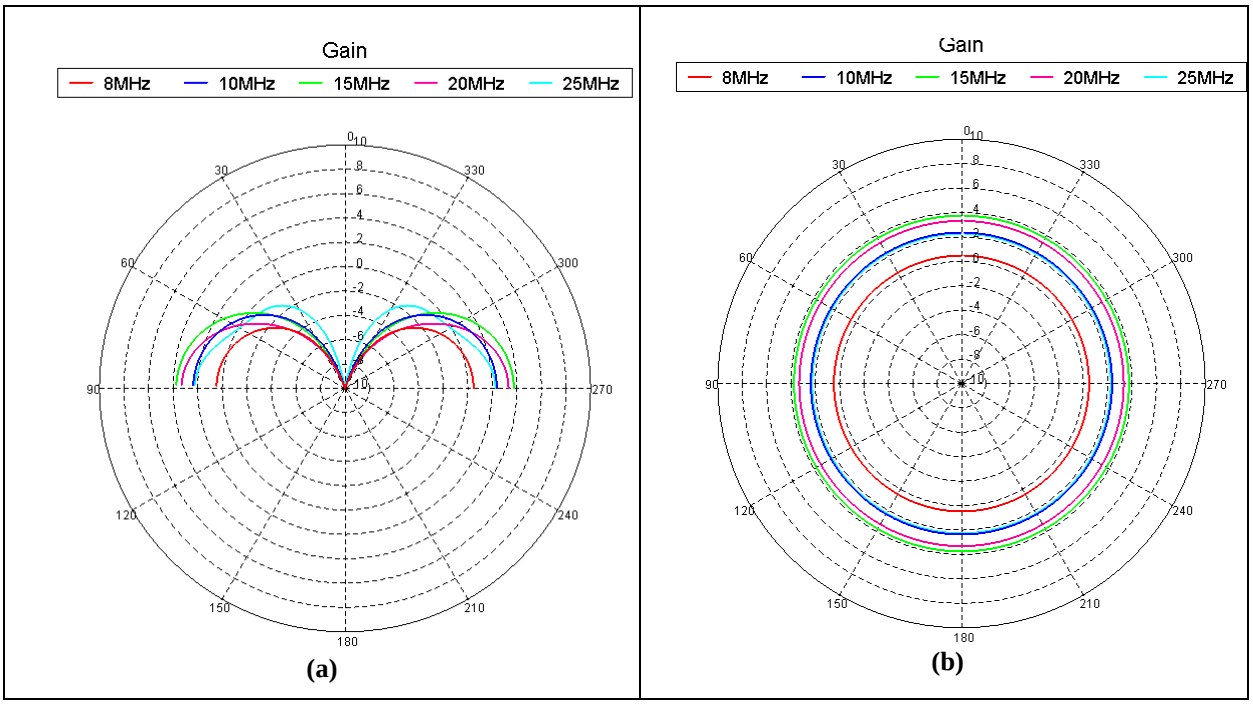

Figure 2.8 – Antenna with the modified design radiation pattern at 7MHz: (a) E plane; (b) H plane.

The radiation patterns are more stable in shape according to the frequency.

2.3 Mutual coupling in phased arrays

The scanning performance of the array is generally determined by the element spacing, which is limited by the element size. For wideband antennas the operating band is very broad, making the electrical distance between the elements larger as the frequency increases. Ideally, less than λ/2 spacing is desired over the frequency band. When the element size is large, the spacing will easily exceed the λ/2 spacing at high frequency so the scanning performance of the array is degraded. However, if the distance between the radiating elements is reduced, mutual couplings phenomena are inevitable. The better solution is a continuous study of a trade-off between the two aspects: the stand alone broadband antenna and the antenna inside the array in the nearby of other identical elements.

The mutual coupling between the elements also depend on the shape of the array, the radiation pattern of the single element, on the frequency and the pointing direction [12], [13], [14].

The impedance matching of a standalone antenna is different and more complicated from the impedance matching of the same antenna inside the array.

The parameter which in a phased array takes into account all these variables is the *active reflection coefficient* and its formulation for the *m*-th radiating element in the array is [14]:

$$\Gamma_m(\vartheta_0,\varphi_0) = \frac{e^{jk\sin\vartheta_0[x(m)\cos\varphi_0+y(m)\sin\varphi_0]}}{V_{0,m}} \sum_{n=1}^{N} |S_{mn}| e^{j\angle S_{mn}} V_{0,n} e^{-jk\sin\vartheta_0[x(n)\cos\varphi_0+y(n)\sin\varphi_0]} \qquad (2.1)$$

where:

- θ_0, φ_0 indicate the generic pointing direction,
- $V_{0,i}$ is the voltage feeding of the generic radiating element *i*,
- *x(i), y(i)* are the coordinates of the generic element *i*,
- *S* is the scattering matrix at a generic frequency *f*,
- $k = 2\pi/\lambda$ is the wave number.

If we consider constant source amplitude for each element in the array, the *active reflection coefficient* can be written as follow:

$$\Gamma_m(\vartheta_0,\varphi_0) = S_{mm} + e^{jk\sin\vartheta_0[x(m)\cos\varphi_0+y(m)\sin\varphi_0]} \sum_{n=1,n\neq m}^{N} S_{mn} e^{-jk\sin\vartheta_0[x(n)\cos\varphi_0+y(n)\sin\varphi_0]}. \qquad (2.2)$$

In order o reduce the mutual coupling in a phased array, the active reflection coefficient Γ_m has to be minimized.

The parameter S_{mm} is the active reflection coefficient of the *m*-th element fed and the other elements terminated on 50Ω. The last term is the only one of the sum which is independent from the frequency. The second term of the sum is frequency dependent. Because all the terms S_{mn} are generally lower than the term S_{mm}, the active reflection coefficient can be minimized if the term S_{mm} is minimized. This last assumption is necessary in order to minimize Γ_m, but not sufficient, because sometime it can happen that a coherent summation of the S_{mm} parameters can cause the Γ_m increase, producing high mutual couplings.

In Figure 2.9 an active VSWR of a circular phased array of 50 elements has been reported, in order to show how even if the antenna are broadband well-matched, the mutual coupling creates a mis-match of the entire array.

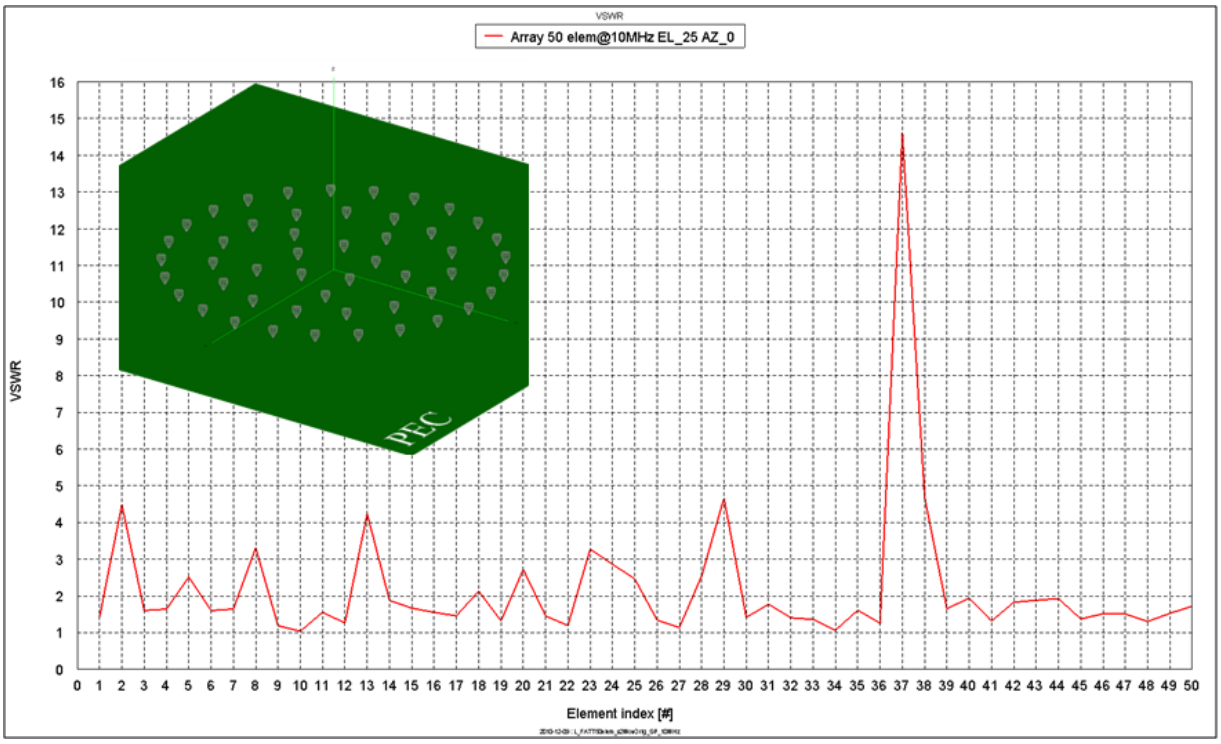

Figure 2.9 – Active VSWR of a circular phased array according to the element inside the array.

Because each radiating elements in practice, is used with amplifiers, which support a VSWR at maximum equal to 3, the active VSWR realized by each element in the array doesn't must exceed 3, and the active reflection coefficient doesn't must exceed the value 0.5. Further, it is necessary that especially at lower frequencies of the HF band used for OTH radar purposes (8-16MHz at least), the generic *m* antenna in the array has to realize the S_{mm} as small as possible.

We took into account all these requirements for the study of the stand alone antenna, which has been explained in the following paragraphs.

2.4 *Miniaturizing the stand alone antenna*

In order to reduce the mutual couplings coming from the use of the antenna in the array, a modified configuration has been studied into respect the two versions presented before (§2.2).

By observing the imaginary part of the input impedance of the original antenna according to the frequency, an inductive behaviour can be notice in the range 7.3MHz-13.27MHz, otherwise the antenna has got a capacitive behaviour.

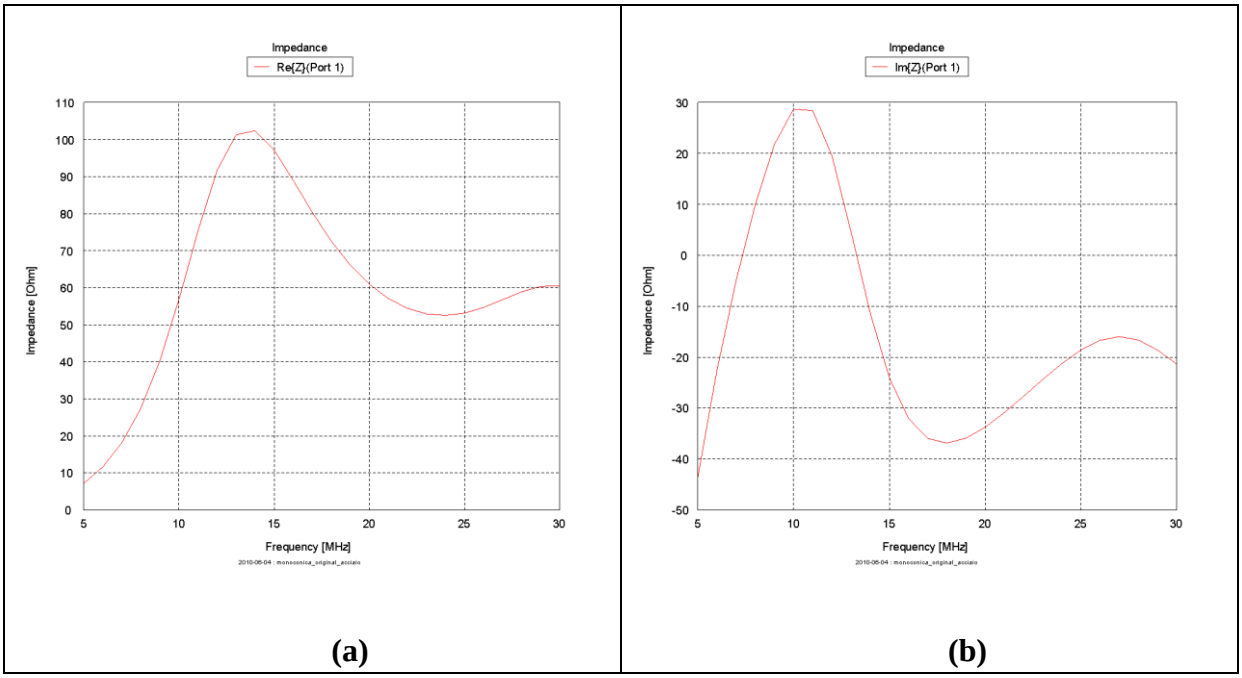

Figure 2.10 – Antenna input impedance: (a) RE (Zin); (b)IM (Zin).

Two different approaches have been studied and compared with the original antenna case: the first one by using a folded pin [17] near the antenna and the second one by using a coupled pin [18]. The first pin has been used because of its inductive behaviour, in order to compensate the capacitive behaviour of the input impedance of the antenna at lower frequencies of the HF band (as shown in Figure 2.11). The second pin behaves as a capacitance and it could compensate the inductive behaviour of the antenna in the range 7.3MHz-13.27MHz.

At the same time, the new configuration has to match the real part of the antenna to 50Ω. In the here proposed configurations only the antenna was fed and not the pin.

Both cases have widely been studied with a parameterization of the segments constituting the pins. For the optimization, the input impedance and the VSWR of the antenna have been taken into account.

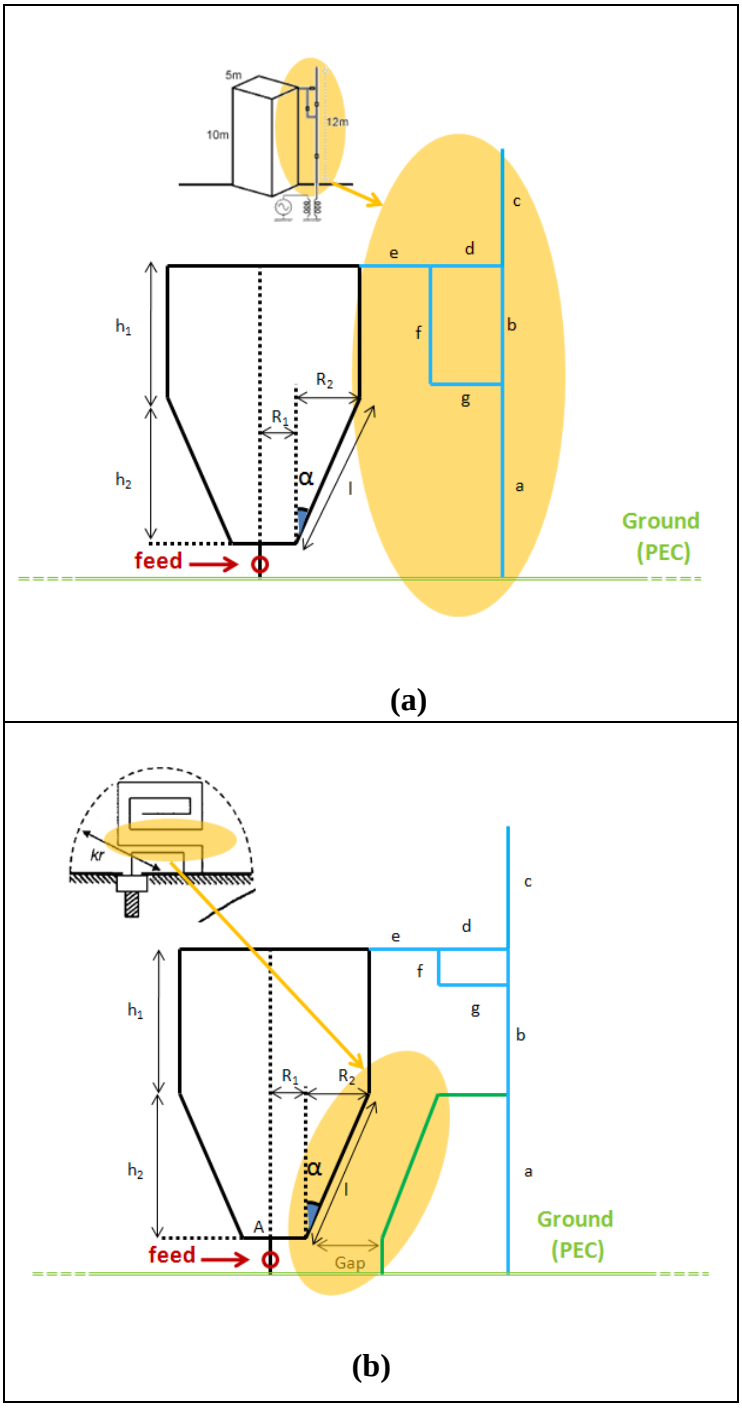

Figure 2.11 – Antenna design: (a) with folded pin; (b) with folded coupled pin.

2.4.1 Antenna with inductive pin: matching

For the folded pin case (Figure 2.11 (a)), the lengths of the segments have been investigated and the VSWR has been observed.

First of all we fixed the length of the segments *e*, *d* and *g* equal to 1m and we varied *f*, *b* and *a*.

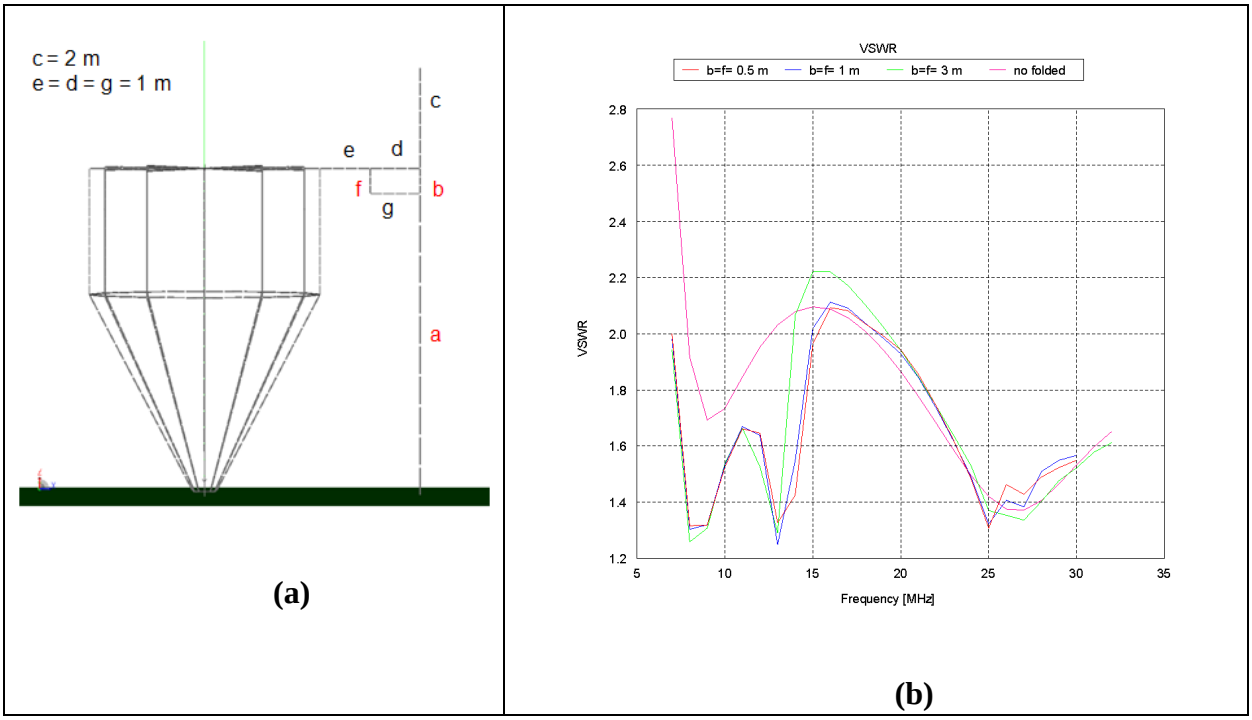

Figure 2.12 – Antenna with folded pin: (a) segments parameterization; (b) VSWR parameter according to the frequency and parameters *b* and *f*.

As it can be seen from VSWR (Figure 2.12 (b)), a very good matching of the antenna at the lower frequencies of the HF band, has been obtained.

The solution with *b* and *f* equal to 0.5m has been considered for further investigations, because it realizes the better VSWR performances.

Then, fixing *f* and *b* equal to 0.5m, we varied the length of the segments *d* and *g*, studying the behaviour of the antenna with three different values of the segment *e* (Figure 2.13 - Figure 2.15).

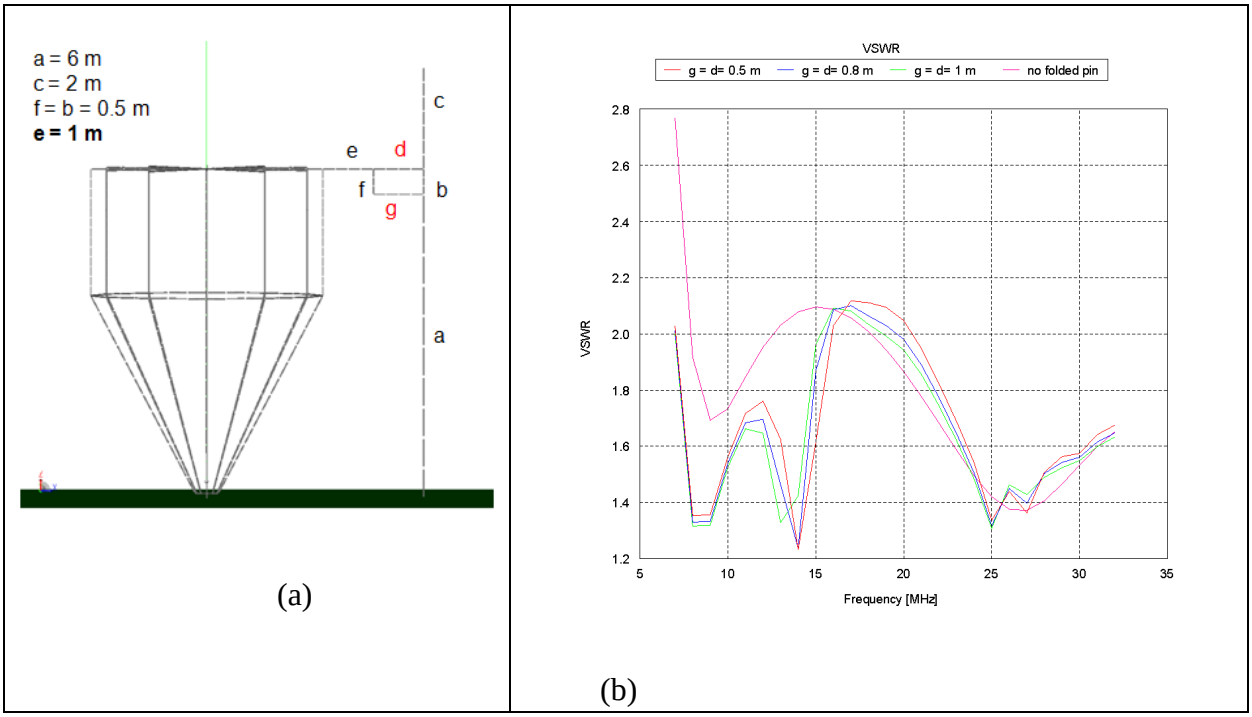

Figure 2.13 – Antenna with folded pin: (a) segments parameterization; (b) VSWR parameter according to the frequency and parameters *d* and *g*.

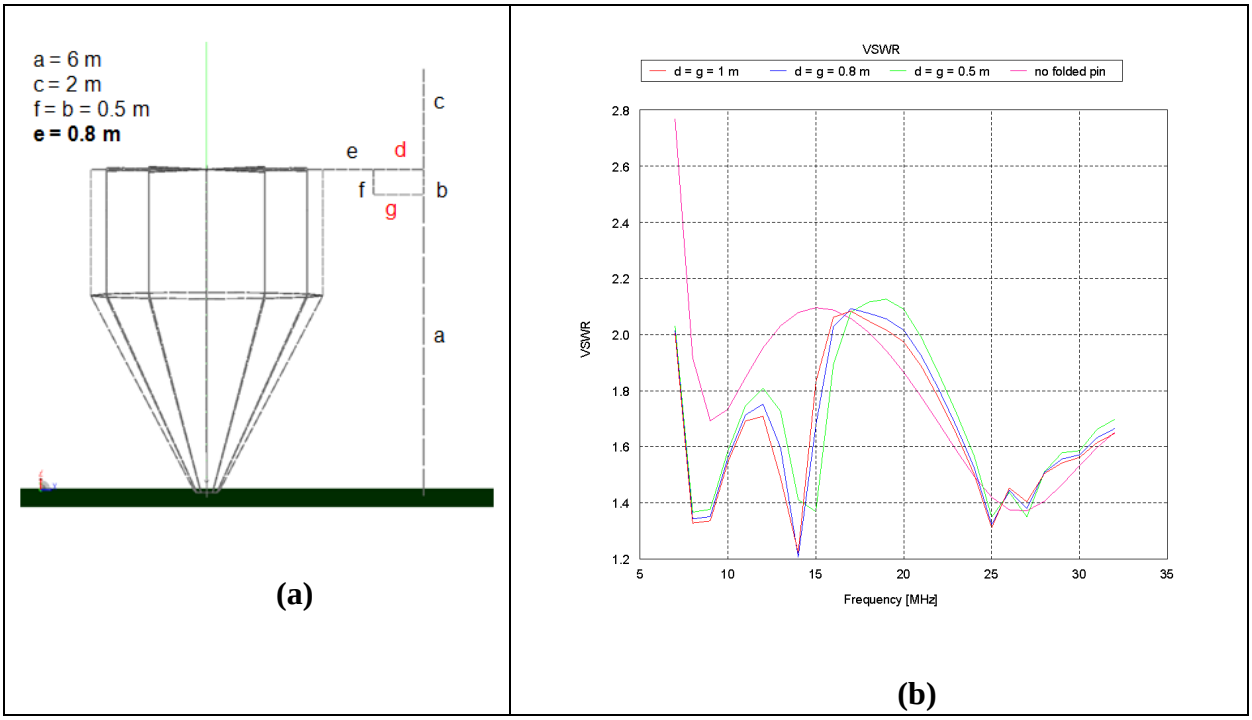

Figure 2.14 – Antenna with folded pin: (a) segments parameterization; (b) VSWR parameter according to the frequency and parameters *d* and *g*.

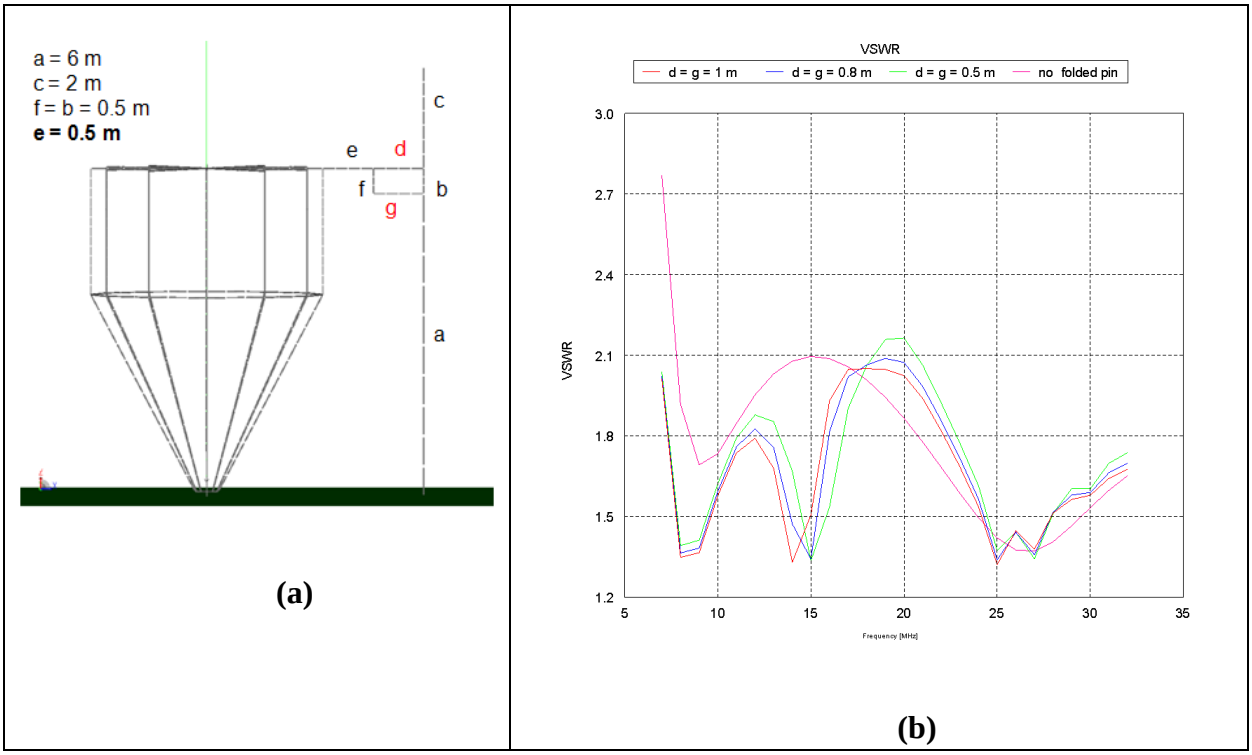

Figure 2.15 – Antenna with folded pin: (a) segments parameterization; (b) VSWR parameter according to the frequency and parameters *d* and *g*.

We observed that good performances have been obtained in the case of *d* and *g* equal to 1m.

2.4.2 Antenna with inductive coupled pin: matching

While the introduction of the simple folded pin, as described in the previous paragraph, produced a capacitive load for the antenna, which compensates the inductive behaviour of the antenna especially in the range 7.3-13.27MHz, after the introduction of a further grounded pin, we noticed a compensation of the capacitive behaviour of the antenna in the center of the considered band.

So we investigated the performance of the antenna according the width of the gap, which operates like an inductive load. At the beginning we chose a width of the gap, as the segment *e* equal to 1m and then we fixed the gap and the segment e to 0.2m. Thus we compared the results between the antenna loaded with original folded pin and with the unloaded antenna.

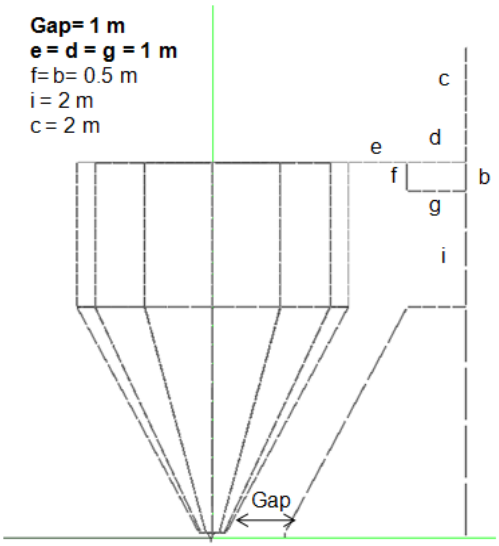

Figure 2.16 – Antenna with folded coupled pin.

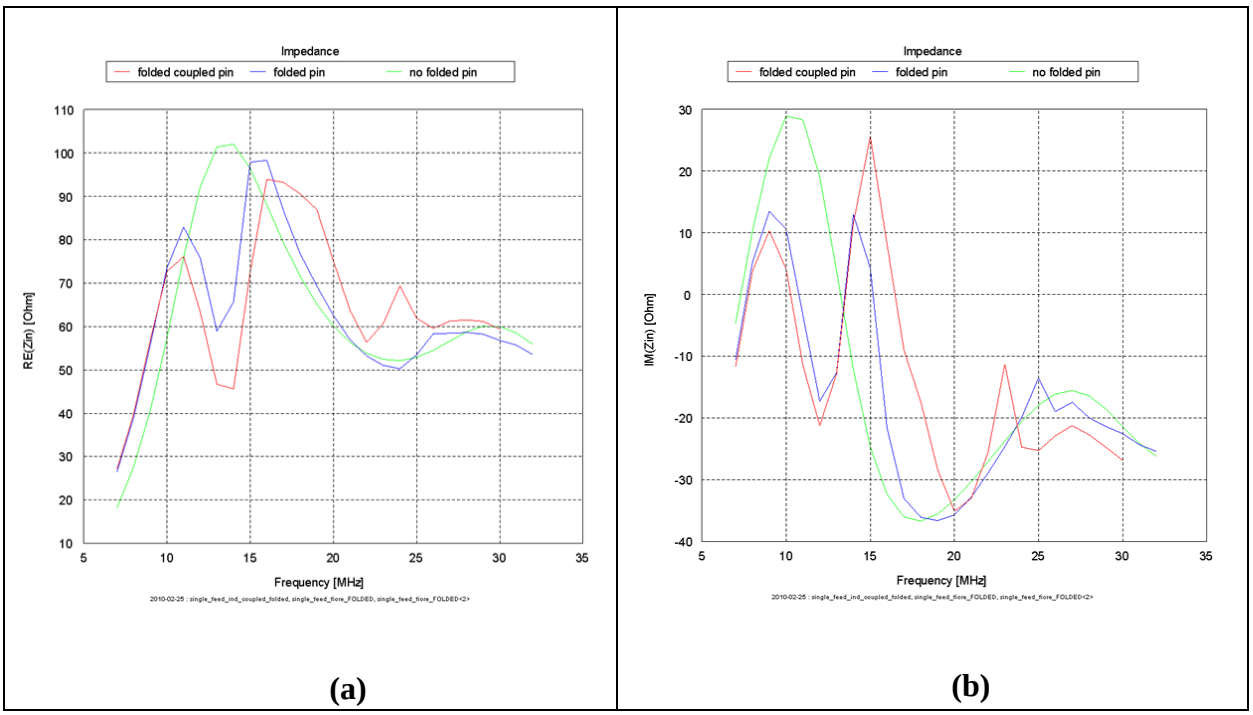

(a) **(b)**

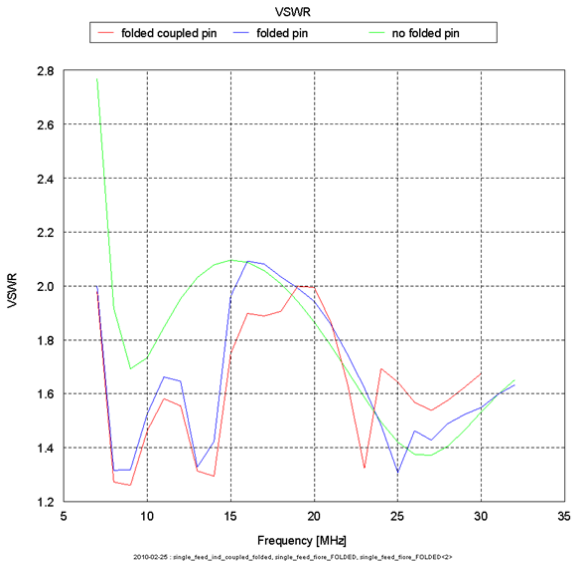

(c)

Figure 2.17 – Antenna with folded coupled pin: (a) RE(Zin) according to the frequency; (b) IM(Zin) according to the frequency; (c) VSWR according to the frequency.

A good matching has been obtained until 18MHz. At higher frequencies, the effect was not so significant.

According to the latter observations, we studied the combination of the folded coupled pin and the simple one, by varying the gap between the antenna and the pin as follows.

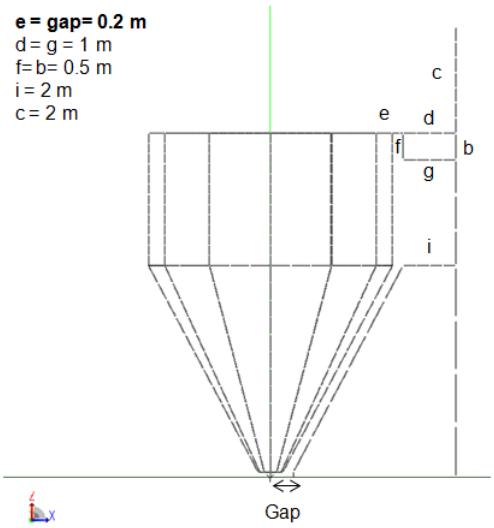

Figure 2.18 – Antenna with folded coupled pin by varying the gap.

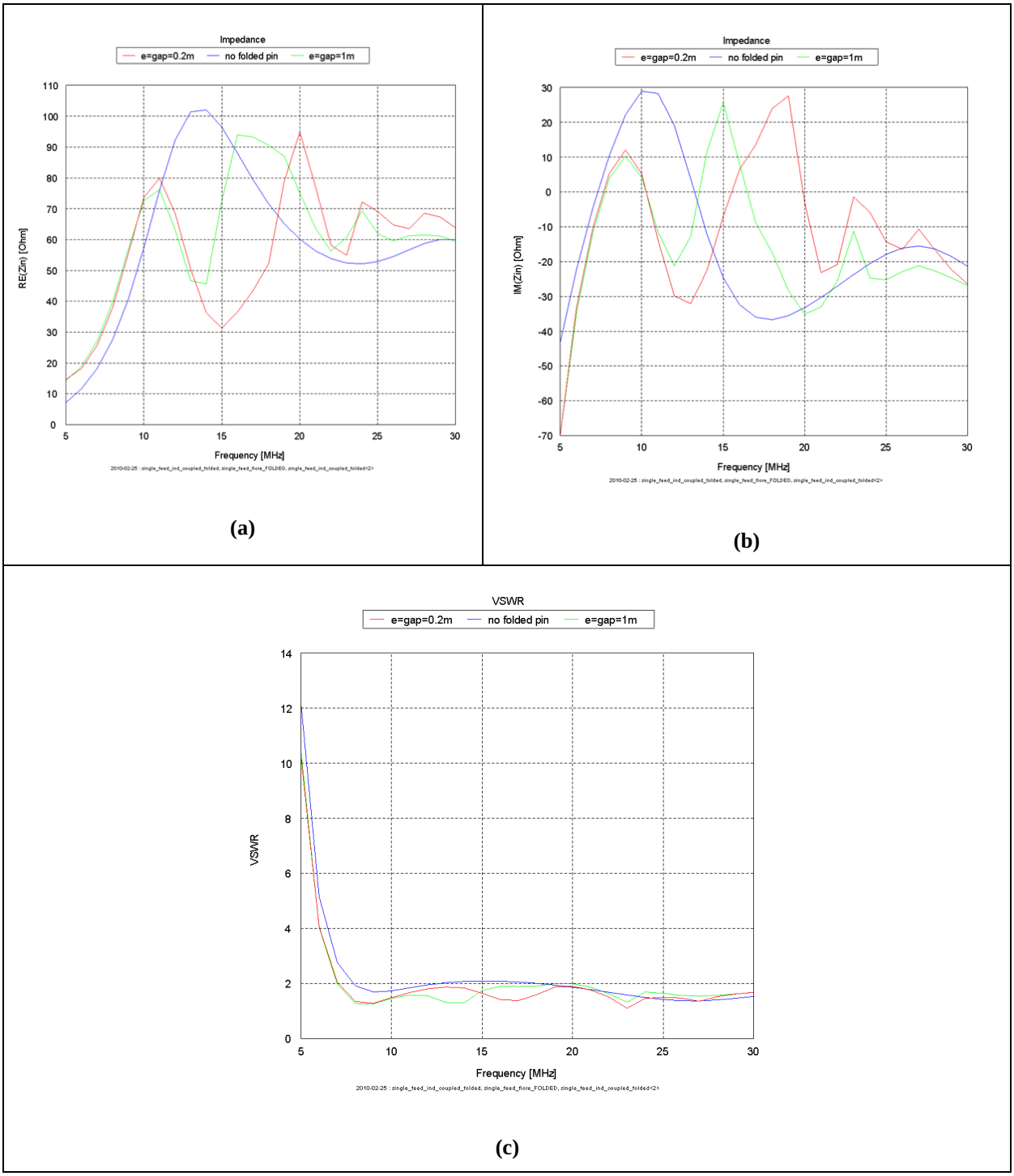

Figure 2.19 – Antenna with folded coupled pin: (a) RE(Zin) according to the frequency; (b) IM(Zin) according to the frequency; (c) VSWR according to the frequency.

By using a much closed grounded pin to the antenna, the coupling was stronger especially in the center frequencies of the band. The last transformation causes more

oscillations of the input impedance, leading to an overall improvement of the matching. However the effect of the reduction of the gap was no significant at lower frequencies of the HF band, so a further study was required.

We thought to introduce other conductive paths to the original pin in order to enhance its inductive behaviour. As it can be seen in Figure 2.20, we added a new path parallel to the existent path *i*, having the same length of *i*.

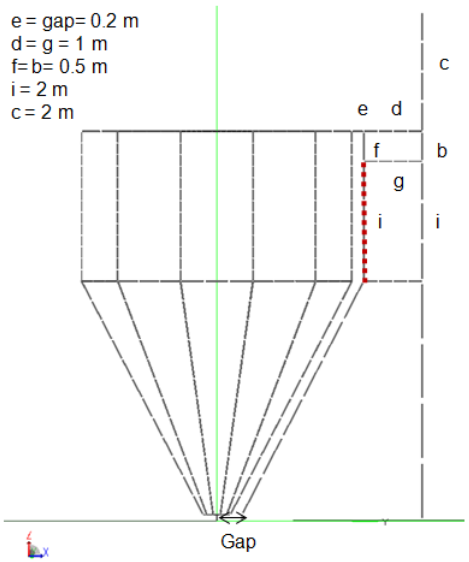

Figure 2.20 – Antenna with folded coupled pin with a further path parallel to *i*.

In the following Figure 2.21, the results in terms of input impedance and VSWR have been shown. The introduction of the segment parallel to *i* produced a better matching of the antenna, especially at lower frequency and further the positive effect is present also at other frequencies.

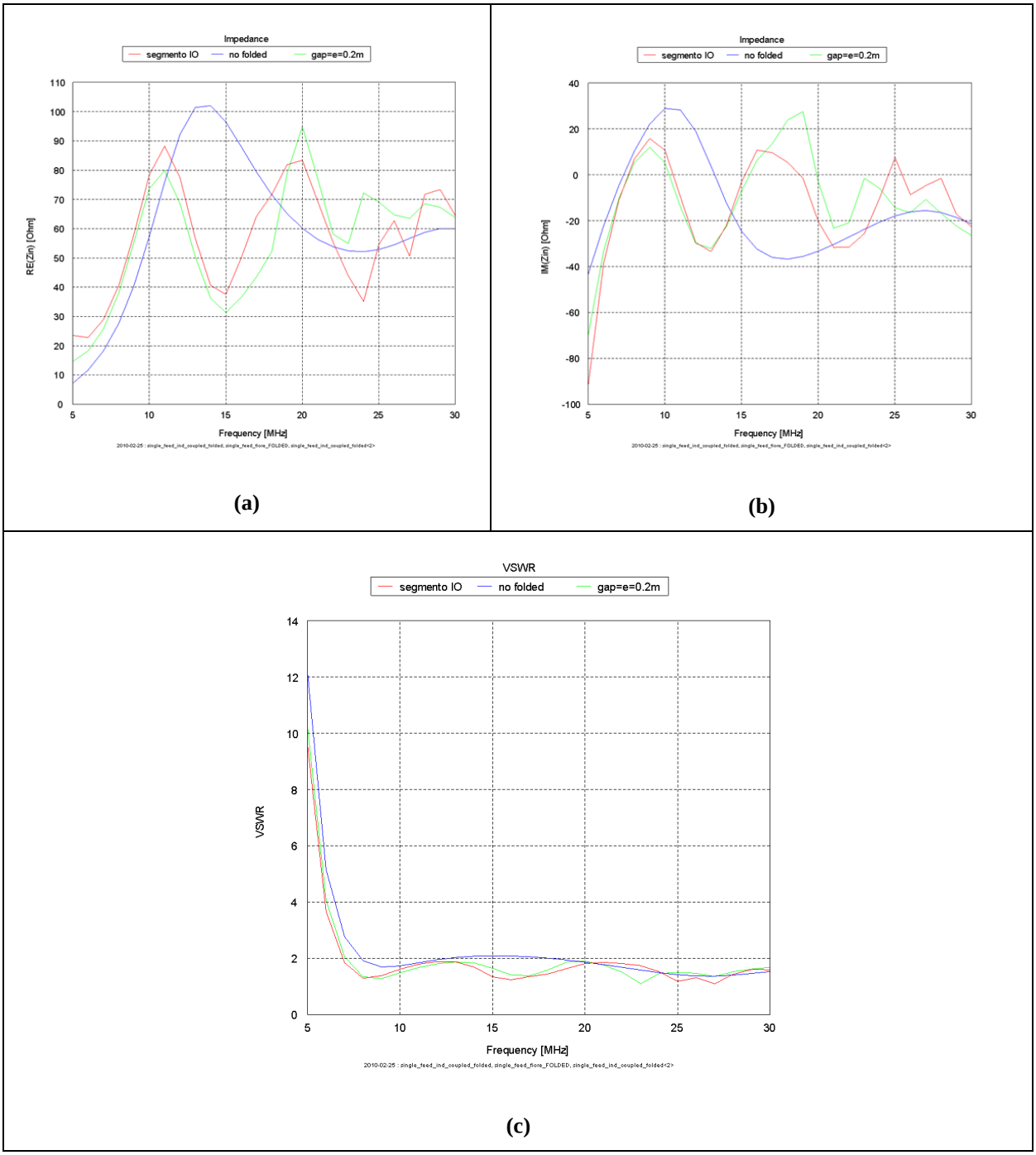

Figure 2.21 – Antenna with folded coupled pin and a further segment parallel to *i*: (a) RE(Zin) according to the frequency; (b) IM(Zin) according to the frequency; (c) VSWR according to the frequency.

Finally, the best performances in terms of matching for our purposes have been obtained with the last solution, which takes into account the combination of a simple folded pin, together with a path coupling the antenna with a very small gap and finally, having a further vertical path.

In the last results we didn't show the performances of the new solution of the antenna in terms of radiation pattern. They are very important, especially in radar application, in which specifics radiation patterns on the principal planes have to be realized. They are showed in the following paragraph.

2.4.3 Antenna with folded coupled optimized pin: radiation pattern

The antenna with different type of the folded pin presents a very good matching, and the target of a very good matching at lower frequencies was obtained. Together with the matching analysis, the radiation pattern of the antenna has been observed according to the frequency, and on the principal planes: E plane at phi=0° and E plane at phi=90°, which coincide with the *xz* plane and the *yz* plane respectively and H plane, which coincides with the *xy* plane.

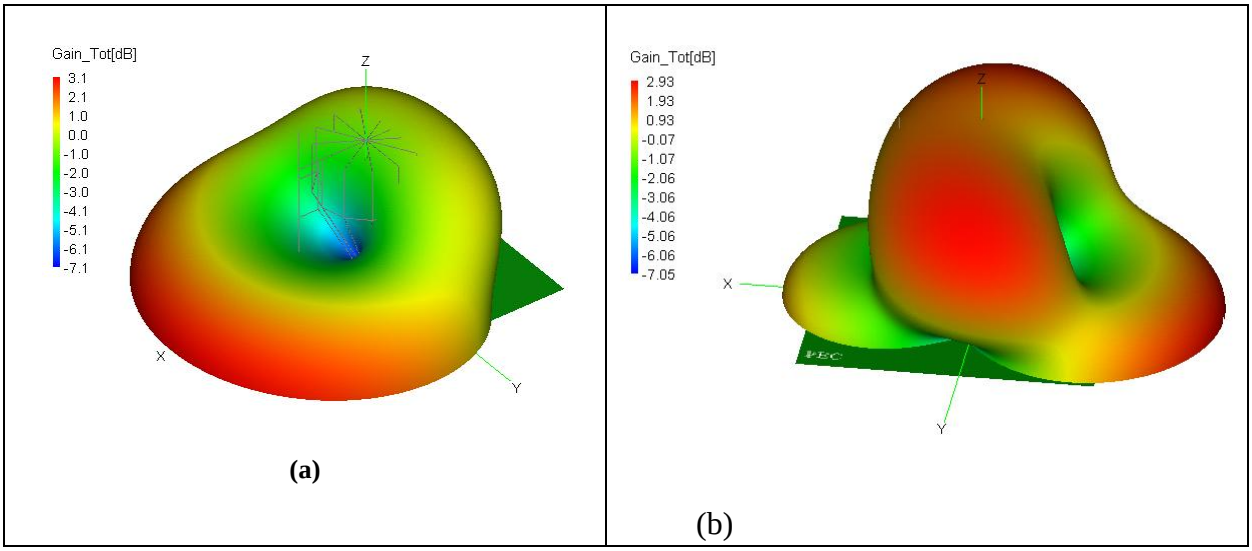

Figure 2.22 – Antenna with folded coupled optimized pin tri-dimensional radiation pattern: (a) 14MHz; (b) 17MHz.

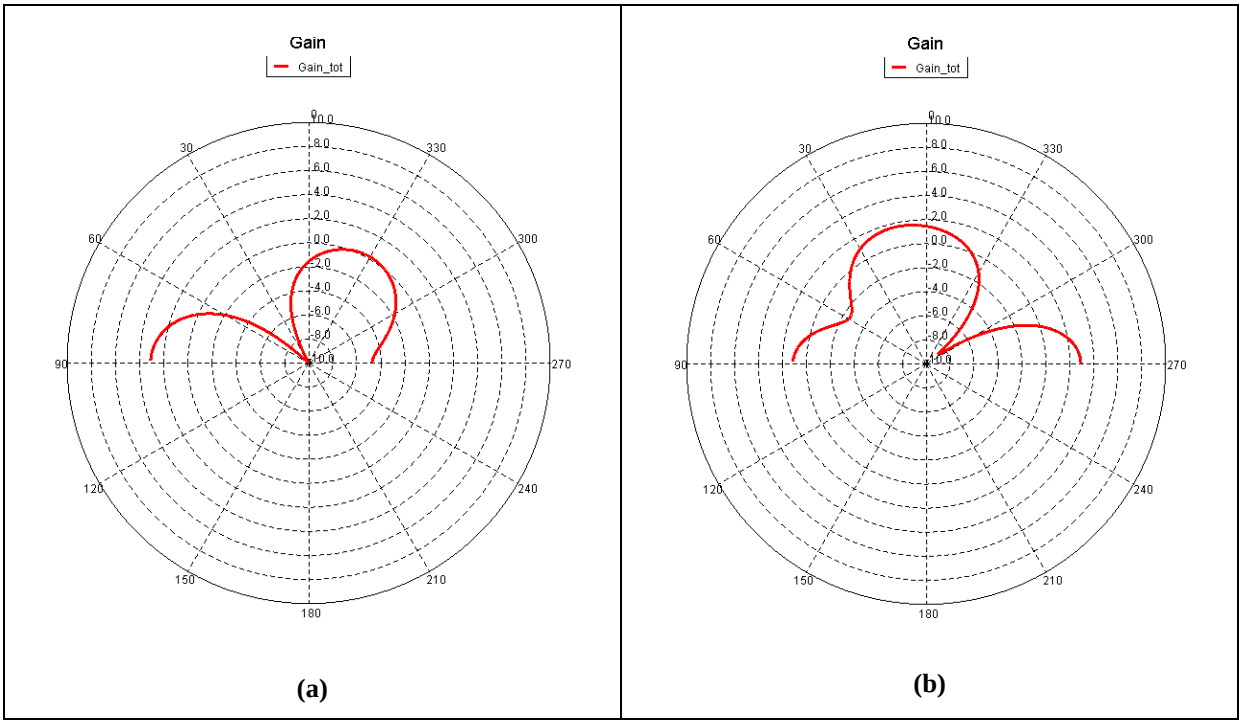

(a) **(b)**

Figure 2.23 – Antenna with folded coupled optimized pin radiation pattern, phi=0°: (a) 14MHz; (b) 17MHz.

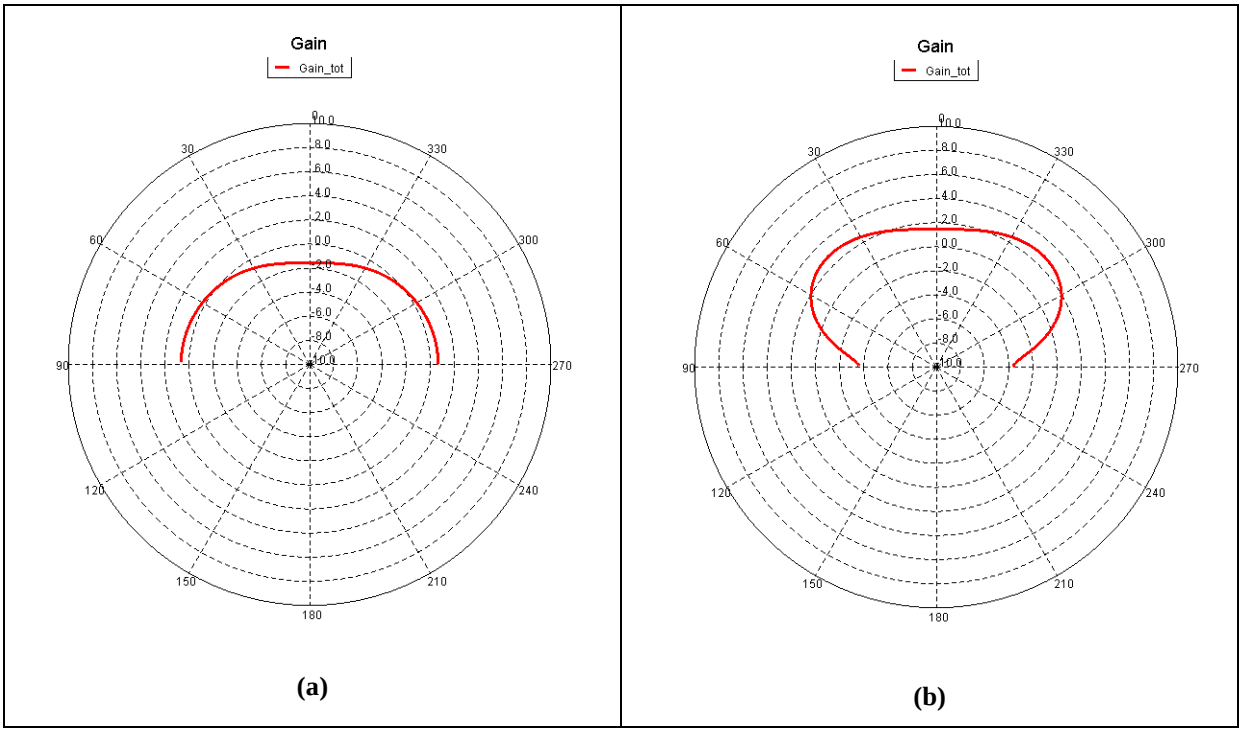

(a) **(b)**

Figure 2.24 – Antenna with folded coupled optimized pin radiation pattern, phi=90°: (a) 14MHz; (b) 17MHz.

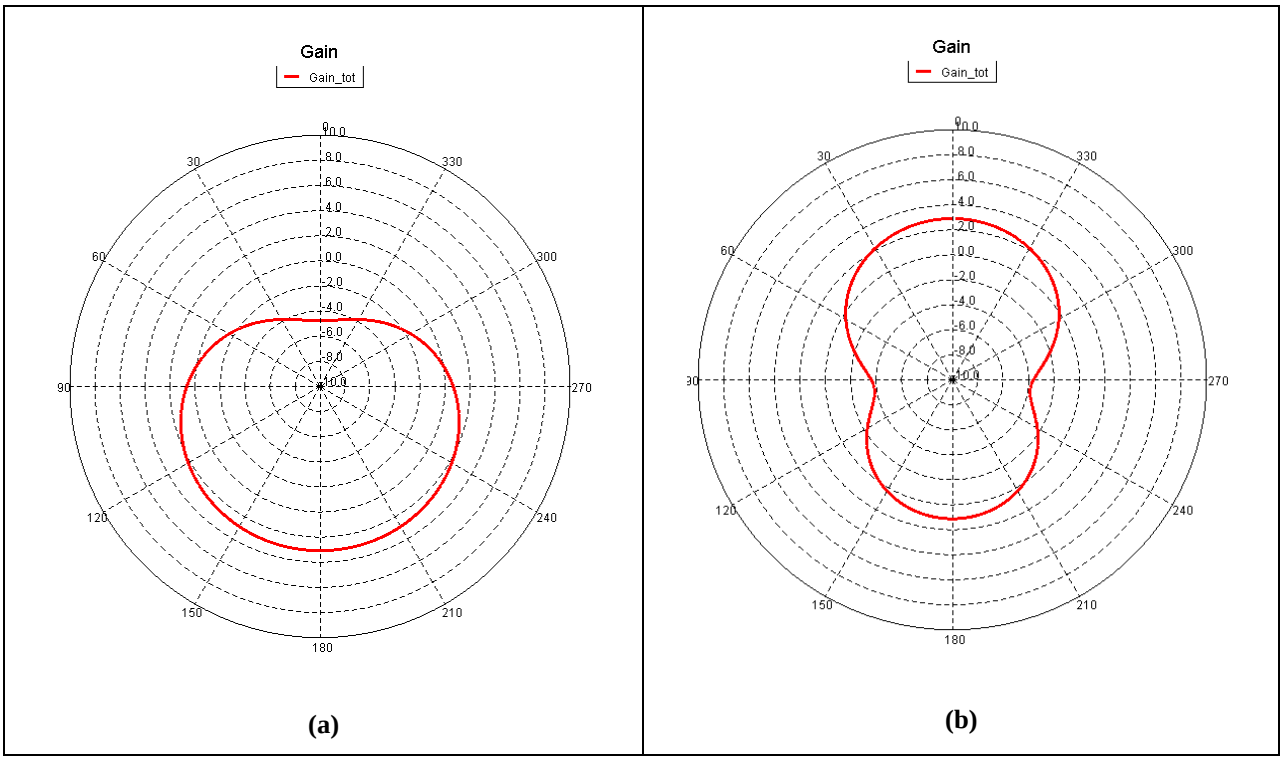

(a) **(b)**

Figure 2.25 – Antenna with folded coupled optimized pin radiation pattern, H plane: (a) 14MHz; (b) 17MHz.

The radiation pattern on the H plane was no more omni-directional and no more symmetrical on the E plane, especially for some frequencies, as it can be seen in Figure 2.25. In some cases, it presented many differences between two closed frequencies.

In Figure 2.23 to Figure 2.25 the radiation patterns at 14MHz and 17MHz are shown respectively. The radiation pattern of the antenna at these latter frequencies in fact, differs so much.

The target on the radiation characteristics of the antenna was lost with the use of a single folded pin because the antenna is no more electrically small. We needed to reduce its size in order to maintain the symmetry of the radiation pattern on the E plane, and the omni-directional behaviour on the H plane.

2.4.4 Antenna with folded coupled optimized pin: miniaturization

The antenna with the folded coupled optimized pin has been miniaturized in two different ways. First, we applied a factor equal to 0.5 to all the original sizes of the antenna,

and then we reduced the size in order to reach all the sizes contained on a sphere having the radius compliant with the Wheeler limit [6] at the central frequency of the band. For the latter reason we chose a radius equal to 3x3x3 m^3. Actually, according to the Wheeler limit, the antenna should be contained in the sphere having radius equal to *1/k*. In our case the segment *c* is not exactly contained in that radius, nevertheless we decided to use it because it is a key point for the antenna matching.

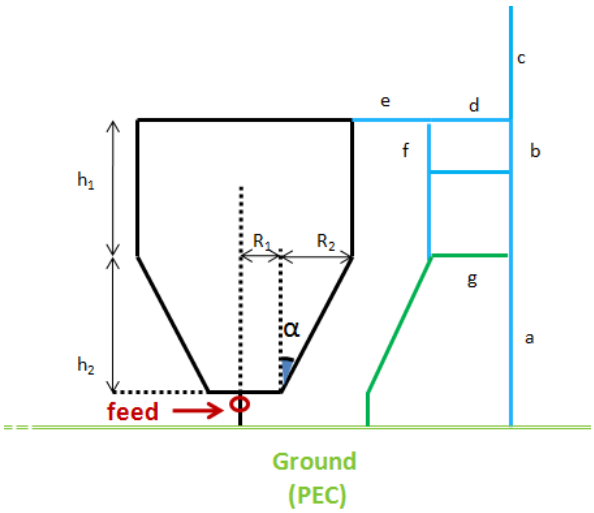

Figure 2.26 – Antenna miniaturized design.

Table 2.1 – Size description of the miniaturized antennas.

	Feed, p [m]	h_1 [m]	h_2 [m]	R_1 [m]	R_2 [m]	a [m]	b,f [m]	c [m]	d,g [m]	e, gap [m]	n [m]
Original	0.1	2.5	3.9	0.23	2.07	4	2.5	2	1	0.2	4.41
Miniaturized (Factor 0.5)	0.1	1.25	1.95	0.115	1.035	2.05	1.25	1	0.5	0.1	2.21
Miniaturized (3x3x3)	0.1	1.9	1	0.1	1.4	2.1	1	1	0.5	0.1	2.44

Table 2.2 – Size comparison between the original and the miniaturized version of the antenna.

	Height [m]	Width [m]
Original	6.5	4.6
Miniaturized (Factor 0.5)	3.3	2.3
Miniaturized (3x3x3)	3	3

In the following Figure 2.27, we showed the results obtained with the size reduction, and we compared the results between the original antenna, the antenna with the folded coupled pin and finally the two versions of the miniaturized antenna.

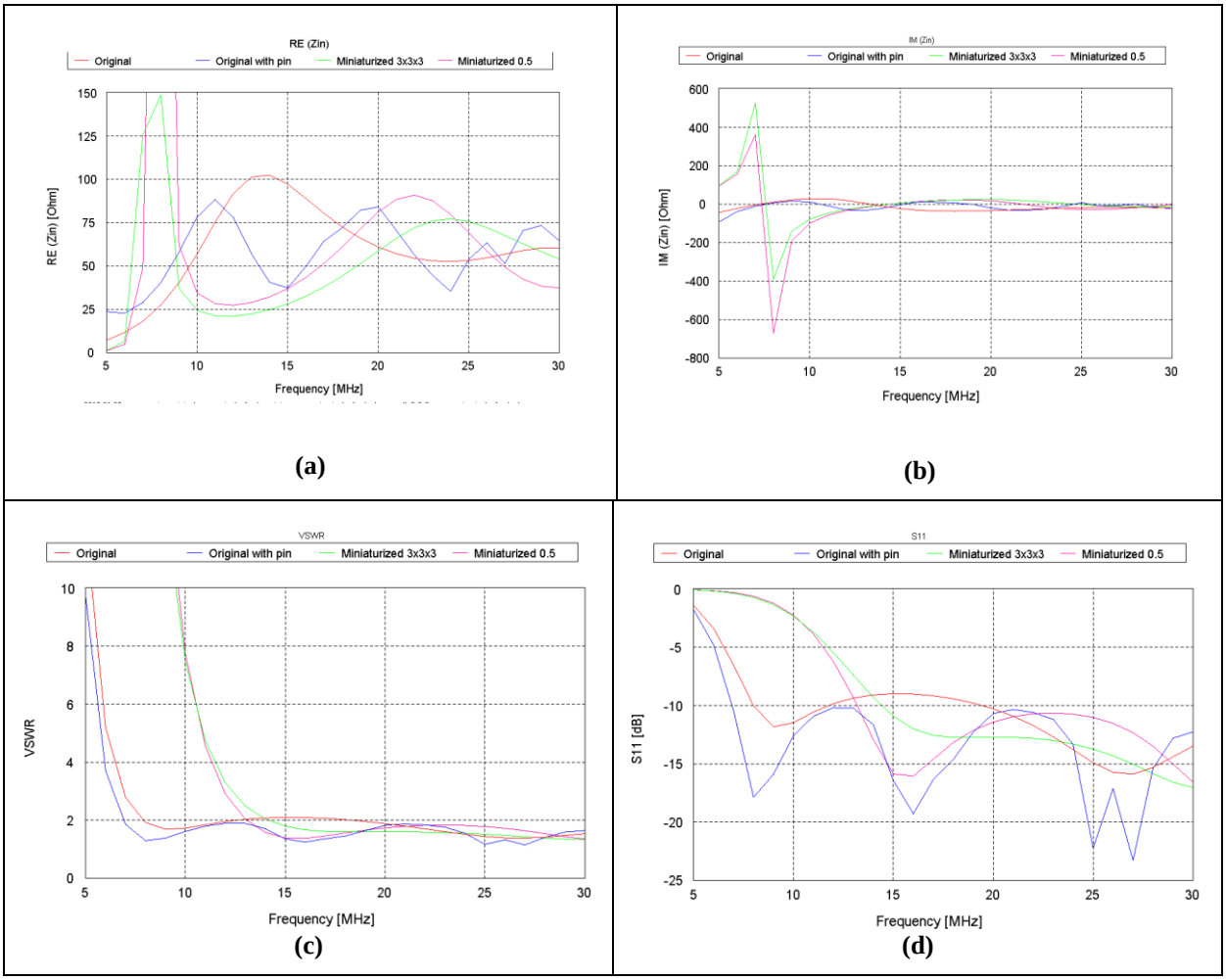

Figure 2.27 – Antenna and its miniaturization versions comparison: (a) RE(Zin) according to the frequency; (b) IM(Zin) according to the frequency; (c) VSWR according to the frequency; (d) S11 in dB according to the frequency.

In terms of matching, by observing the S11 in dB, the miniaturized antenna with a factor equal to 0.5 had very good performance for frequencies in the range 13-21.07MHz. At lower frequencies it is mismatched and at higher frequencies it presents a worst matching than the original antenna. The miniaturized antenna with the use of the Wheeler limit had good performances up to 13.86MHz and the matching is always better than the original one; however it is mismatched at lower frequencies. In both cases, the mismatching is due to the

fact that the size of the antennas at lower frequencies is very small compared to the wavelength, and it behaves like an ideal dipole (e.g. at 5MHz its size is around 0.05λ) [16]. The same behaviour can be noticed by observing the real impedance at these frequencies, which is very low (few Ohms) compared to the values obtained at other frequencies. For the latter reasons the proposed antennas could only be used for our purposes in the higher part of the HF band.

It can be notice that by using a miniaturized version of the antenna with the pin, we reached again the symmetry on the radiation pattern on the E plane q.e.d. (Figure 2.29- Figure 2.30). The radiation pattern is again omni-directional on the H plane (Figure 2.31); however a decrease of the maximum gain of the antenna is inevitable, because the antenna has got smaller size than the original one.

The shape of the radiation pattern according to the frequency is almost the same.

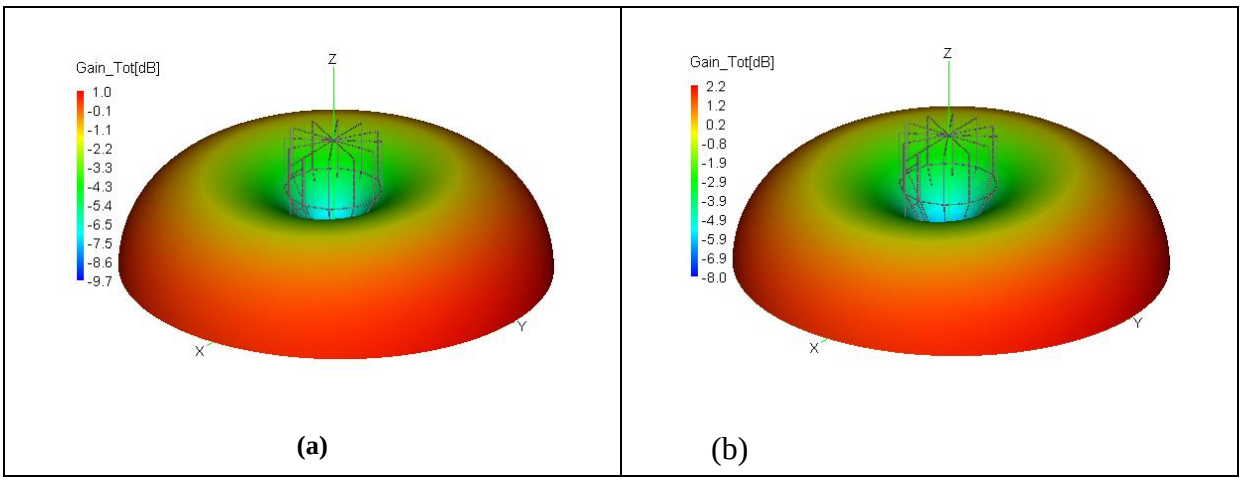

Figure 2.28 – Antenna with folded coupled optimized pin miniaturized (0.5 factor) tri-dimensional radiation pattern: (a) 14MHz; (b) 17MHz.

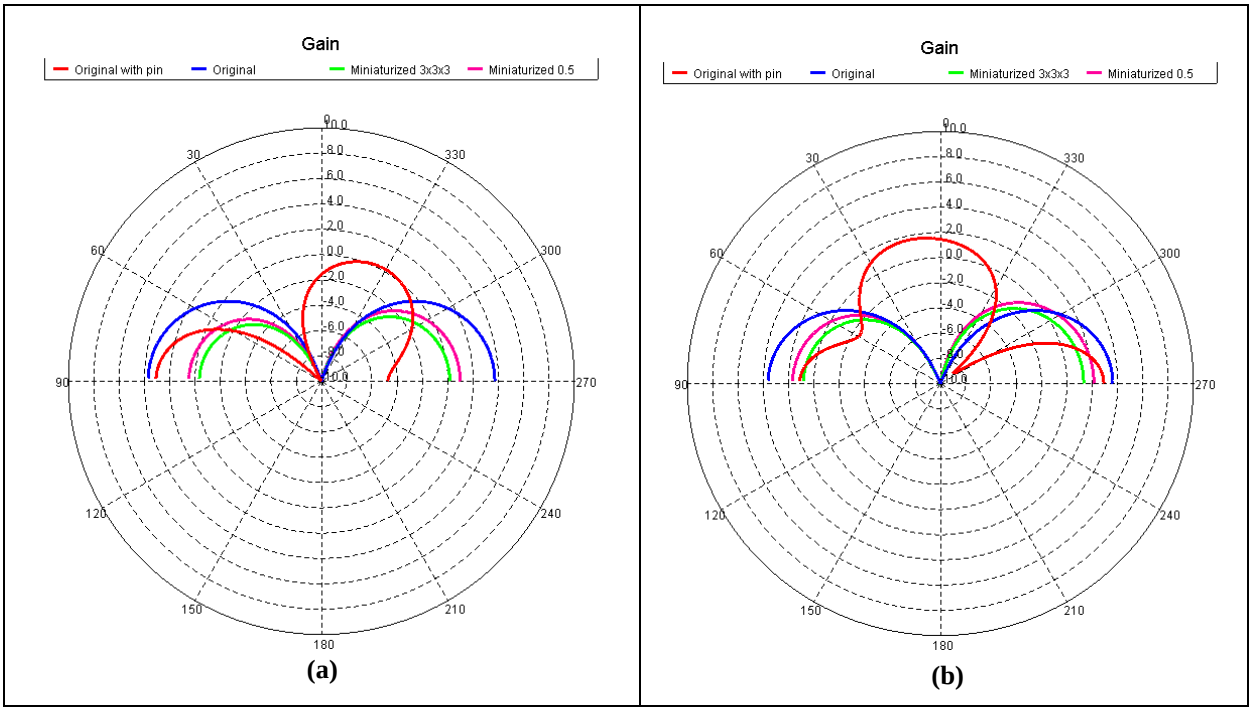

Figure 2.29 – Antenna with folded coupled optimized pin radiation pattern, phi=0°: (a) 14MHz; (b) 17MHz.

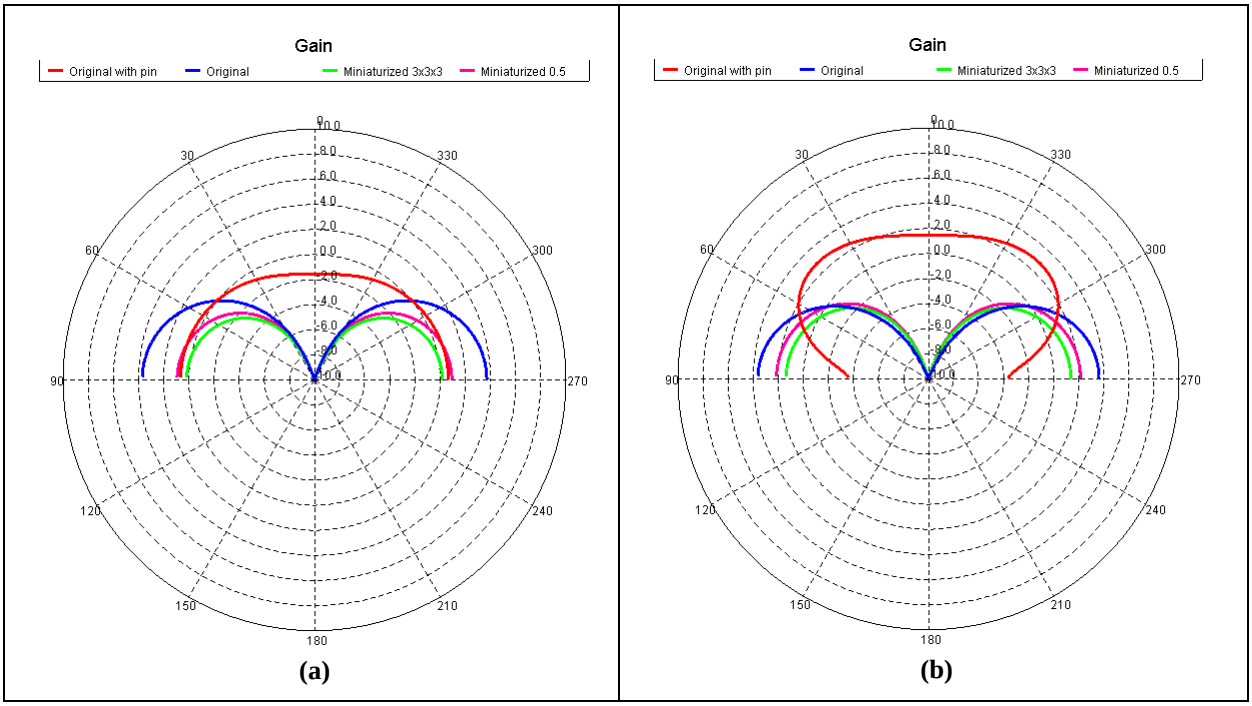

Figure 2.30 – Antenna with folded coupled optimized pin radiation pattern, phi=90°: (a) 14MHz; (b) 17MHz.

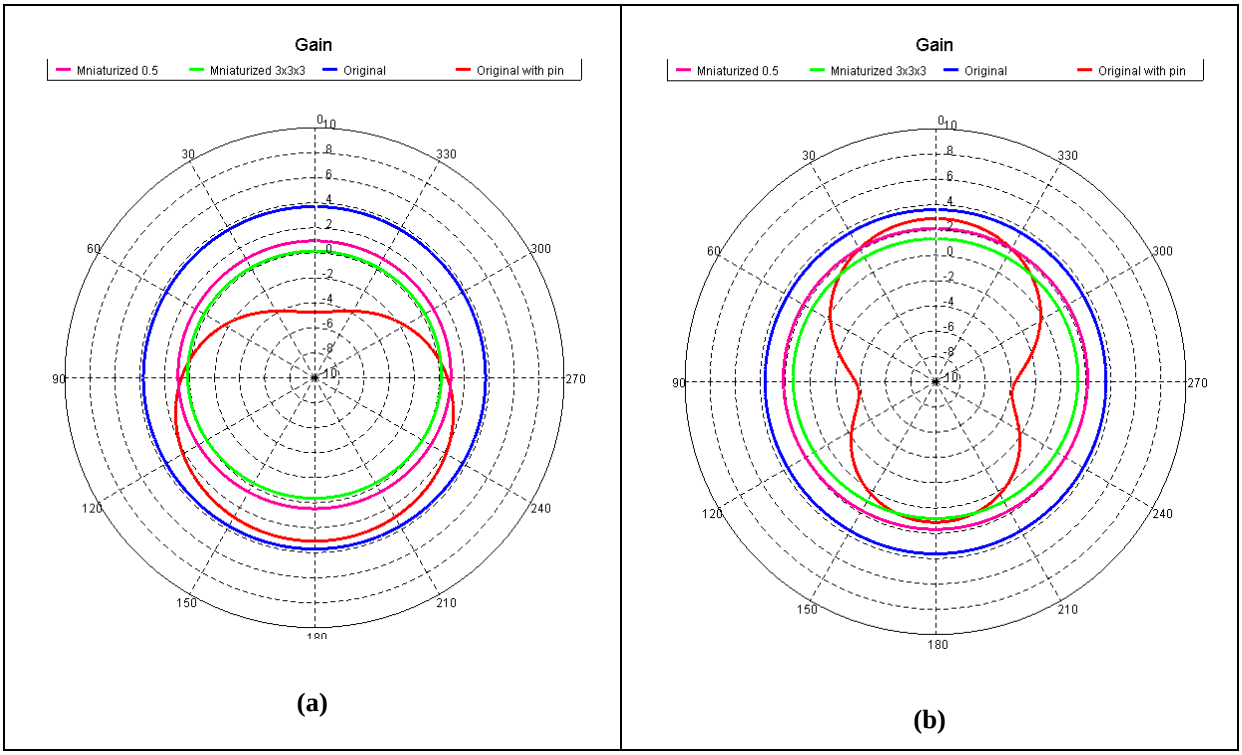

Figure 2.31 – Antenna with folded coupled optimized pin radiation pattern, H plane: (a) 14MHz; (b) 17MHz.

In Table 2.3 we compared the maximum gain of the original antenna, with the maximum gain obtained with the two miniaturized versions. With the reduction of the size of the antenna, we reached again the performances on the shape of the radiation pattern, but we lose in terms of the gain, especially if we consider the $3x3x3m^3$ version of the antenna.

Table 2.3 – Gain comparison between the original and the miniaturized versions of the antenna.

	Maximum gain @ 14MHz [dB]	**Maximum gain @ 17MHz [dB]**
Original	3.72	3.63
Miniaturized (Factor 0.5)	1.0	2.2
Miniaturized (3x3x3)	0.23	1.43

We can conclude that both the miniaturized antennas don't cover the whole frequency range in the HF band, but just the higher frequencies. For our purpose, the last solution obtained is far from the specifics of OTH radar.

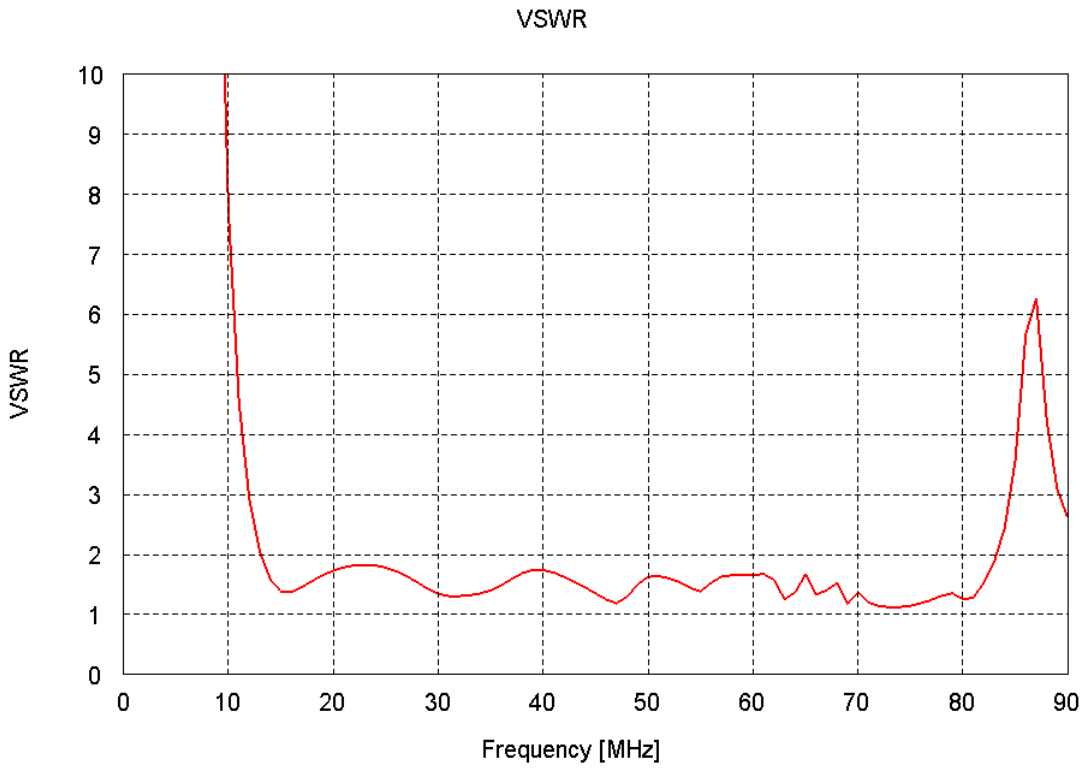

Figure 2.32 – VSWR of the 0.5 factor miniaturized antenna according to the frequency.

However, it should be noted that the two miniaturized antennas are capable of operating over a very wideband in the range 13-90MHz (Figure 2.32), and then they can be proposed for VHF applications.

For phased array radar application, we have to use another kind of solution, like e.g. some matching networks, which can realize very good matching at single frequencies (narrowband matching) or on a wide range of frequencies (wide band matching network). The theory and performances of different matching networks have been widely investigated in the following chapter.

3 IMPEDANCE MATCHING NETWORKS

In the previous chapters, we showed how the mutual coupling is strong at lower frequencies of HF band. For OTH radar array purposes, the lower frequencies are important because they allow covering high distances in space with respect to the radar site.

Several stand alone antenna configurations have been investigated. The stand alone original antenna doesn't allow reaching very good performances at lower frequencies, where the mutual coupling is strongest. So, other configurations, with inductive pins causing the capacitance compensation have been studied. However, a miniaturization is required, in order to maintain the performances of the antenna in terms of radiation pattern. The miniaturized version realizes a translation of the operating bandwidth of the antenna. In order to compensate the capacitive behaviour of the antenna, the use of impedance matching network is inevitable.

Further, as mentioned in §2.3, the stand alone antenna has to realize a VSWR as small as possible. All the presented radiating elements respect the constraint on the VSWR<3, which corresponds to a S11<-6dB. The last constraints for the phased radar array are not good enough, because the mutual couplings.

For these reasons, we rearranged the specifics on the stand alone antenna matching, making them stricter. The stand alone antenna has to be realize an S11<-17dB in the range 8-21MHz, where the mutual couplings are stronger; a S11<-6dB are enough for higher frequencies (21-30MHz), where the mutual coupling is less strong.

In order to reach those performances, the antenna used with the matching networks is 0.5m higher than the antenna presented in previous chapters and it consists of 18 arms and the radius of the wires is equal to 0.020m. This antenna configuration presents better impedance matching performance than the previous one, especially in the centre of the HF band.

The Figure 3.1 shows the active VSWR of the new antenna in the circular phased array of 50 elements at 12MHz, according to the pointing direction of the beam.

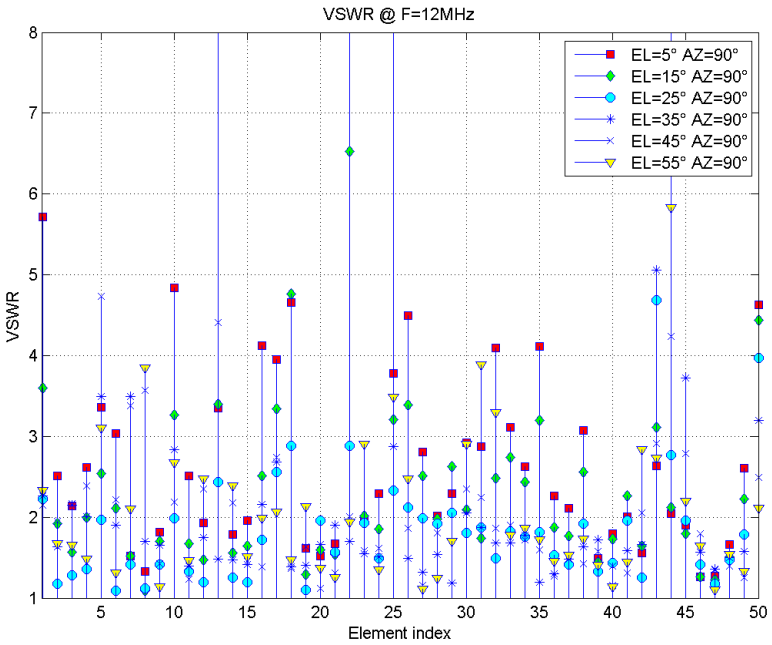

Figure 3.1 – Active VSWR of the circular phased array at 12MHz.

A narrowband matching network has been designed for the stand alone antenna and then it has been used for each element (Figure 3.2) of the circular array reported in Chapter 2.

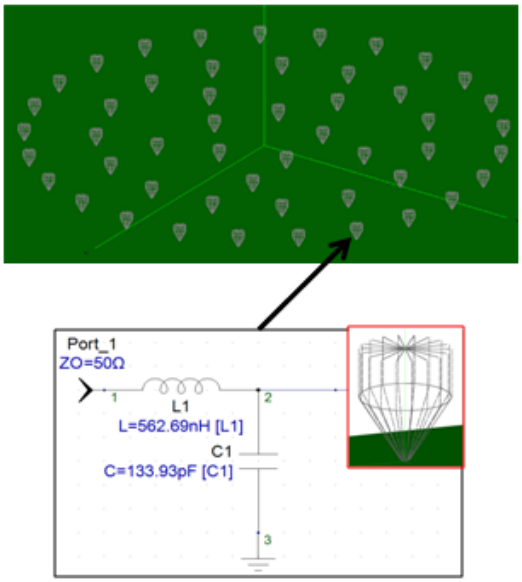

Figure 3.2 – Narrowband matching network of each radiating element of the circular phased array.

The vantage of the use of a very well-matched antenna in the array is showed in Figure 3.3: it can be notice that the mutual coupling is less strong.

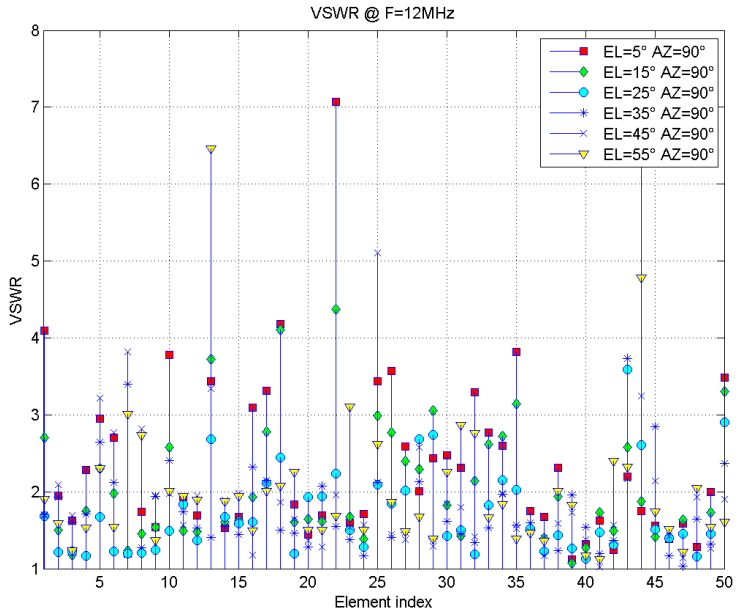

Figure 3.3 – Active VSWR of the circular phased array at 12MHz: each element matched with a narrowband matching network.

Because the interest is to reduce the mutual coupling also according to the frequency, let assume that the number of frequencies of interest are equal to M and the number of the elements of the phased array are N, with A and φ the amplitude and the phase of the sources respectively.

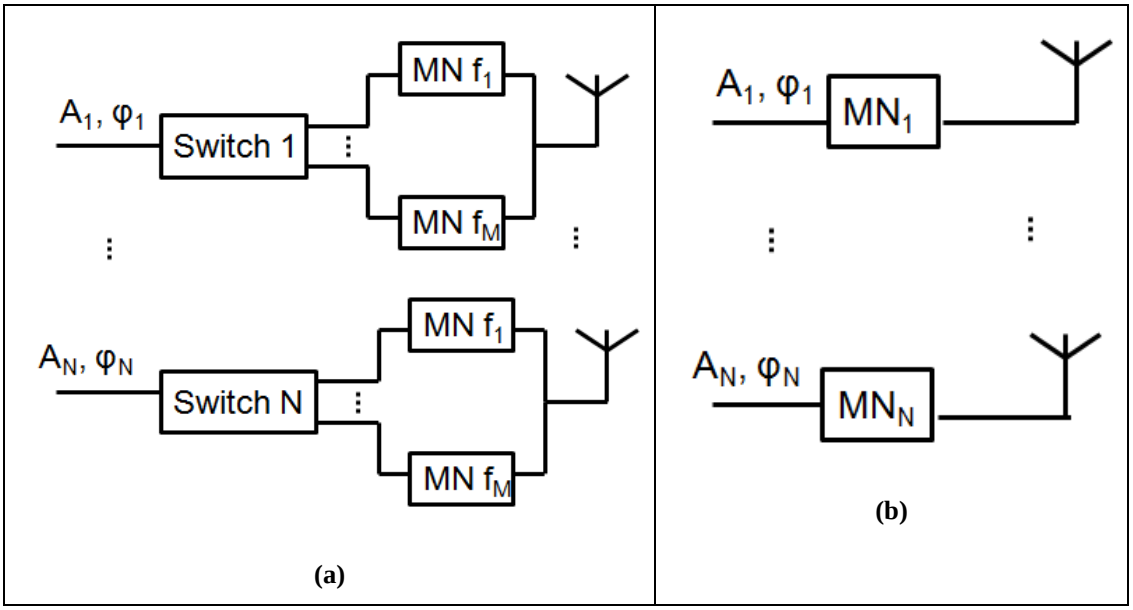

Figure 3.4 – Matching networks in the phased array: (a) use of MxN narrowband networks; (b) use of M wide-band matching networks.

Thus, two possible approaches of the use of matching networks have been thought and investigated:

1. the use of MxN narrowband matching networks (Figure 3.4 (a)),
2. the use of N wideband matching networks (Figure 3.4 (b)).

The first approach can be useful in the case in which the transmission of the radar signal is made with a discrete occupation of the frequencies in the range 8-30MHz.

The second approach can be fit with the need of a continuous occupation of the frequencies in the range 8-30MHz.

At the beginning, according to literature a several number of matching networks topologies have been designed. After that, we provide a new methodology in order to obtain good compromise in terms of bandwidth, combining the analytical design with optimization algorithms.

3.1 Narrowband impedance matching networks

The performance of an impedance matching network depends on the factor of quality Q, inversely proportional to the operating bandwidth. A network designed with a high Q factor is a narrowband network; otherwise small Q values imply wideband networks. Different topologies are used in literature in order to realize the matching, and they depend on the number of the lumped element used. For the purposes of this work, we avoid to use resistances in the matching network, in order to maximize the efficiency of the antenna, reducing the losses. An L topology matching network allows obtaining a good matching at a specified frequency with just two elements, like the combination of a capacitance and an inductance. Instead, the T and π topologies allow obtaining the matching with three lumped elements, as a combination of capacitance and inductance as well.

3.1.1 L topology matching network

With L topology matching network is possible to reach the matching with the maximum factor Q achievable with a matching network. However, because the Q factor depends on the impedance of the load and the impedance of the source, it is fixed and it cannot be modified.

For the design of an L network, in literature there is a specific criterion, just by knowing the impedance of the load R_L, the impedance of the source R_s and the frequency [24].

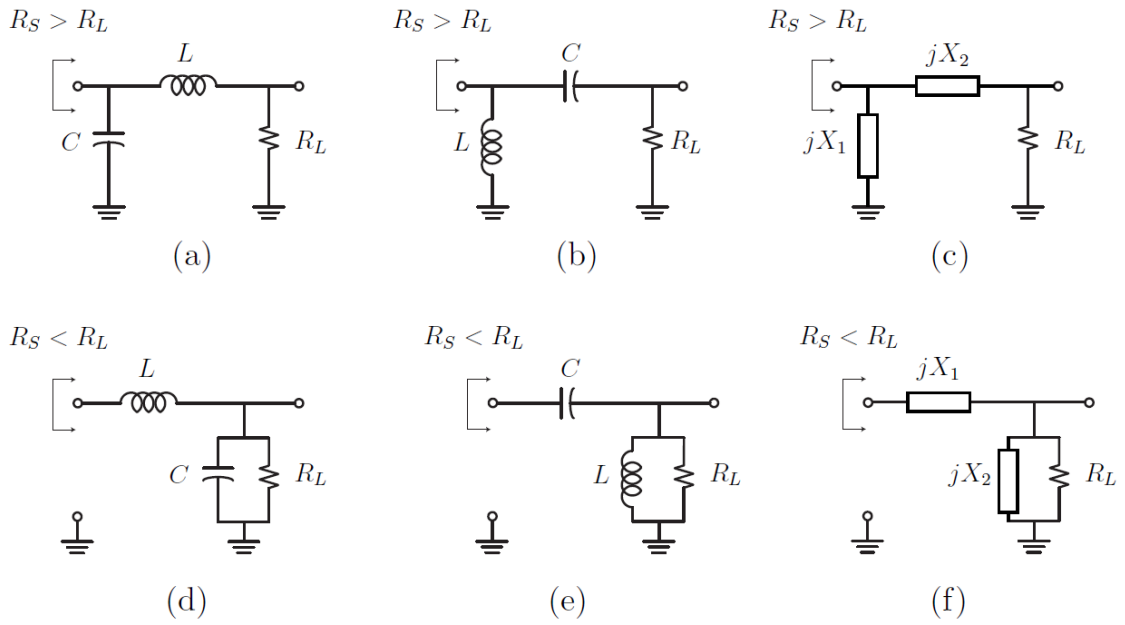

Figure 3.5 – Several combinations of *L*-matching networks. In (a)–(c) the load is connected in series with the reactance boosting the input resistance. In (d)–(f) the load is in shunt with the reactance, lowering the input resistance.

Let $R_{\max} = \max(R_S, R_L)$ and $R_{\min} = \min(R_S, R_L)$, the L-networks shown in Figure 3.5 are designed as follows:

1. Calculate the factor $m = R_{\max}/R_{\min}$.
2. Compute the required circuit $Q = \sqrt{m-1}$.
3. Choose the topologies from Figure 3.5(a)-(c) if you are boosting the resistance, i.e. R_S>R_L, then $X_s = Q \cdot R_L$. If you are dropping the resistance, i.e. R_S<R_L, choose (d)-(f), then $X_p = R_L/Q$.
4. Compute the effective resonating reactance. If R_S>R_L, calculate $X_s^{'} = X_s(1+Q^{-2})$ and set the shunt reactance in order to resonate, $X_p = -X_s^{'}$. If R_S<R_L, then calculate $X_p^{'} = X_p/(1+Q^{-2})$ and set the series reactance in order to resonate, $X_s = -X_p^{'}$.
5. For a given frequency of operation, pick the value of L and C to satisfy these equations as follows: $L = X/\omega$ and $C = 1/\omega X$.

Actually, in the most of the cases the impedance of the load has a reactance part, e.g. $R_L \pm jX_L$, which has to be compensated, in order to reach the matching. This behaviour is found when different kind of loads are used, e.g. antennas, mixer, transmission lines, etc.

There are two basic approaches in handling complex impedances [23]:

1. Absorption: To actually absorb any stray reactance into the impedance-matching network itself. This can be done through prudent placement of each matching element such that element capacitors are placed in parallel with stray capacitances, and element inductors are placed in series with any stray inductances. The *stray* component values are then subtracted from the *calculated* element values, leaving new element values (*C'*, *L'*), which are smaller than the calculated element values.
2. Resonance: To make resonant any stray reactance with an equal and opposite reactance at the frequency of interest (Figure 3.6).

For our purposes we will use the resonance approach.

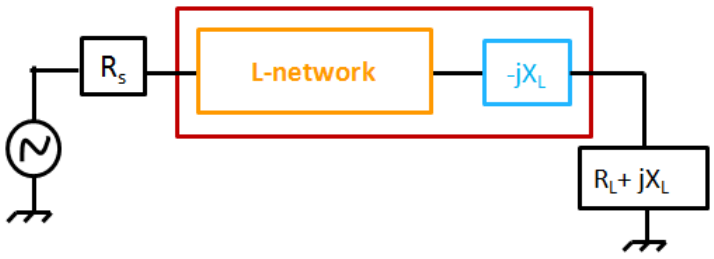

Figure 3.6 – L-network: Resonance approach.

Most of the cases, during the design of an impedance matching network, both the techniques are used. However, if the *stray* element values are larger than the calculated element values, absorption cannot take place. In a situation such as this, when absorption is not possible, the concept of resonance coupled with absorption will often do the trick. The two methods presented are valid also for T or π matching networks design.

Sometime it is easier to implement some known formulas, present in literature, which take into account the complex load characteristic. There are eight combinations of L and C (shown in Figure 3.7) in order to cover all complex loads on the Smith chart [20].

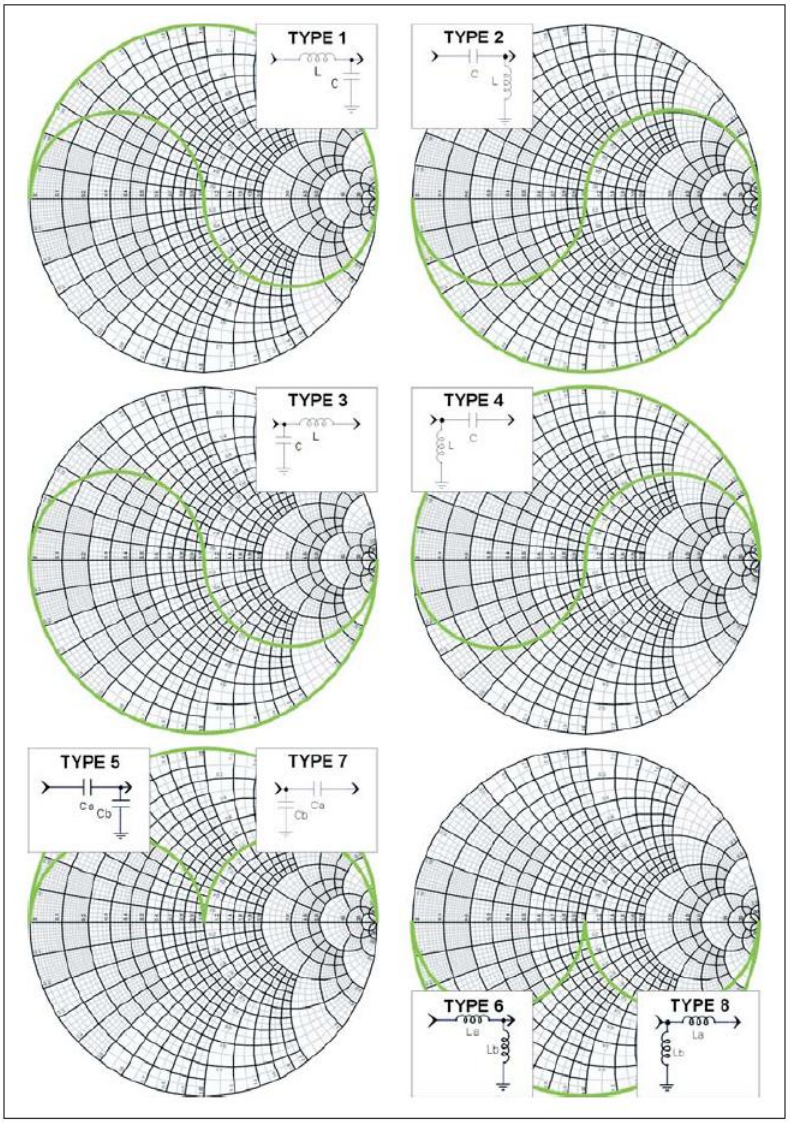

Figure 3.7 –Yin-Yang regions on the Smith chart for L-matching networks design.

Each green zone describes a region of impedances on the Smith chart (Yin-Yang region) which can be matched with the correspondent LC-network combination.

Let $Z_L = R_L + jX_L$, the load impedance, and R_s, the source impedance, it can be possible to choose one of the eight combinations (Figure 3.7) which perfectly match the load to the source and to calculate the values of each components with the formulas described in Appendix A.

3.1.2 T and π topologies matching networks

With T and π topologies matching network is possible to reach a narrowband matching because the Q factor depends on the virtual resistance, on the source and the impedance of the load, so it is controllable.

The π topologies matching network are designed with three lumped elements, shaped as a pi-greco. They can best be described as two "front-to-front" L networks that are both configured to match the load and the source to an invisible or "virtual" resistance located at the junction between the two networks, as shown in Figure 3.8.

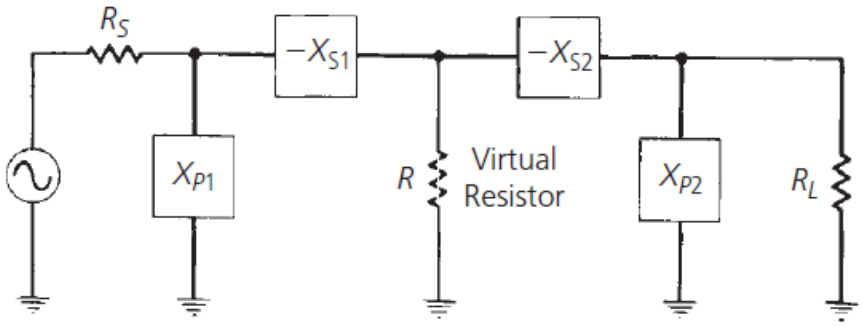

Figure 3.8 – π - network designed as two *front-to-front* L topologies.

The significance of the negative signs for −Xs1 and −Xs2 is symbolic. They are used merely to indicate that the Xs values are the opposite type of reactance from Xp1 and Xp2, respectively. Thus, if Xp1 is a capacitor, Xs1 must be an inductor, and vice versa. Similarly, if Xp2 is an inductor, Xs2 must be a capacitor, and vice versa. They do not indicate negative reactances (capacitors).

The virtual resistance (R) must be smaller than either *Rs* or *RL* because it is connected to the series arm of each L section but, otherwise, it can be any value you wish. Most of the time, however, R is defined by the desired loaded *Q* of the circuit that you specify at the beginning of the design process. For our purposes, the loaded *Q* of this network will be defined as:

$$Q = \sqrt{\frac{R_{\max}}{R} - 1} \tag{3.1}$$

where $R_{\max} = \max(R_S, R_L)$. Although this is not entirely accurate, it is a widely accepted Q-determining formula for this circuit, and is certainly close enough for most practical work.

Proceeding from the load to the source, further it is necessary to define Q_L e Q_S, which are the quality factor of the first L-network and the second L-network respectively. They are defined as follows:

$$Q_L = \sqrt{\frac{R_L}{R} - 1}$$
$$Q_S = \sqrt{\frac{R_S}{R} - 1} \tag{3.2}$$

Assuming a total quality factor equal to Q and described as in (3.3), from (3.3) it can be possible to get the virtual resistance R from the inverse formulation, as follows:

$$R = \frac{R_{\max}}{Q^2 + 1} \tag{3.3}$$

Finally, the reactances of the π-network are described as:

$$X_{p1} = \frac{R_S}{Q_S},\ X_{s1} = RQ_S,\ X_{s2} = RQ_L,\ X_{p2} = \frac{R_L}{Q_L} \tag{3.4}$$

In the design of a π-network, it must be defined the subsequent quantities:

$$Q_{\min} = \sqrt{\frac{R_{\max}}{R_{\min}} - 1}\ ,\ R_{\min} = \min(R_S, R_L) \tag{3.5}$$

In order to verify these conditions [22]:

$$Q > Q_{\min} \Leftrightarrow R < R_{\min} \tag{3.6}$$

So, the Q factor of a π-network is always maximum than Q_{min}, i.e. the minimum Q factor, just realizable with a single L matching network.

The T topologies matching network are designed with three lumped elements, shaped as a "T" (Figure 3.9). They can best be described as two "back-to-back" L networks. The load and the source are matched through these two L-type networks, to a virtual resistance that is *larger* than either the load or source resistance.

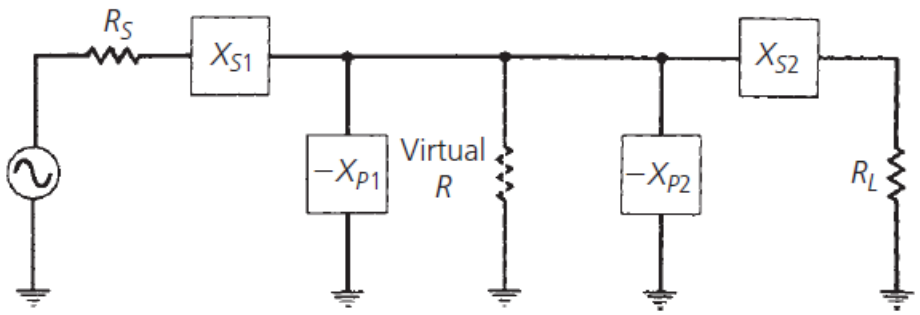

Figure 3.9 – T-network designed as two *back-to-back* L-topologies.

The loaded *Q* of the T network is determined by the L section that has the highest *Q*.

By definition, the L section with the highest *Q* will occur on the end with the *smallest* terminating resistor. Remember, too, that each terminating resistor is in the *series* leg of each network. Therefore, the formula for determining the loaded *Q* of the T network is:

$$Q = \sqrt{\frac{R}{R_{\min}} - 1} \tag{3.7}$$

where $R_{\min} = \min(R_S, R_L)$.

Proceeding from the load to the source, further it is necessary to define Q_L e Q_S, which are the quality factor of the first L-network and the second L-network respectively. They are defined as follows:

$$\begin{aligned} Q_L &= \sqrt{\frac{R}{R_L} - 1} \\ Q_S &= \sqrt{\frac{R}{R_S} - 1} \end{aligned} \tag{3.8}$$

Assuming a total quality factor equal to Q and as described in (3.9), from (3.9) it can be possible to get the virtual resistance R from the inverse formulation, as follows:

$$R = R_{\min}(Q^2 + 1) \tag{3.9}$$

Finally, the reactances of the π-network are described as:

$$X_{s1} = R_S Q_S, \;\; X_{p1} = \frac{R}{Q_S}, \;\; X_{p2} = \frac{R}{Q_L}, \;\; X_{s2} = R_L Q_L \tag{3.10}$$

Actually, the impedances of the load are never real, for this reason, the absorption and resonance methods can be applied in order to compensate the reactance of the load, as described in chapter 3.3.

3.1.3 Narrowband antenna matching with L, T and π networks

In order to understand the behaviour of each topologies of narrowband matching network, the proposed antenna has been matched at a specific frequency, by comparing the three topologies presented.

In the project of the matching network, the central frequency 17MHz of the entire bandwidth has been considered. By applying the formulations described before, the comparison has been showed in Figure 3.14. For the design of the L-network, we had to consider the impedance of the antenna on the Smith chart, in order to choose the best type, as shown Figure 3.7. At 17MHz the impedance of the antenna fall inside the regions of the type 1 and type 2 L-networks. In these two cases we calculated the lumped elements values, for both the networks and we plotted the results in terms of S11dB in Figure 3.12 - Figure 3.13.

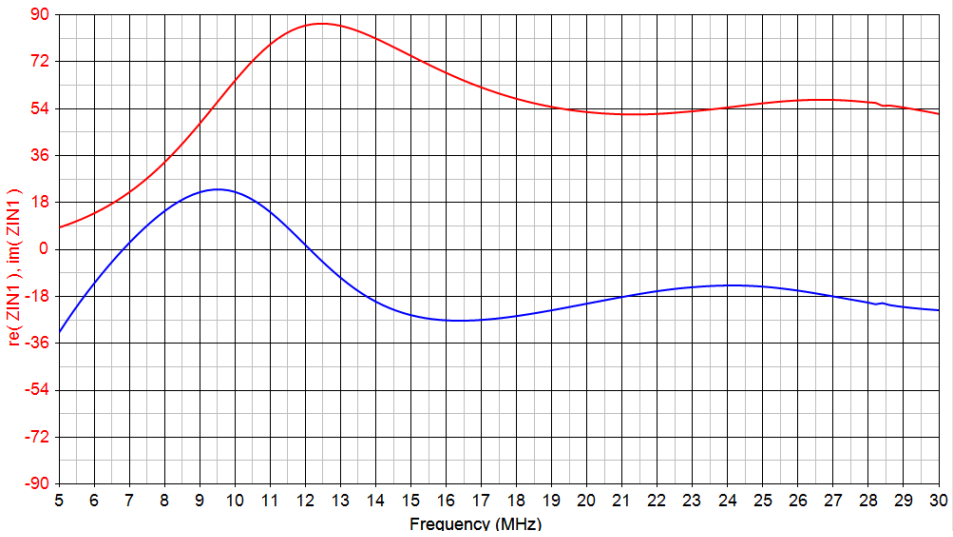

Figure 3.10 – Real and imaginary part of the impedance of the antenna.

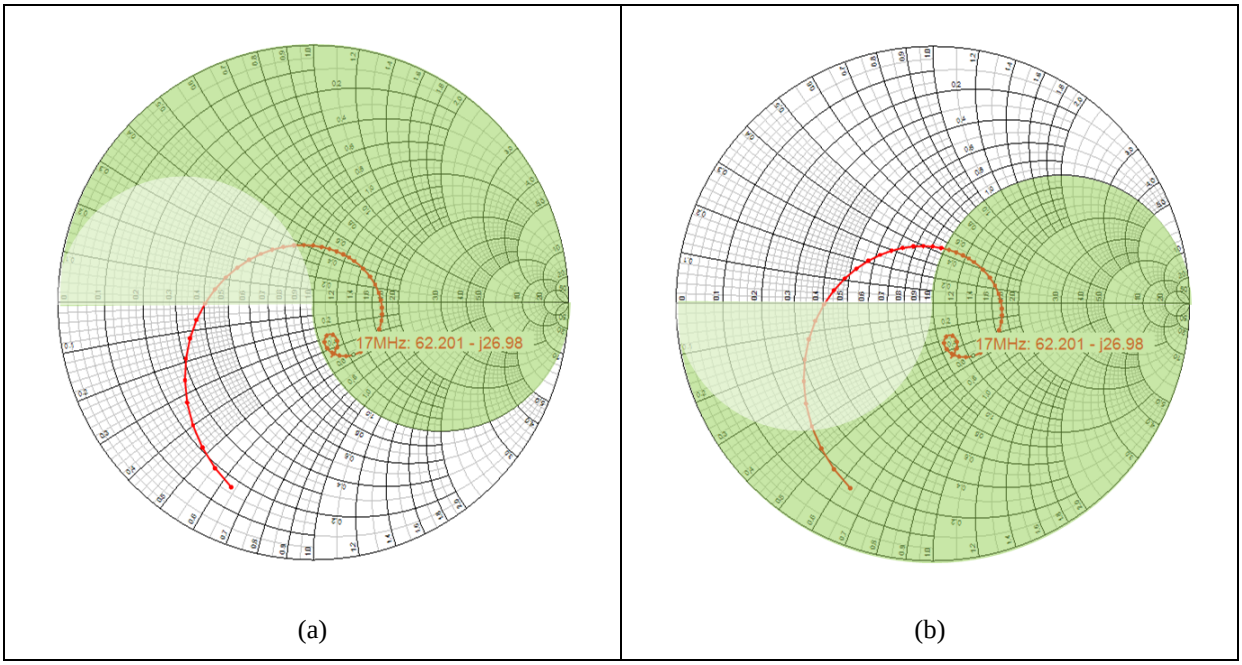

Figure 3.11 – Real and imaginary part of the impedance of the antenna on the Smith chart with Yin Yang region: (a) L type 1; (b) L type 2.

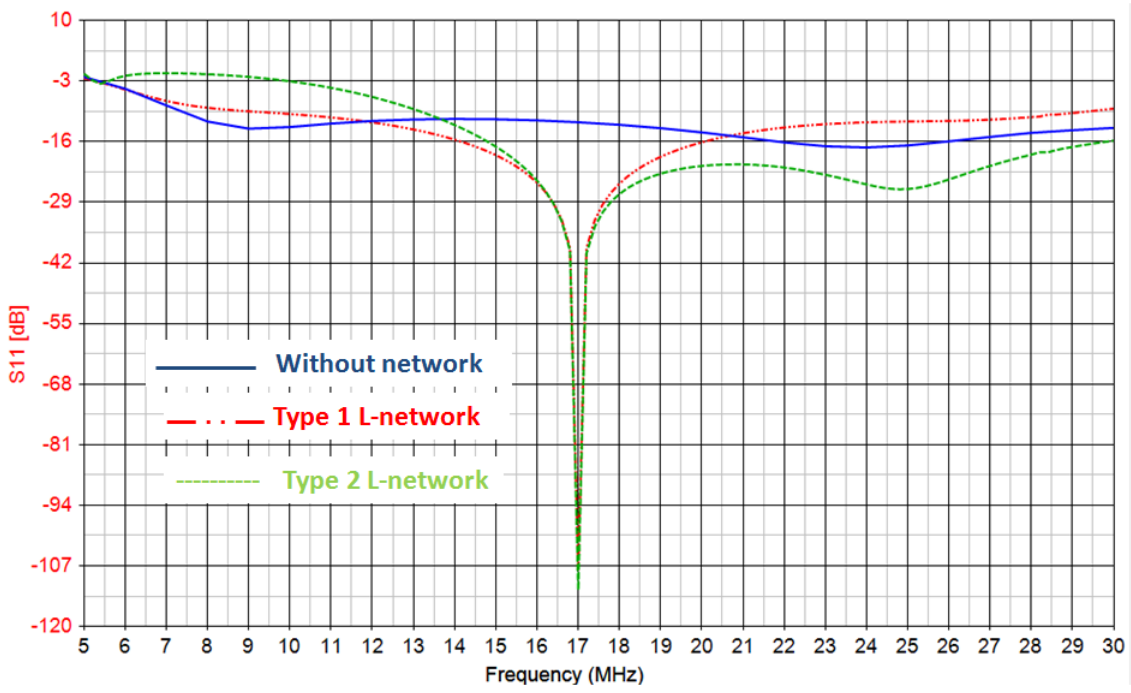

Figure 3.12 – S11 parameter comparison between L, T and π matching networks.

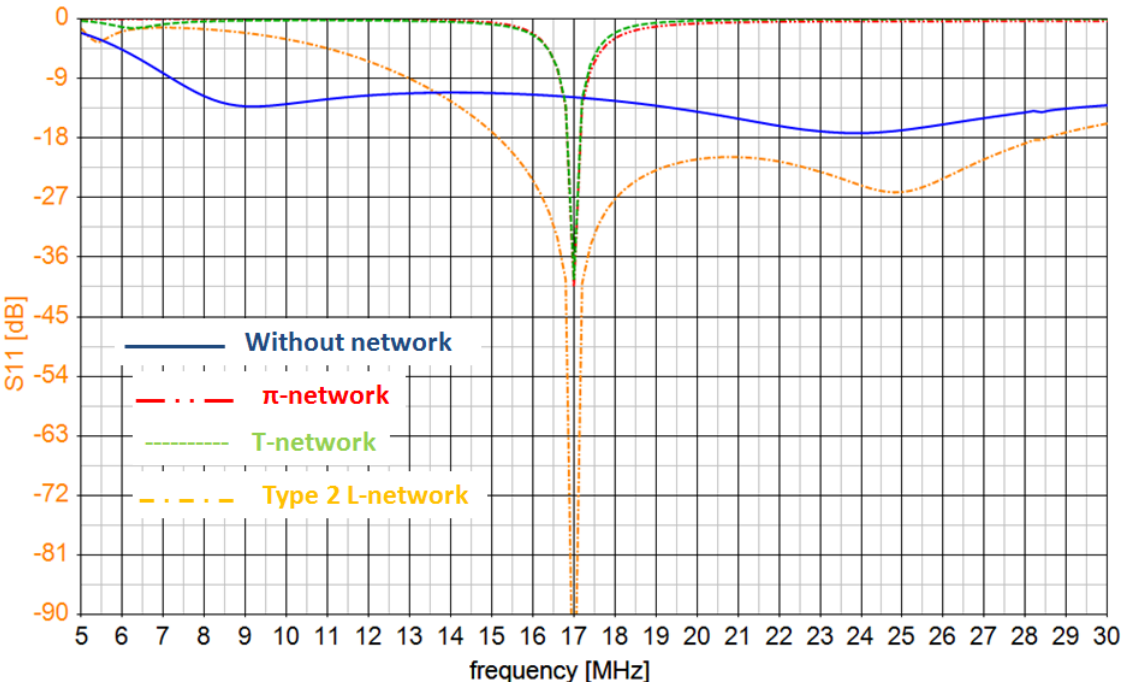

Figure 3.13 – S11 parameter comparison between L, T and π matching networks.

It can be seen that, using an L matching network, we obtained the maximum bandwidth achievable, that it means a minimum Q factor. However we don't have control on the value of the Q factor, because it is fixed by the impedance of the load and the impedance of the source. By using a T or π matching network, it can be possible to control the value of the Q factor, however it always will be lower than Q realized by an L-network.

3.2 Wideband impedance matching networks

At a specific resonance frequency it can be possible to reach a desired matching by choosing a certain Q, very high as well. The *perfect* impedance match can occur only at one frequency. That is the frequency at which the $+jX$ component exactly equals the $-jX$ component and, thus, cancellation or resonance occurs. At all other frequencies removed from the matching center frequency, the impedance match becomes progressively worse and eventually nonexistent. This can be a problem in broadband circuits where we would ideally like to provide a perfect match everywhere within the broad pass-band. There are methods, however, of increasing the bandwidth of the match (low Q matching network) and a few of these methods will be presented in this work and used to reach the performances of the proposed antenna.

3.2.1 L cascade matching network: analytical approach

A wideband matching can be possible with an easy and completely analytical way, e.g., arranging in cascade a certain number of L-networks having the same Q factors (Figure 3.14) [23].

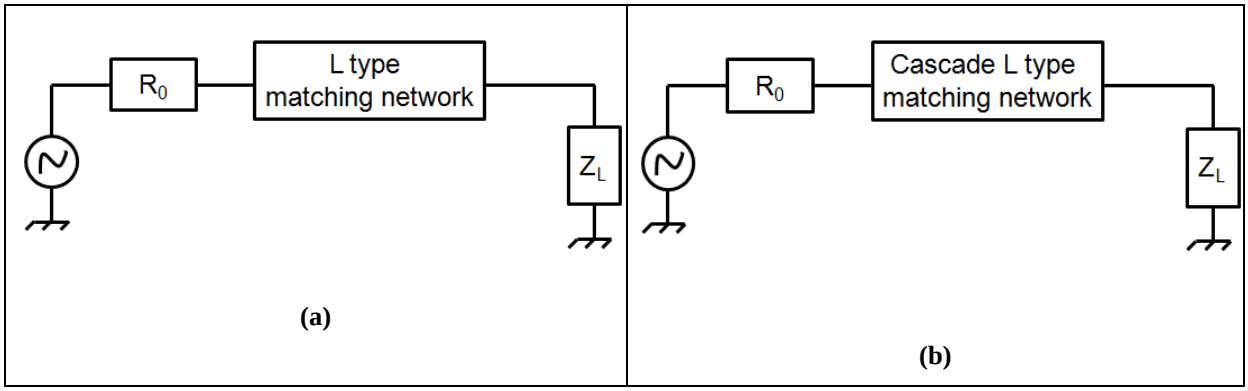

Figure 3.14 –RF circuit source-matching network-load: (a) single L-network; (b) L-networks cascade.

The Q factor obtained with different L-networks, arranged in cascade is lower than the Q factor obtained with a single L, π or T-network therefore the bandwidth is wider.

For the design of a cascade L-network, the following cases have to be distinguished (Figure 3.15): resistance of the load R_L higher than the resistance of the source R_s; resistance of the load R_L lower than the resistance of the source R_s.

The maximum bandwidth (minimum Q) available from this network is obtained when the virtual resistor (R) is made equal to the geometric mean of the two impedances being matched.

$$R = \sqrt{R_s R_L} \tag{3.11}$$

The loaded Q of the network, for our purposes, is defined as:

$$Q = \sqrt{\frac{R}{R_{\min}} - 1} = \sqrt{\frac{R_{\max}}{R} - 1} \tag{3.12}$$

where $R_{\max} = \max(R_S, R_L)$ and $R_{\min} = \min(R_S, R_L)$.

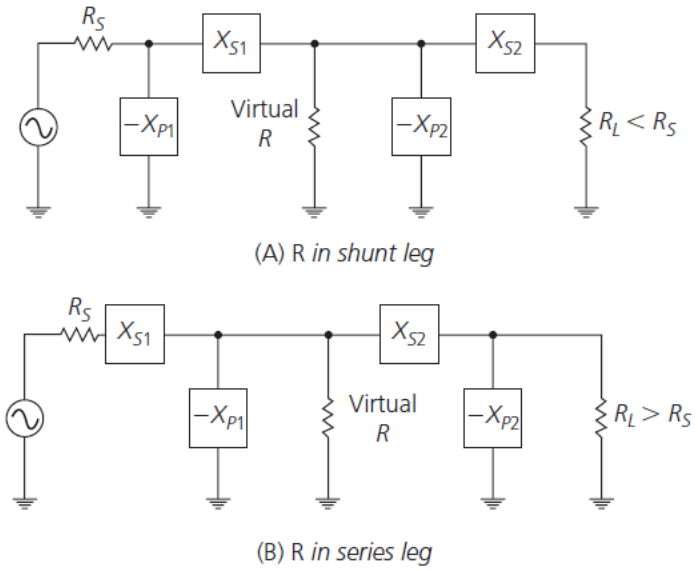

Figure 3.15 – Cascade of two L-networks: (A) $R_L<R_S$; (B) $R_L>R_S$.

As described for the narrowband case, the negative reactances shown in Figure 3.15 are symbolic, in order to indicate that the reactances with opposite signs have to be designed as opposite type (chapter 3.1).

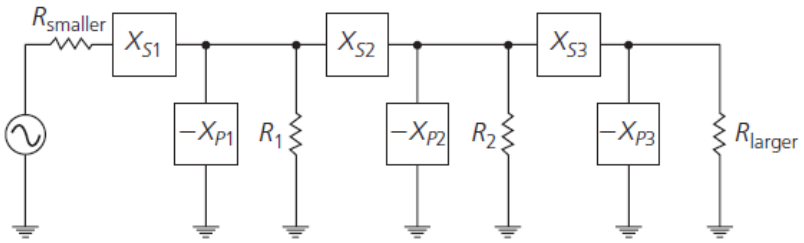

Figure 3.16 – Three L networks cascade: $R_L>R_S$ case.

If even wider bandwidths are needed, more L networks may be cascaded with virtual resistances between each network. Optimum bandwidths in these cases are obtained if the ratios of each of the two succeeding resistances are identical; therefore the maximum bandwidth (minimum Q) is obtained if the subsequent relation is respected:

$$\frac{R_1}{R_{\min}} = \frac{R_2}{R_1} = \frac{R_3}{R_2} = \ldots = \frac{R_{\max}}{R_N} = 1 + Q^2 \tag{3.13}$$

By knowing the resistances of the load and the source, it can be possible to solve a system of equations obtained from (3.13), where the unknowns are the virtual resistances and the Q factor.

The reactances of the N cascade networks can be obtained from the virtual resistances and the Q factor, as described in § 3.1.

Finally, by respecting the symbolic signs of the reactances, it can be possible to obtain the values of the inductances and the capacitances of the network.

For further instructions on the design of an L cascade matching network, several examples have been showed in the subsequent paragraph.

3.2.2 Wideband antenna matching with L cascade networks: optimization

The presented theory on impedance matching networks has been applied for very broadband matching at lower frequency of the HF band, in the proposed antenna configuration. In order to obtain good performances in terms of bandwidth, the presented merely analytical approach, has been combined with optimization algorithms. The latter algorithms act on the values of the lumped elements of the networks chose a priori, realizing a specific goal on the S11 parameter of the antenna. The definition of wide band matching is strictly related to the application, where the antenna has to be used (see Chapter 1).

For our purposes, these latter specifics are equal to an S11 in the frequency range 8-21MHz, equal at least to -17dB. This condition allows reducing the high mutual coupling between the antennas inside the radar array.

However, the proposed methodology can be applied for different configurations of electrically small antennas, which need to operate in a very wide frequency range.

We chose the central frequency of the band 5-30MHz which corresponds to 17MHz, in order to design different number of L cascade networks by using the antenna as load and finally we compared the performances of the networks on the HF band.

We chose the network shown in Figure 3.15(a) because the real part of the impedance of the antenna at 17MHz is bigger than the source impedance (equal to 50Ω) and equal to 62.2Ω, for designing the single L network. After that we chose two, three and four cascades of the single L networks. The matching networks and the corresponding values of the lumped element are reported in Figure 3.17.

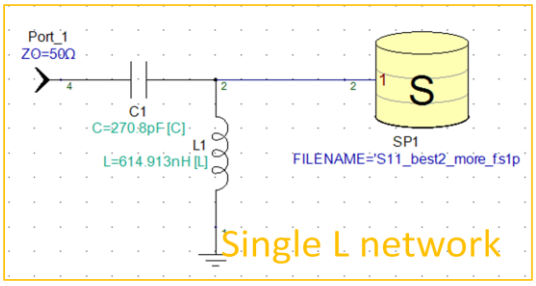

(a)

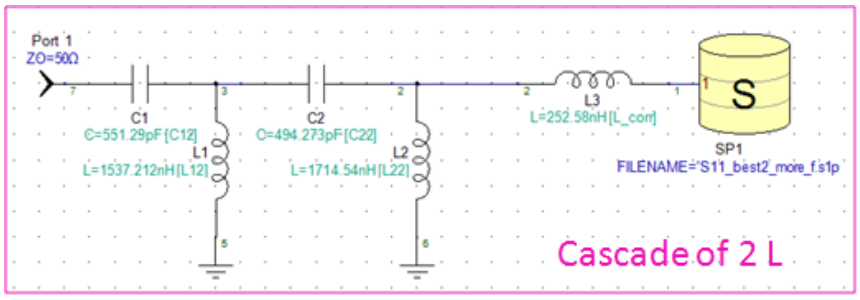

(b)

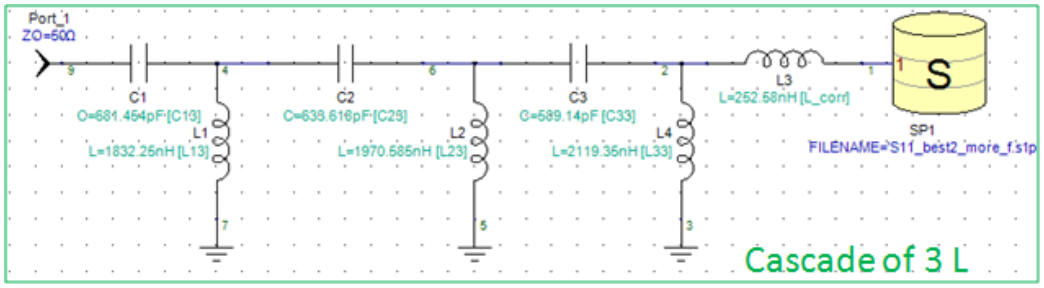

(c)

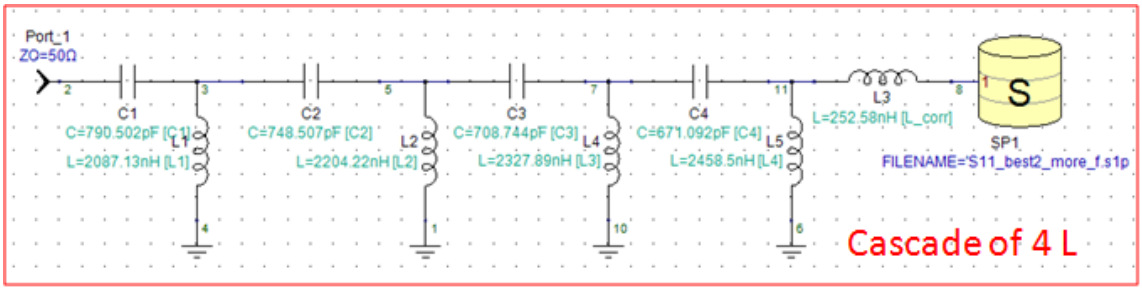

(d)

Figure 3.17 – Different L-networks cascade comparison for antenna matching.

We applied the resonance approach by using an inductor, in order to compensate the reactance of the antenna at 17MHz, which is equal to -26.98Ω.

The results in terms of S11 parameter are reported in Figure 3.18.

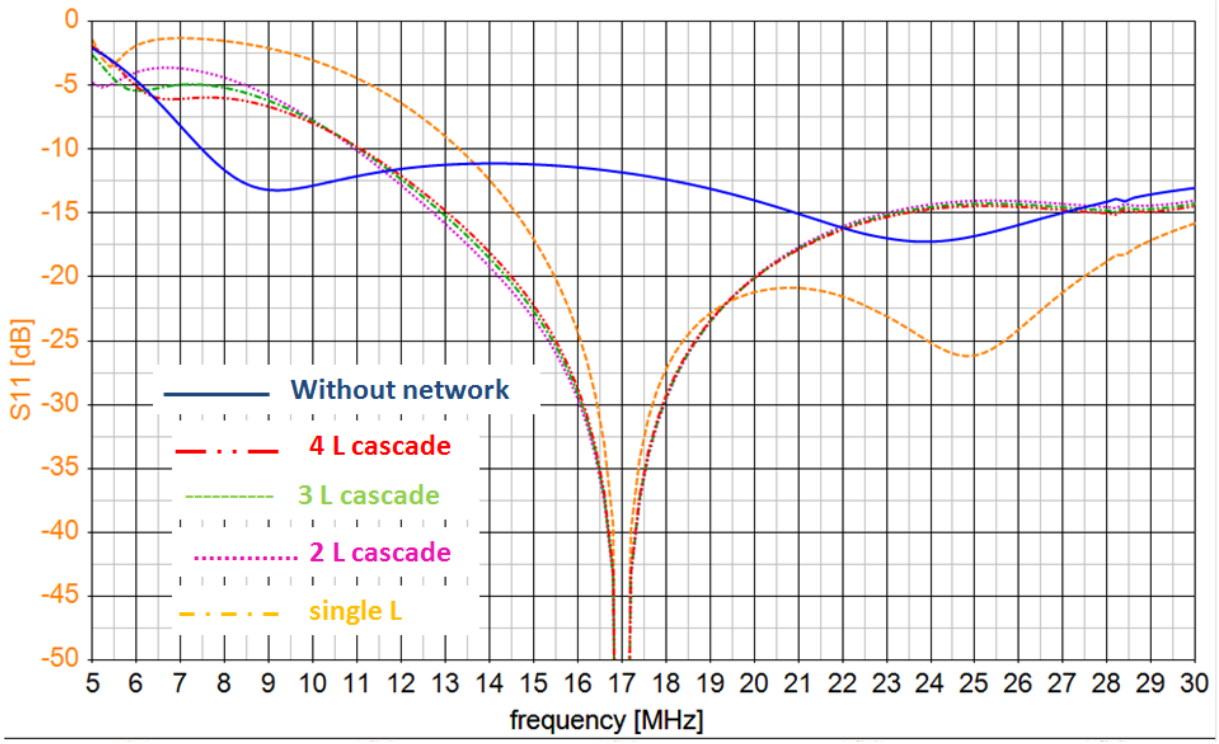

Figure 3.18 – S11 parameter of the antenna by using different L-networks cascade.

We noticed that by using the four L network cascade, the S11dB parameter has got a good behaviour in terms of bandwidth, especially at lower frequencies. Therefore we chose the latter matching network to match the antenna on the whole band.

All the values of the lumped elements belonging to the matching network have been parameterized. We fixed a goal for the S11dB parameter, which corresponds to the wideband specifics described before and we used subsequent optimizations of the values of the lumped element in order to reach the goal. According to the procedure, we obtained the network shown in Figure 3.19, with good performances of the S11 parameter Figure 3.20, but not good enough for our strict purposes.

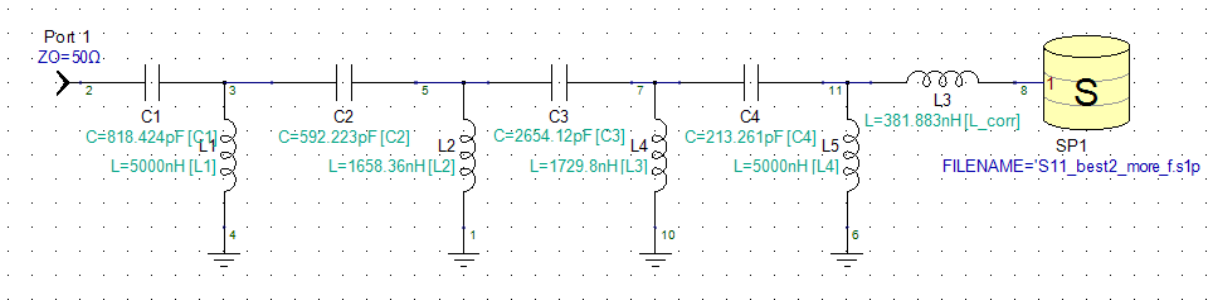

Figure 3.19 – 4 L networks cascade after optimization of the lumped elements.

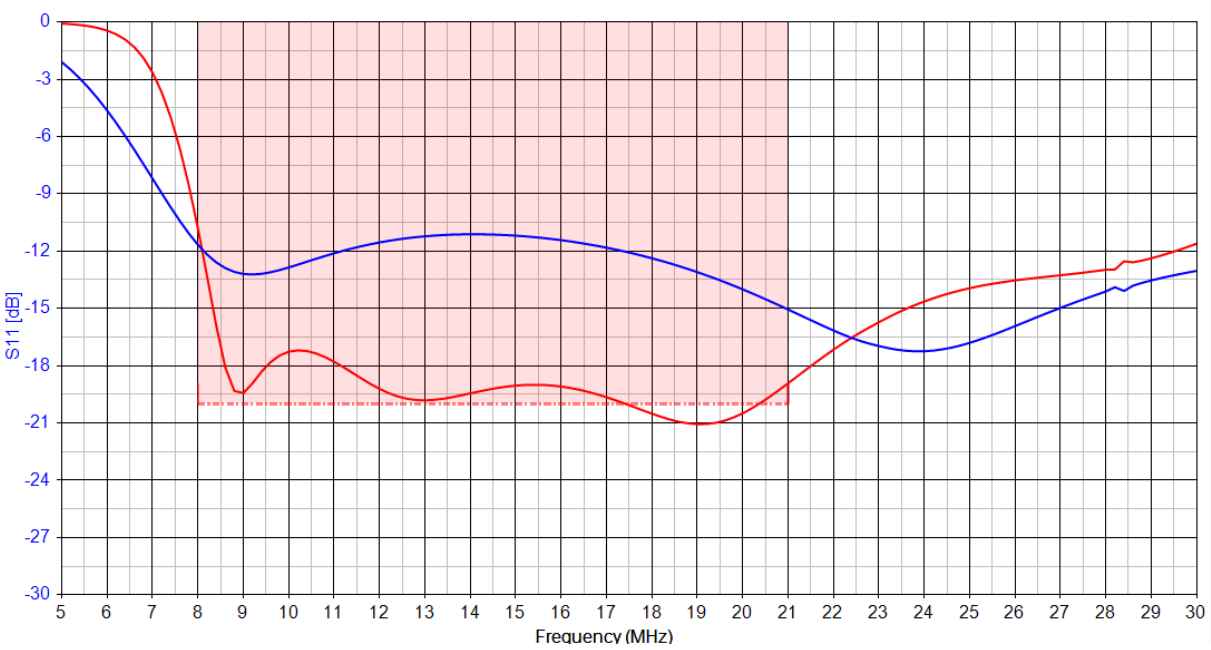

Figure 3.20 – S11 parameter of the antenna by using 4 L-networks cascade after optimization.

At 8MHz the S11dB realized by the network doesn't respect the goal.

In some cases further L networks in cascade could be used, but by using real lumped elements, losses have to be considered in the gain of the whole system consisting of the source, the matching network and the antenna as load.

Actually, until now we considered ideal lumped elements, without losses, but in the real case the Insertion Loss (IL) has to be taken into account. As the IL depends on the elements type, the number of the lumped elements has to be optimized as well in order to reduce the losses in the system. Even if optimizations of the elements have been considered, by using a simple L-networks cascade, the goal has not been realized.

3.2.3 Wideband antenna matching with T cascade networks: optimization

For the latter reason we thought to another type of matching networks cascade, realized with T-networks. With this last solution it can be possible to realize the desired matching, especially at lower frequencies, with a lower number of lumped elements.

We translated the reference frequency for designing the single T matching network, in order to approach the frequencies where the matching we demonstrated has been very hard. We chose 10MHz and then we arranged a cascade of three T-networks, having the same Q factor. The Q factor has been chosen accordingly to the condition (3.7), i.e. it has to be higher than the Q factor realized by a single L-network at the same frequency. We applied the resonance approach, putting a corrective capacitance *C_corr* in series to the network, in order to compensate the reactance of the antenna at 10MHz.

After subsequent optimizations of the values of the elements we obtained the network shown in Figure 3.21.

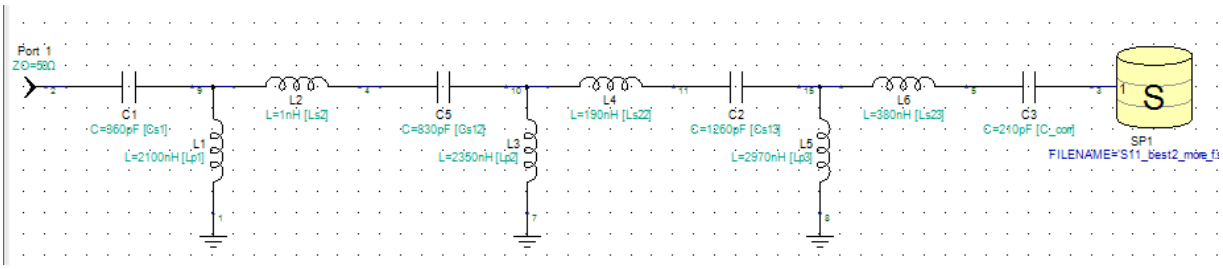

Figure 3.21 – 3 T networks cascade after optimization of the lumped elements.

We reached the desired goal on the S11dB, i.e. on the matching of the antenna on a very large band as shown in Figure 3.22.

According to the bandwidth definition (1.1), and our constraints on the impedance matching of the antenna, we obtained B_p=89% in the range 8-21MHz and B_p=35% in the range 21-30MHz. Finally the goals for obtaining a very good matching of the proposed antenna have been reached.

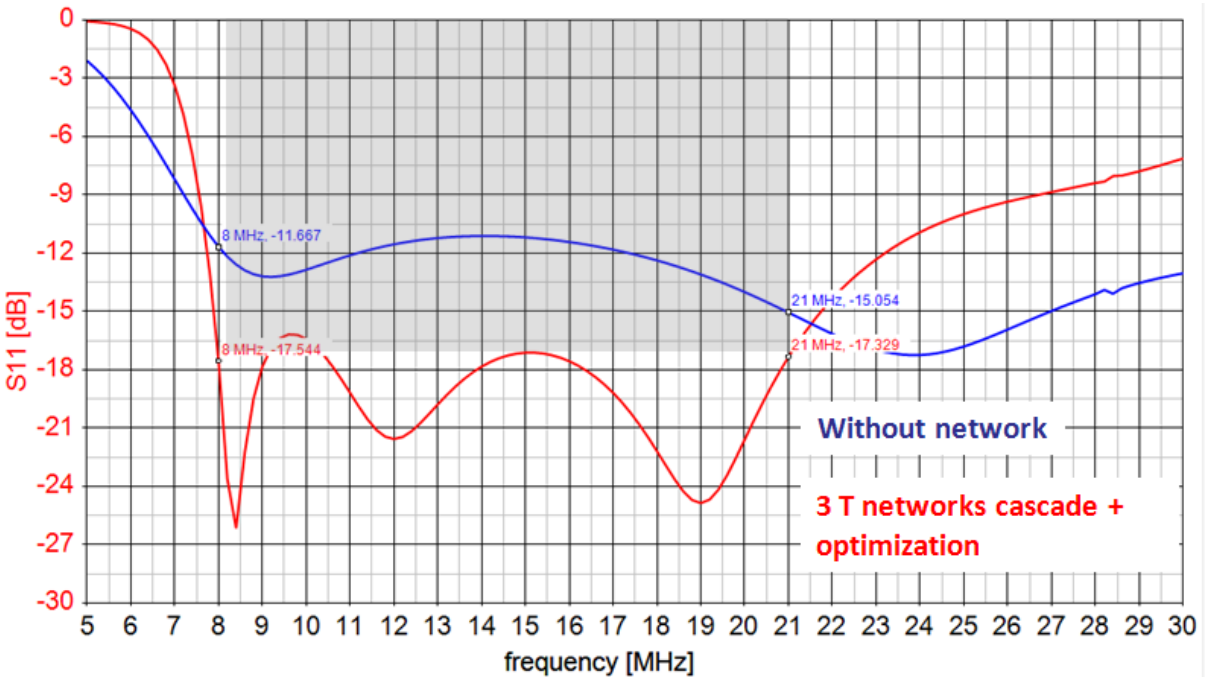

Figure 3.22 – S11 parameter of the antenna by using 3 T networks cascade after optimization.

4 MRI RADIO FREQUENCY COILS SIMULATION

The Magnetic Resonance Imaging includes different devices in order to guarantee the acquisition of the image of the sample under test. The main ones are:

1. The magnet, which produces a constant magnetic field in the region of interest (typically in the centre of the system);
2. The gradient's coils, which produce three magnetic field along x, y and z axis respectively;
3. Finally, the Radio Frequency (RF) coils, which produce an electromagnetic field in the region of interest at the Larmor's frequency.

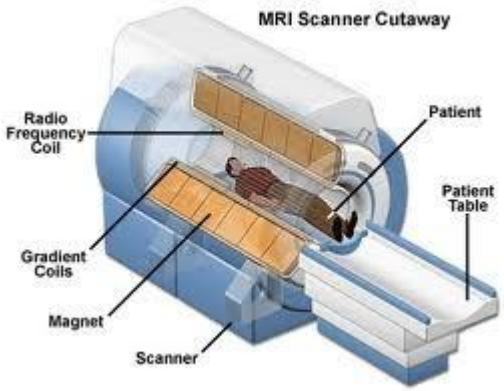

Figure 4.1 – MRI scanner system.

The Magnetic Resonance is based on the Nuclear Magnetic Resonance (NMR) which consists in the resonance of the atomic nuclei. The NMR concerns with the measure of the signals coming from the nuclei. The hydrogen's (^{1}H) nucleus is one of the most used in order to construct the image of a tissue, because it is the most present element in the human body. For instance, the water contains two atom of hydrogen, while lipid and proteins contain many more. It can be possible obtaining the image of a body under test, by using the MR Spectroscopy, which consists in the resonance of the phosphorus (^{31}P) or sodium (Na) nuclei.

The different signals coming from the nuclei resonate at different frequencies, which can be calculated with the following expression:

$$f_0 = \frac{\gamma}{2\pi} B_0 \tag{4.1}$$

where B_0 is the static magnetic field produced by the permanent magnet and γ is the gyromagnetic ratio, which depends on the proton (nucleus) of the element that it is considered for the spectroscopy. A relation between some of the gyromagnetic ratios and the resonance frequencies of typical nuclei are reported in Table 4.1- Table 4.2.

Table 4.1 – Giromagnetic ratios and resonance frequency relationship (B_0=1.5T).

Element	$\gamma/2\pi$ (MHz/T)	f_0 (MHz)
^{1}H	42.5756	≈63.86
^{31}P	17.2348	≈25.85

Table 4.2 – Giromagnetic ratios and resonance frequency relationship (B_0=7T).

Element	$\gamma/2\pi$ (MHz/T)	f_0 (MHz)
^{1}H	42.5756	≈298
^{31}P	17.2348	≈120.64

One of the main issues for a MRI system design is the RF coils design and testing. There are two main types of RF coils used for MRI purposes: the surface coils and the volume coils. The RF coils have to be able to transmit the excitation at Larmor's frequency of the nuclei, to the body under test and to register the response, in order to reconstruct its electromagnetic image. There are different parameters that guarantee the quality of a MRI RF coil:

1. Correct tuning at the Larmor's frequency (it depends from the static magnetic field and from the tissue);
2. Correct matching with the body under test at the Larmor's frequency;
3. High spatial and temporal resolution of the images (high SNR): it means an high homogeneity of fields produced by the coils (in a certain Region Of Interest (ROI));
4. Low Specific Absorption Rate (SAR) in order to respect the exposure guidelines [27].

So far, the RF coils project was related to an equivalent lumped circuit model of the coil, represented by inductances and capacitances. The last assumption is right since the RF coils can be considered as electrically small structures.

For the birdcage RF coils (volume coil), for examples, there some of different equivalent models with lumped elements networks, which depend on the low pass or high pass characteristics of the birdcage [29].

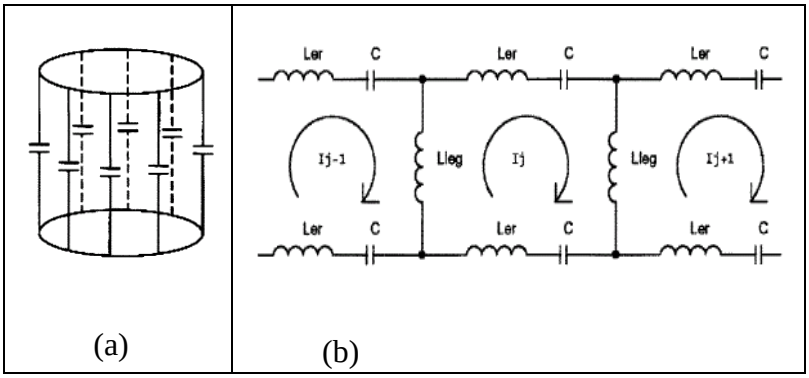

Figure 4.2 – Low pass birdcage coil and its equivalent model.

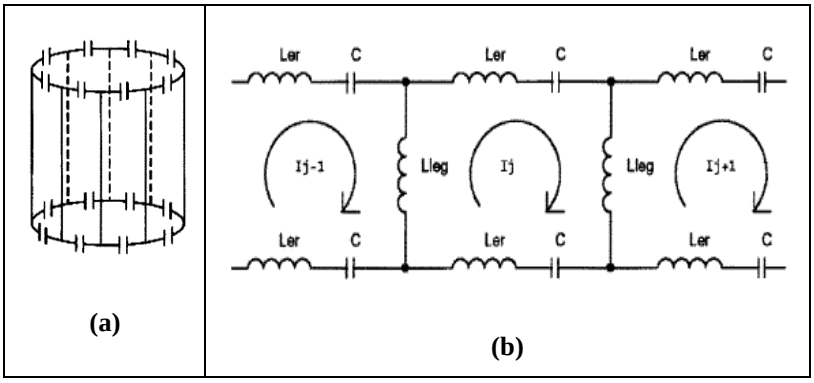

Figure 4.3 – High pass birdcage coil and its equivalent model.

With the traditional approaches of modelling a surface or a volume coil is possible to simulate and study the tuning, the matching and the magnetic field distribution of the coil. The MRI coil has to be tuned and matched at the resonance frequencies of the nuclei of a specific atom (depending on the Larmor's frequency of the atom); the nucleus is excited by a static magnetic field B_0, realized by the permanent magnet in the MRI system. Further, the amplitude B_1 of the radio frequency magnetic field distribution has to be as homogenous as possible in a predefined region around the coil in order to reach a good resolution of the image on the area under test.

The traditional approach is accurate if the dimension of the coil is small compared to the wavelength. E.g., an RF coil with the largest size equal to 0.14m and working under a static magnetic field strength B_0 equal to 0.18T, can resonate at 7.66MHz. The size of the latter coil compared to the wavelength is very small, so the model is very accurate.

The trend of the future MRI systems is the use of high static magnetic fields, e.g. B_0=7T, in order to obtain an increased image resolution [30]. High magnetic fields imply higher operating frequencies for RF coils. For example, in order to measure the spin-angle of the proton with B_0 (static magnetic field) equal to 7T, a RF coil resonance frequency of around 300 MHz is needed.

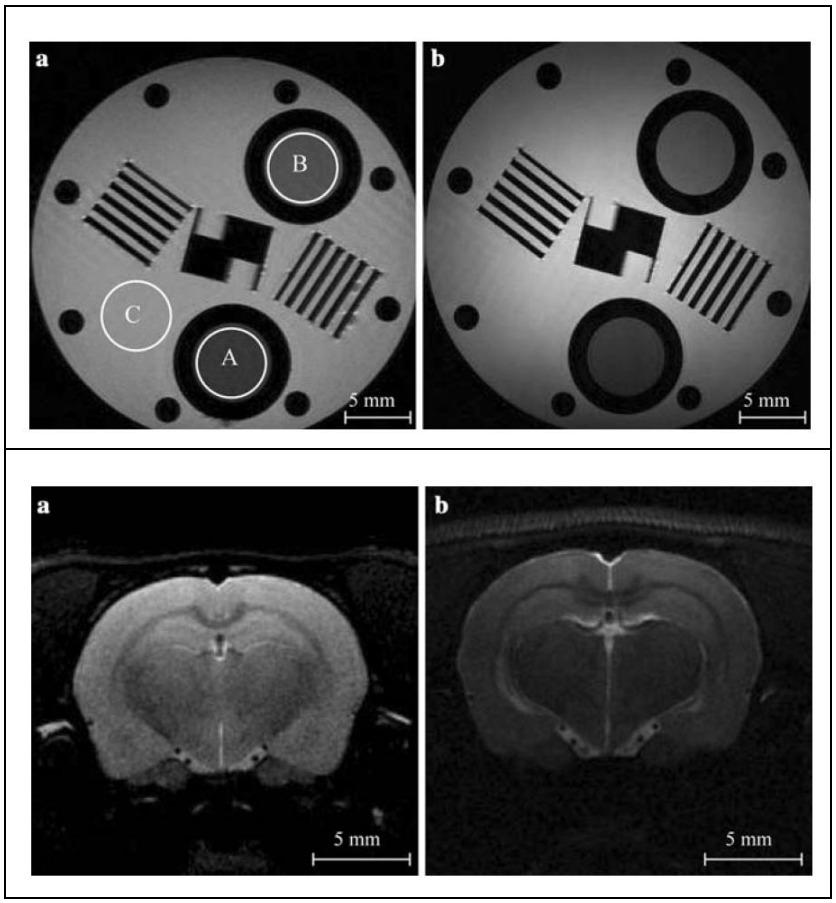

Figure 4.4 – MRI images obtained with 1.5T (a) and 7T (b) scanner respectively.

Typical sizes of RF coils operating at these frequencies are for instance, around 0.2m. This last size compared with the wavelength at the resonance frequency is not smaller, so the lumped element networks model is not more accurate: a full-wave approach is necessary. The

full-wave approach is helpful to estimate both the magnetic and the electric field as well, which was not possible with the traditional approach.

A further increasing interest is related to the interactions between RF coils and implants that could happen in the human body during the MRI exam. In this dissertation, after a complete full wave simulation of a surface MRI coil, we studied its interaction with a pacemaker system inside the human body.

First of all, we wanted to investigate a new approach, taking into account the presence a detailed and heterogeneous human model together with the RF coil, in order to compare the results with the simulation made with a simplified phantom and the measurements obtained in previous studies [25].

Afterwards we wanted to simulate the interaction of the RF coil together with the human body model and a simplified model of a common implant.

4.1 Example of RF coil EM numerical analysis: unloaded case

According to the mentioned topic, we investigated the case of a surface coil which operates at 64MHz, that is the resonance frequency of the hydrogenous atom with a static magnetic field B_0=1.5T.

The name of the RF coil is Figure of Eight (Fo8) coil (Figure 4.5), previously proposed [25], and widely simulated [26]-[28], in order to validate the measurements.

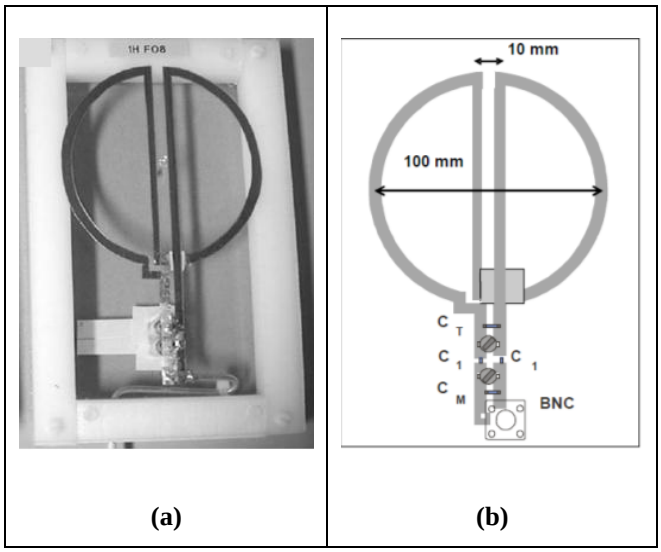

Figure 4.5 – Figure Of Eight RF surface coil.

This particular configuration allows obtaining a homogenous magnetic field in its central region. It is made with strip-lines of copper and the size and materials are described in details in Table 4.3.

Table 4.3 – Figure Of Eight RF surface coil: materials and size.

	Material	**Thickness**
Coil	Adhesive copper strips	100micron
Support	Plexiglass	1mm
Top	Plexiglass	16mm
Separator	Teflon	2cm

It has to be noticed that, in order to resonate, the coil has to be loaded with capacitances placed along the structure. The self resonance frequency of this RF coil is around to 300MHz, so far from the operating frequency 64MHz. Actually, just some of the capacitances are fixed, some of them are trimmers which can be used for the tuning and the matching of the coil. The values of the fixed capacitances in the unloaded case are shown in Table 4.4.

Table 4.4– Figure Of Eight RF surface coil: values of the capacitances, S11 and Q parameters.

	C_T	C_1	C_M	$\|S_{11}\|$dB	Q
Unloaded Fo8 coil	5.1pF	15pF	124pF	-26	100

For the electromagnetic simulation and for better estimate all the parameters of the RF coil, two approach have to be taken into account: a) the coil without load; b) the coil with a load in the nearby. The first approach allows designing the coil tuned at a specific resonance frequency, which in this particular case is equal to 64MHz. The second approach allows obtaining a good estimation of the matching of the coil with a dielectric simplified phantom and eventually to tune again the coil. The effect of the dielectric load is in fact, a translation of the resonance frequency and a consequently effect on S11 value, that is strictly related to the dielectric constant value.

The presented structure is very narrowband and electrically small compared to the wavelength at its frequency of resonance and it requires long simulation time when a FDTD solver is used. Furthermore the width of the strip-lines of the Fo8 coil is very thin compared to the wavelength. For the last reasons it is more convenient to use a Frequency domain numerical method. In our studies we distinguished two cases. For the e.m. simulation of the unloaded coil and of the loaded coil with a very simple phantom (like a sphere, a cylinder, etc…), it's preferable to use a Finite Element Method (FEM), in order to reach the convergence of the solver and finally the results very quickly. Then, if we are interested on the e.m. analysis of the coil with the presence of a very detailed numerical model of the human body, a Time Domain solver is inevitable.

The un-loaded case has been investigated with two numerical electromagnetic methods in the frequency domain applied to a numerically designed CAD of the coil (Figure 4.6): specifically with FEM and MoM.

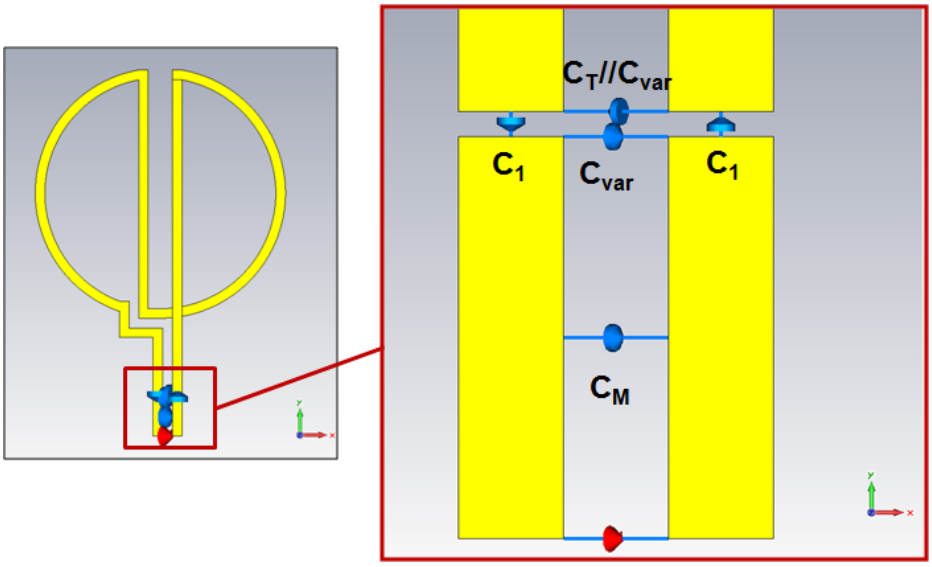

Figure 4.6 – Numerical CAD of the Fo8 coil: unloaded case.

In order to reach the right operating frequency, a preliminary parameterization and optimization of the values of the trimmers (in the range 1-25pF) have been realized. For the last purposes, we observed the S11dB parameter. After subsequent optimizations, we obtained the results shown in Figure 4.7.

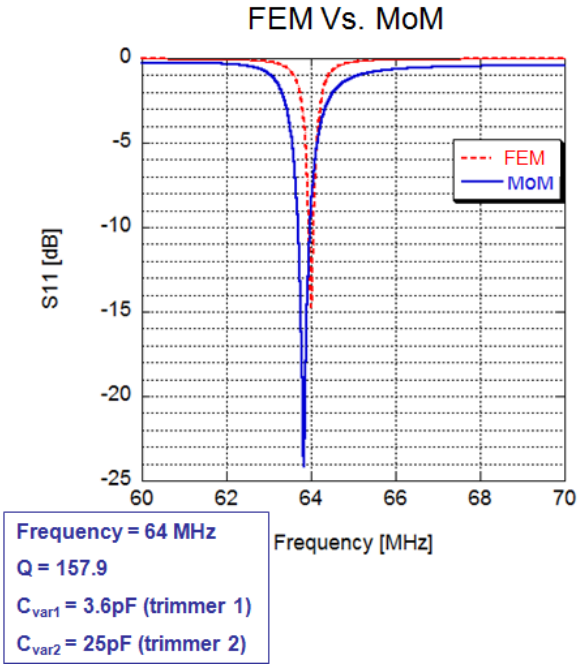

Figure 4.7 – S11 parameter of the un-loaded Fo8 coil: FEM Vs. MoM results.

4.2 Example of RF coil EM numerical analysis: loaded case

In order to validate the electromagnetic methods for RF coils analysis, we studied the case of the loaded coil and we compared the results with measurements made in a real MRI scanner. We maintained the characteristics of the load, which is a simple cylinder, filled with a material having the dielectric properties of the muscle at 64MHz [31]. In Figure 4.8 we showed the measurements configuration of the coil into respect the cylindrical phantom and the MRI scanner at 1.5T.

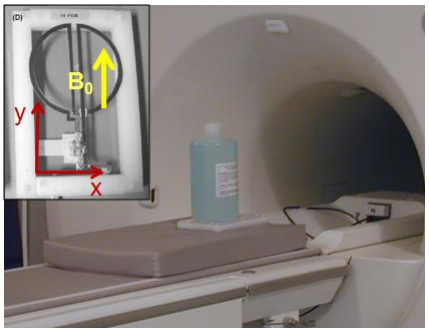

Figure 4.8 – Configuration of the RF coil during the measurements.

The configuration of the coil with respect to the cylindrical phantom during the simulation made with the MoM and the FEM is shown in Figure 4.9.

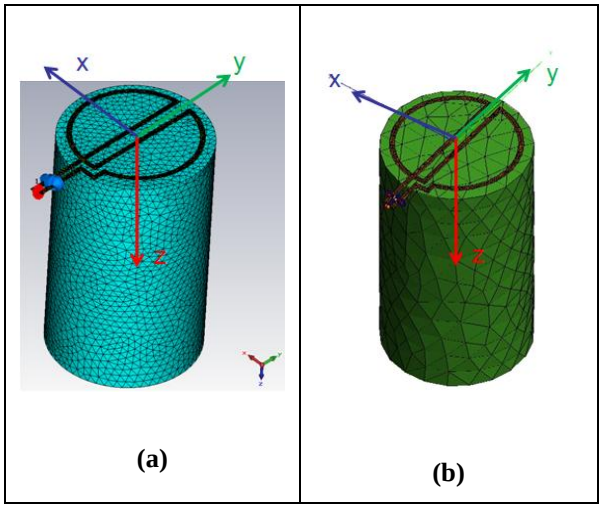

Figure 4.9 – Numerical CAD of the Fo8 coil, unloaded case: (a) FEM; (b) MoM.

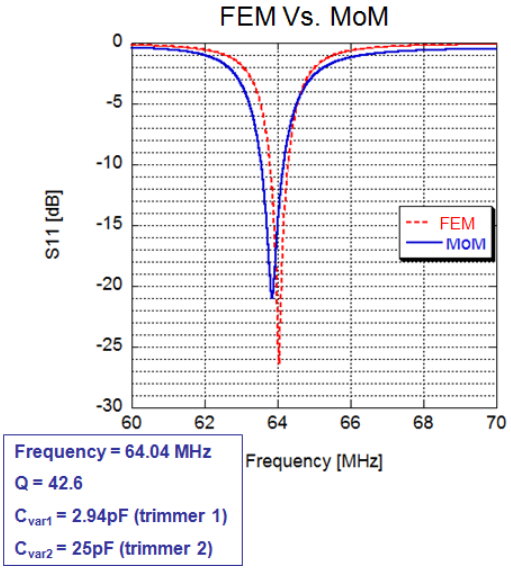

Figure 4.10 – S11 parameter of the loaded Fo8 coil: FEM results versus MoM results.

In Figure 4.10 it can be noticed the effect of the presence of the load on the matching of the coil: the curve of the S11 parameter is larger (i.e. lower factor Q) than the case in which the coil is unloaded. We tuned again the coil with subsequent optimizations of the trimmer, in order to reach the original resonance frequency, equal to 64MHz and finally we compared again the results carried out with the two methods.

In the loaded case it is interesting to estimate also the field's distribution inside the phantom, in order to verify the homogeneity of the magnetic field and to predict the electric field, which was not predictable with the traditional approaches.

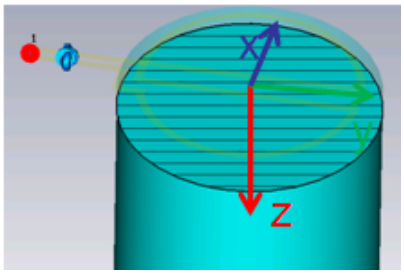

Figure 4.11 – Plane of calculation of the field's distributions.

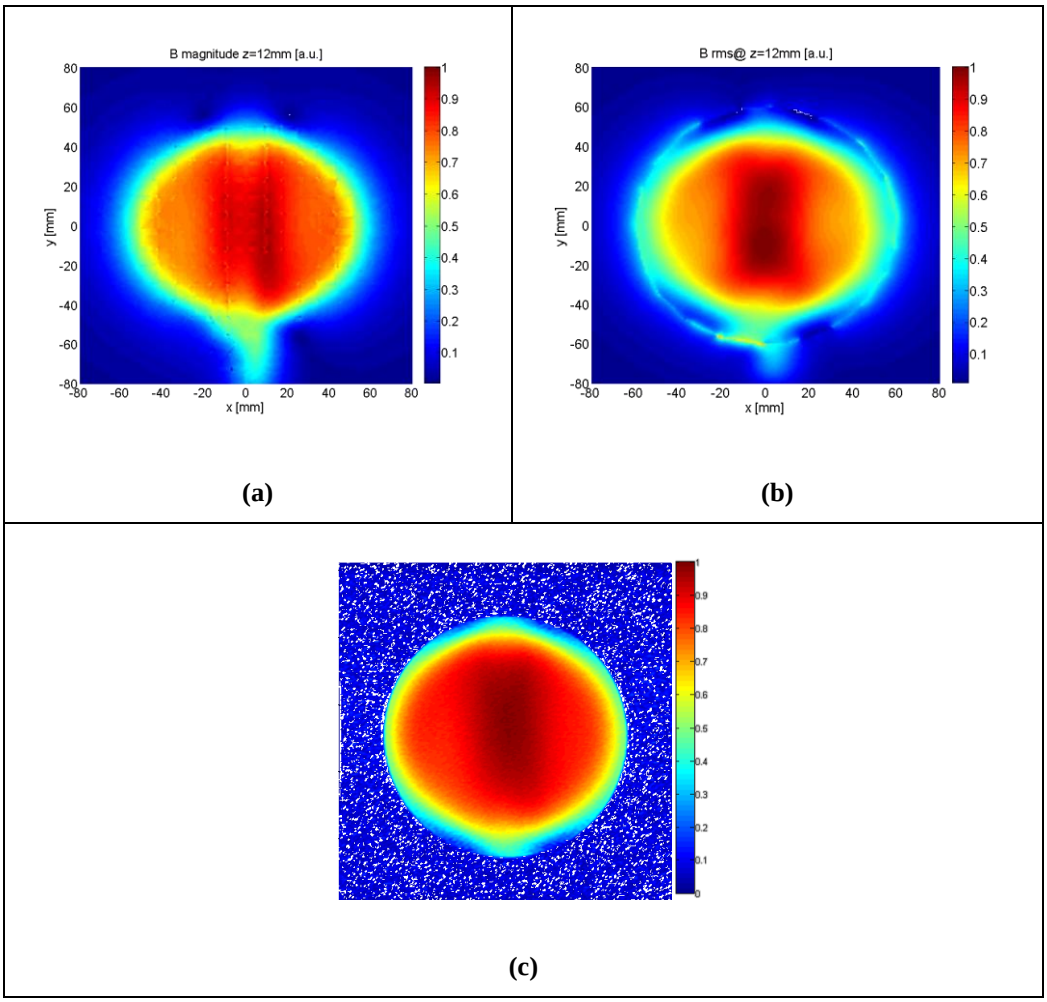

Figure 4.12 – Magnetic field distribution at 64MHz on the plane at z=12mm: (a) FEM; (b) MoM; (c) MRI scanner.

The field's maps at 64MHz have been plotted on a plane corresponding to z=12mm, parallel to the plane of the coil. Finally we compared the results obtained with FEM, MoM and measurements. We obtained good agreements between the two numerical methods and the measurements.

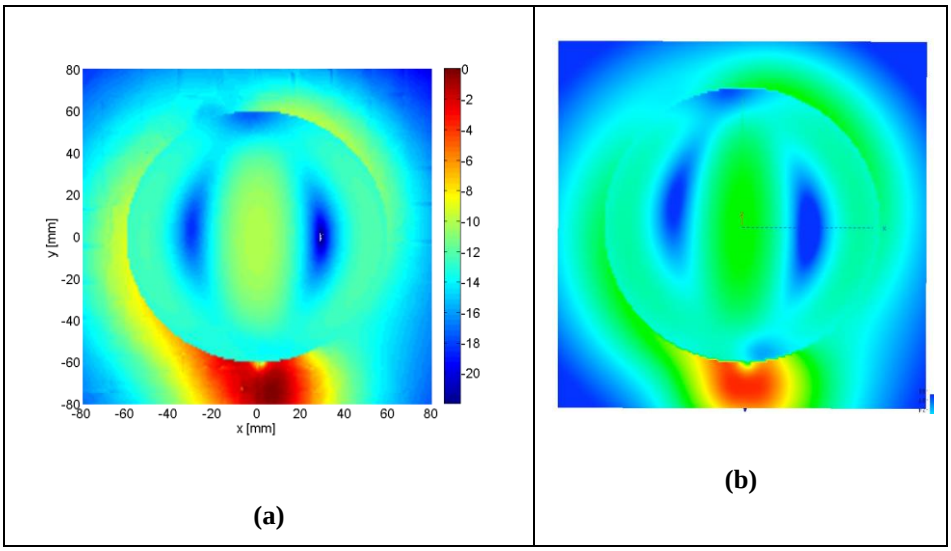

Figure 4.13 – Electric field distribution at 64MHz on the plane at z=12mm [logarithm scale]: (a) FEM; (b) MoM.

We obtained good agreements between the electric fields results distribution estimated with the two methods.

We can conclude that the numerical simulation of the RF coils has been preliminarily validated and they represent a useful tool for predicting mechanisms related to the resonance imaging.

4.3 Electromagnetic analysis of interaction between RF coils, human body and implants

In medicine, proper diagnosis, treatment and management of several diseases are possible with the Magnetic Resonance Imaging (MRI), a widely used and well-established technique. MRI is contraindicated for patients implanted with medical metal devices because potential effects might occur due to the static magnetic field, the Radio Frequency (RF) magnetic field and the time-varying magnetic gradient fields. So the interaction of RF coils and implants require more investigation [32].

We proposed a new methodology in order to analyze a possible interaction between RF coils and patients implanted with a pacemaker including an equivalent electromagnetic model useful for analyzing RF surface coils. This analysis has been made in order to predict damaging of the device, and to give requirements for the safety of the patient.

The purpose of this work is to validate the numerical method for simulating RF coils, by using a heterogeneous human body as load implanted with a passive pacemaker system.

The heterogeneous human body used for our purposes is just available in time domain simulation. Typically, the surface coils for MRI are electrically small and complicated structures, so the full-wave approach used in the previous paragraph is quite time consuming. For the last reasons, an equivalent model of system consisting of the RF coil and the human body has been studied.

In the case of the Fo8 coil, as it can be seen from Figure 4.14, the convergence of the time solver has been reached by modifying the numerical CAD of the coil; however the simulation was very long and onerous.

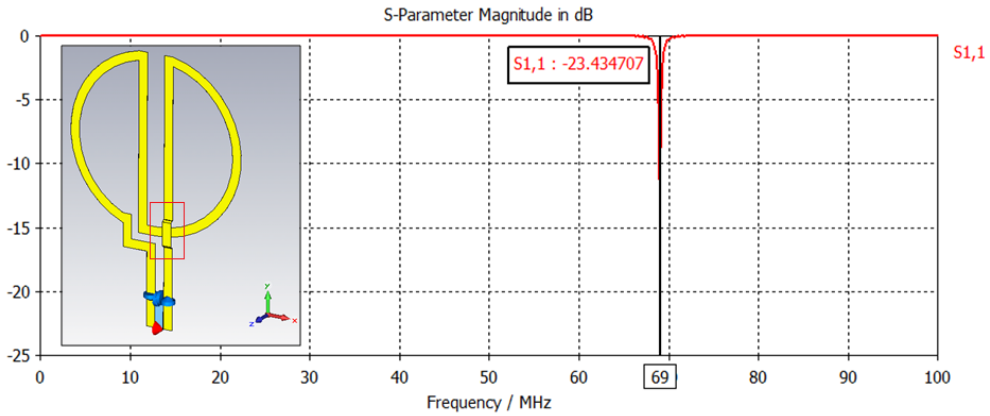

Figure 4.14 – S11 parameter of the modified Fo8 coil with time domain simulation.

4.3.1 Electromagnetic equivalent model of the RF coil: validation

The fields have been evaluated from the solver used for the analysis, by applying the Equivalence Principle in the frequency domain on a box surrounding the original model of the coil at 64MHz.

Then we separately simulated the box representing the equivalent model of the coil in free space, by using the time domain solver. Both the numerical models of the RF coil work at 64MHz.

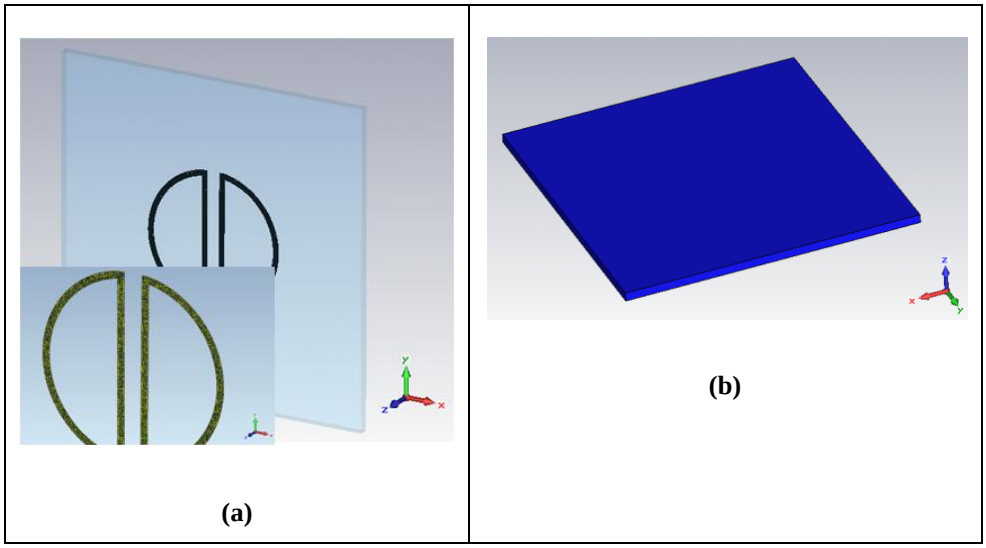

Figure 4.15 – Numerical model of the coil: (a) Original; (b) equivalent.

All the steps are resumed in the flow chart shown in Figure 4.16.

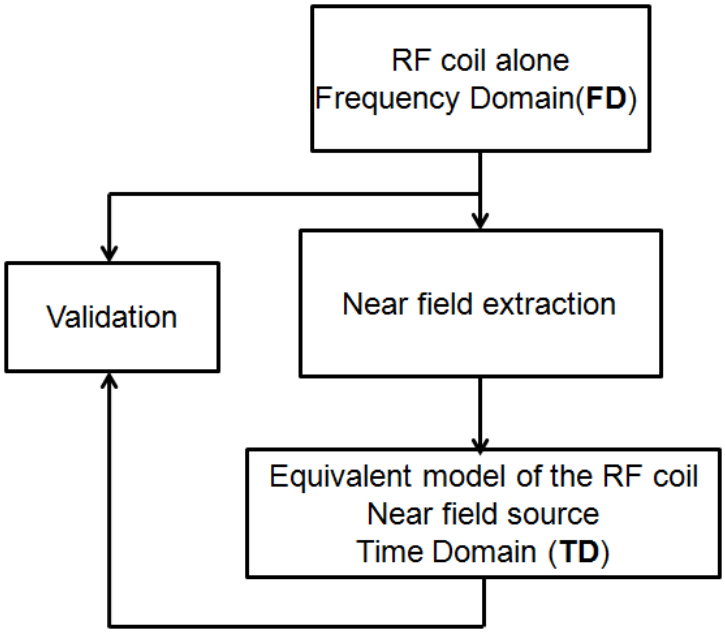

Figure 4.16 – Steps for equivalent model of the RF coil validation.

All the results refer to an input power equal to 1W, at 64MHz, on a plane at z=12mm parallel to *xy* plane and the amplitude is normalized. As it can be seen from Figure 4.17, we obtained good agreements between the two studied cases. So the equivalent model has been validated.

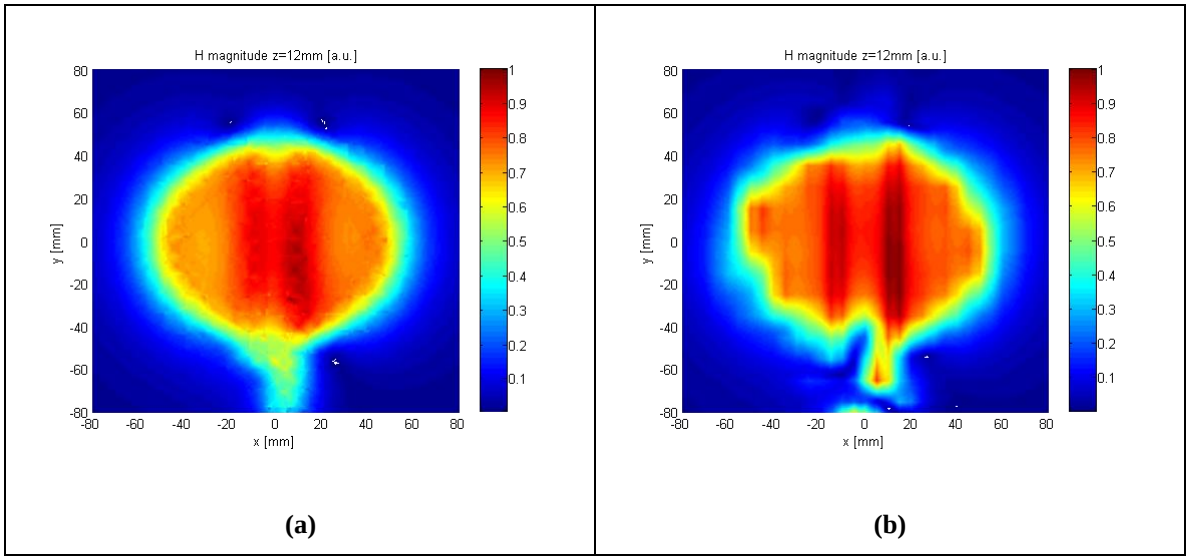

(a) **(b)**

Figure 4.17 – Magnetic field results on z=12mm plane: (a) Original coil; (b) equivalent model of the coil.

Afterwards, the equivalent solution has been applied to the loaded case of the coil. The cases of simplified phantom and realistic human head have been investigated.

The loaded original coil with the simple dielectric cylinder having the dielectric properties of the muscle at 64MHz has been analyzed in frequency domain. Then, the loaded equivalent coil has been analyzed in time domain. Finally, the equivalent model of the coil has been analyzed with the human head. Again, all the results refer to an input power equal to 1W, at 64MHz, on a plane at z=12mm parallel to *xy* plane and the amplitude is normalized.

The results in terms of magnetic field distribution are showed in Figure 4.18: they present good agreements, so we can conclude that the equivalent solution is also validated in the loaded case.

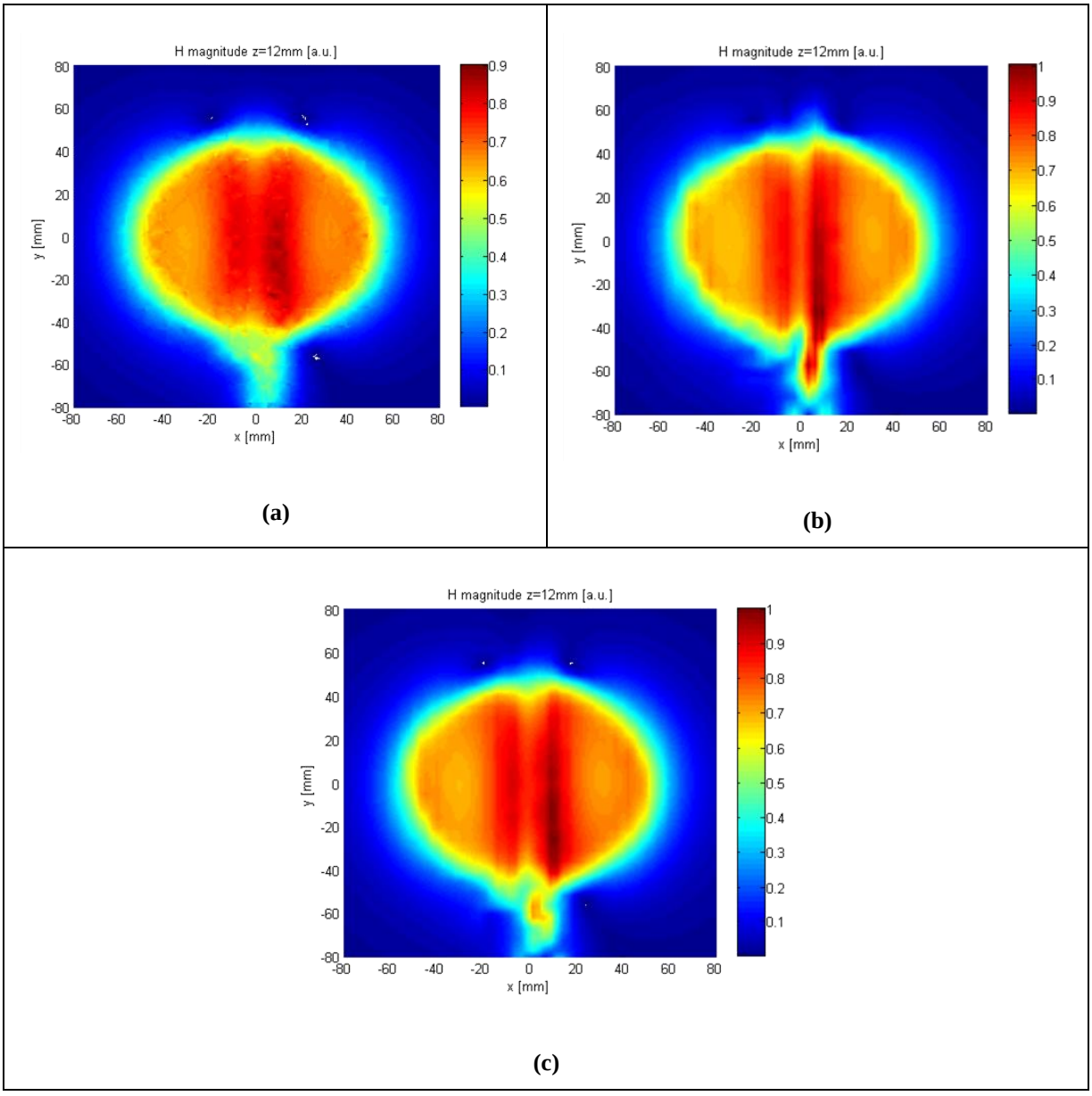

Figure 4.18 – Magnetic field results on z=12mm plane at 64MHz: (a) Original coil loaded with a dielectric cylinder (FD); (b) equivalent model of the coil loaded with a dielectric cylinder (TD); (c) equivalent model of the coil loaded with the realistic human head.

4.3.2 Electromagnetic equivalent model of the RF coil: application

The equivalent model has been used for evaluating the effect of the RF coil on a passive pacemaker system inside the numerical model of the human body.

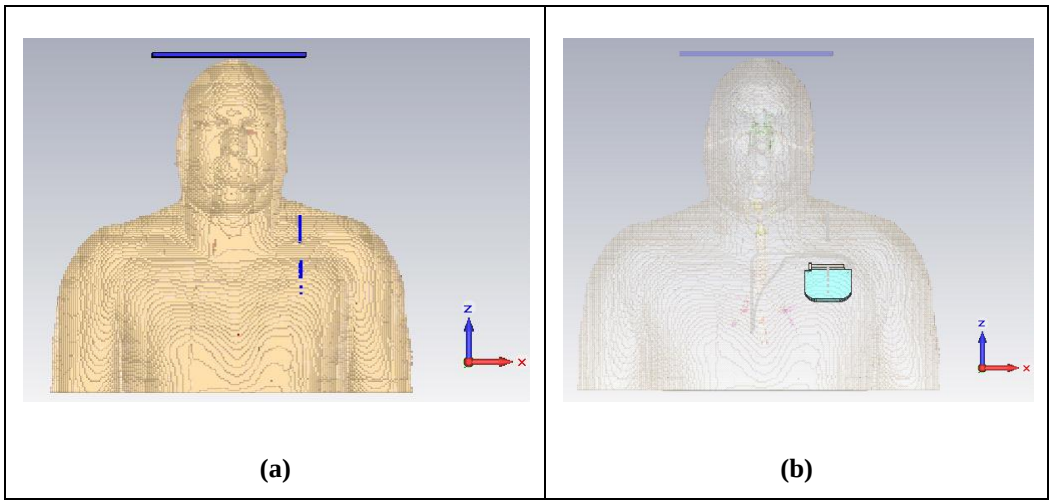

Figure 4.19 – Effect of the RF Fo8 coil on the human body: (a) without pacemaker; (b) with pacemaker.

We evaluated the field's distribution on a line crossing the pacemaker case. By comparing the results, we noticed that in the case of the presence of the pacemaker, some spikes of the electric field and the magnetic field appeared. The peak of the electric and the magnetic field are due to the presence of the wires belonging to the system. It can be noticed that the maximum electric field value, obtained with the presence of the pacemaker is five times the electric field obtained in the case of absence of the pacemaker in the same region. The peaks might cause an unwanted rise of the temperature of the tissues surrounding the wires, causing a higher Specific Absorption Rate (SAR). The spikes might also be able to damage the device. This latter result suggests to take into account a redesign of the device in a realistic MRI environment, in order to consider the use of this diagnosis technique also for implanted patients.

The comparison between the results showed us how some spikes around the pacemaker system are present Figure 4.20.

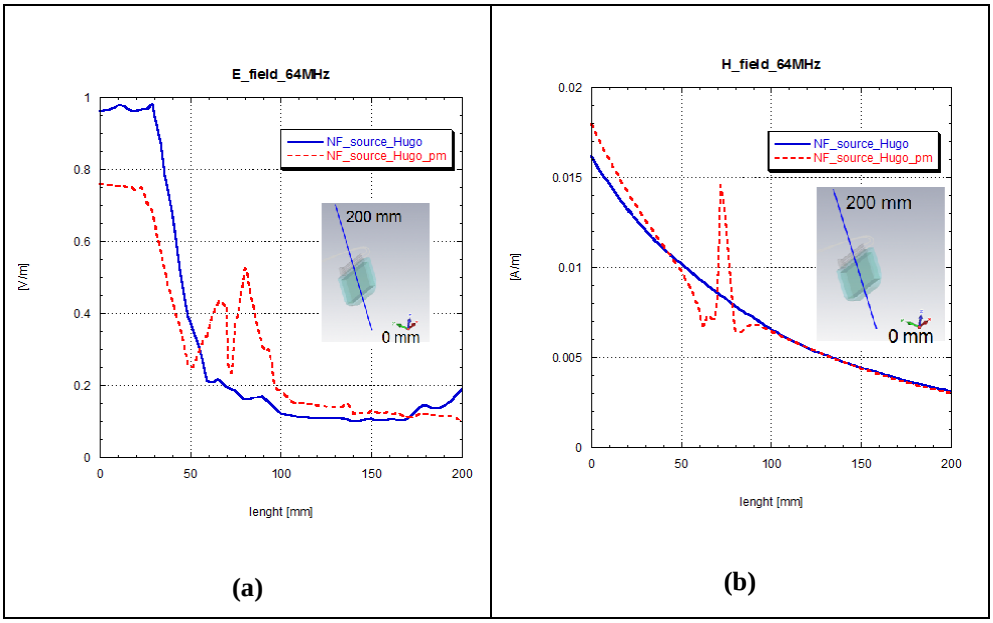

Figure 4.20 – Field's distribution comparison with and without the pacemaker: (a) E field; (b) H field.

The proposed methodology allows simulating resonant structures, like the RF coils. Further the method is very useful for electrically small structure having complicated geometry. The computational burden of e.m. numerical method in time domain is significantly reduced by using the proposed approach.

CONCLUSIONS

The design methodologies discussed in this work have led to broadband compact antennas able to work both in radar and communication applications. The antenna configuration exploits the concepts related to two different broadband antennas that are well-known in literature: the biconical antenna and the folded antenna. Different techniques have been used for miniaturizing the antenna. The monoconical configuration was obtained by using a perfect electric ground plane. The resonances at different frequencies in the range 7-30MHz were obtained by exploiting the concepts of the meandered antennas: different folds of the wires make it resonant. The aim of this work was to modify an available configuration in order to make it suitable for OTH radar exploiting a phased array.

Moreover, the single element has been studied taking into account mutual coupling phenomena between the elements in the array. First of all, unacceptable matching performances has been noticed in the active VSWR of the array, especially at the lower part of the HF band, which suggested the usage of very well-matched antennas. The single element has to realize a VSWR as small as possible in the range 8-21 MHz at least. For higher frequencies, the mentioned constraint becomes less important.

In order to obtain a better matching of the antenna, two kind of shorting pins which grounded the antenna have been studied. Different configurations of the pin have been investigated by using a parameterization in segment lengths.

The first pin allows realizing a capacitive coupling with the antenna, reaching good matching performances for lower and central frequencies of the HF band. The second pin behaves like an inductance, compensating the capacitive behaviour of the antenna at very low frequencies. The pins made the antenna resonant, with very good matching performances; however the electrical size of the antenna is not small, therefore a disruption on the radiation pattern according to the frequency is inevitable. For the last reason the antenna was miniaturized. The two obtained solution allow reaching again the symmetry of the radiation pattern on the E plane, and the omni-directionality on the H plane lost with the pin introduction. The proposed very small antenna has two disadvantages: a smaller gain, and thus a smaller efficiency; a higher operating frequency. The last issues come from the fact that the

antenna became electrically small. Otherwise the two configurations can be used for different purposes in the VHF band, because in this band they present very broadband performances.

In order to improve the matching of the antenna maintaining the performances on the radiation pattern, the antenna shape has to be preserved. So, another way to make the antenna resonant is the use of impedance matching networks. Two different approaches have been thought: the use of several narrowband matching networks; the use of single wideband matching networks. The analytical design of narrowband and broadband matching networks has been investigated. Then the analytical approach has been combined with optimization approach, obtaining very good results on the matching of the antenna. We reached the constraint fixed for our purposes: a S11 parameter of the single element less than -17dB in the range 8-21 MHz, which implies an operating bandwidth of the antenna equal to 89%.

The final antenna configuration with the very wide-band impedance matching can be used in the phased radar array leading to significant advantages on the coupling.

According to the electrically small antenna theory, a new type of antenna, useful for MRI application has been investigated. An electromagnetic equivalent model of a RF surface coil operating at 64MHz has been validated. The model has been applied for a more complex environment, with the presence of a human model implanted with a pacemaker system. The model has been validated again and it allowed a complete analysis of the complex system represented by the MRI scanner.

REFERENCES

[1] Antenna Standards Committee of the IEEE Antennas and Propagation Society, *IEEE Standard Definitions of Terms for Antennas,* IEEE Std 145-1993, The Institute of Electrical and Electronics Engineers, Inc, New York, 1993.

[2] George H. Brown and O. M. Woodward Jr., *Experimentally Determined Radiation Characteristics of Conical and Triangular Antennas*, RCA review, 1952.

[3] O. Givati and A. Fourie, *Analysis of Wire Skeletal Conical Antennas*, IEEE Transaction

[4] A. Boag et al., *Design of Electrically Loaded Wire Antennas Using Genetic Algorithms*, IEEE Transaction on Antennas and Propagation, 1996.

[5] A. G. Kandoian, *Three New Antenna Types and Their Applications*, Proc. IRE, 1946.

[6] H. A. Wheeler, *Fundamental Limitations of Small Antennas*, Proceedings of the IRE, 1942.

[7] S. R. Best, *A Discussion on the Properties of Electrically Small Self-Resonating Wire Antennas, IEEE Antenna and Propagation Magazine*, 2004.

[8] J. Rashed and C. T. Tai, *A New Class of Resonant Antennas*, IEEE Transactions on antennas and Propagation, 1991.

[9] J. Morrow, *Shorted biconical antenna for Ultra-Wideband Applications*, Radio and Wireless Conference RAWCON, 2003.

[10] A. Amert and K. Whites, *Miniaturization of the Conical antenna for Ultra-wideband Applications*, IEEE Transactions on Antenna and Propagation, 2009.

[11] Y. K. Yu and J. Li, *Analysis of Electrically Small Size Conical Antenna*, Progress in Electromagnetics Research Letters, 2008.

[12] M. I. Skolnik, *Radar Handbook*, McGraw-Hill, 3rd edition, 2007.

[13] T. A. Milligan, *Modern Antenna Design*, Wiley, 2005.

[14] D. M. Pozar, *The Active Element Pattern*, IEEE Transactions on Antennas and Propagation, 1994.

[15] C. A. Balanis, *Antenna Theory*, 2nd edition, 1997.

[16] W. L. Stuztman, G. A.Thiele, *Antenna Theory and Design*, 2nd edition, 1998.

[17] G. Marrocco and L. Mattioni, *Naval Structural Antenna Systems for Broadband HF Communications*, IEEE Transaction on Antennas and Propagation, 2006.

[18] H. Choo and H. Ling, *Design of electrically small planar antennas using inductively coupled feed*, Electronics Letters, 2003.

[19] P.H. Smith, *Electronic Applications of the Smith Chart*, SciTech/Noble Publishing, 1995, 2nd edition.

[20] R. Rhea, *The Yin-Yang of Matching - Part 1: Basic Matching Concepts*, High Frequency Electronics, Agilent Technologies, 2006.

[21] R. Rhea, *The Yin-Yang of Matching - Part 2: Practical Matching Techniques*, High Frequency Electronics, Agilent Technologies, 2006.

[22] S.J. Orfanidis, *Electromagnetic Waves and Antennas*, Rutgers University, 2008.

[23] C. Bowick, *RF circuit design*, Elsevier, 2008, 2nd edition.

[24] A. M. Niknejad, *Electromagnetics for High-Speed Analog and Digital Communications Circuits*, Cambridge University Press, 2007.

[25] M. Alfonsetti et al., Versatile coil design and positioning of transverse-field RF surface coils for clinical 1.5-T MRI applications, MAGMA, 2005.

[26] N. Fontana et al., *RF coil design: A Comparison of Analytical, Numerical and Experimental Methods for RF Field Mapping*, Risonanza Magnetica in Medicina: dalla ricerca tecnologica avanzata alla pratica clinica, ISMRM, 2011;

[27] ICNIRP, *Guidelines for Limiting Exposure to Time-Varying Electric, Magnetic, and Electromagnetic Fields (up to 300 GHz)*, 1998.

[28] R. Stara et al., *RF coil design for Low and High Field MRI: Numerical Methods and Measurements*, IEEE Nuclear Science Symposium and Medical Imaging Conference, 2011.

[29] G. Giovannetti at al., *A fast and accurate simulator for the design of the birdcage coils in MRI*, Magnetic Resonance Materials in Physics, Biology and Medicine, 2002.

[30] Beuf O. et al., *Small-animal MRI: signal-to-noise ratio comparison at 7 and 1.5 T with multiple-animal acquisition strategies*, Magnetic Resonance Mater Phy, 2006.

[31] IFAC, *Dielectric properties of body tissues*, http://niremf.ifac.cnr.it/tissprop/.

[32] F. Duru et al., *Pacing in magnetic resonance imaging environment: clinical and technical considerations on compatibility*, European Heart Journal, 2001.

PUBLICATIONS

JOURNAL PAPERS

[1] M. Ballardin, I. Tusa, N. Fontana, A. Monorchio, C. Pelletti, A. Rogovich, R. Barale, R. Scarpato, *Non-thermal effects of 2.45 GHz microwaves on spindle assembly, mitotic cells and viability of Chinese hamster V-79 cells,* Mutation Research. Fundamental and molecular mechanisms of mutagenesis, pp. 555-564, 2011.

CONFERENCE PAPERS

[2] N. Fontana, A. Monorchio, M. O. Munoz Torrico, Y. Hao, *A Numerical Assesment of the Effect of MRI Surface Coils on Implanted Pacemakers*, submitted to IEEE International Symposium on Antennas and Propagation and CNC/USNC/URSI Radio Science Meeting, Chicago, 2012.

[3] N. Fontana, A. Monorchio, G. Manara, R. Stara, A. Retico, A. Del Guerra, M. Tosetti, G.Tiberi, M. Alfonsetti, A. Galante, A. Vitacolonna, M. Alecci, *RF coil design: A Comparison of Analytical, Numerical and Experimental Methods for RF Field Mapping*, Risonanza Magnetica in Medicina: dalla ricerca tecnologica avanzata alla pratica clinica, ISMRM, 2011.

[4] R. Stara, N. Fontana, A. Monorchio, G. Manara, A. Retico, A. Del Guerra, G.Tiberi, L. Biagi, M. Alfonsetti, A. Galante, A. Vitacolonna, M. Alecci, M. Tosetti, *RF coil design for Low and High Field MRI: Numerical Methods and Measurements*, IEEE Nuclear Science Symposium and Medical Imaging Conference, 2011.

[5] N. Fontana, C. Pelletti, A. Rogovich, A. Monorchio, *On the influence of a glass slide on the SAR distribution in Petri dishes for in vitro exposure to 2.45 GHz EM fields*, IEEE International Symposium on Antennas and Propagation and CNC/USNC/URSI Radio Science Meeting, pp. 1-4, Toronto, Ontario, Canada, 2010.

[6] D. Bianchi, N. Fontana, S. Genovesi, A. Monorchio, A. Vallecchi, M. Cerretelli, M. Linari, G. Biffi Gentili, *Multi-Objective Optimization of Wideband Spiral Arrays*, IEEE International Symposium on Antennas and Propagation and CNC/USNC/URSI Radio Science Meeting, pp. 1-4, Toronto, Ontario, Canada, 2010.

[7] N. Fontana, A. Rogovich, A. Monorchio, *A Numerically Efficient Technique to Evaluate Specific Absorption Rate in Exposures to Pulsed Electromagnetic Fields*, IEEE International Symposium on Antenna and Propagation and USNC/URSI National Radio Science Meeting, Charleston, USA, 2009.

APPENDIX A – FORMULAS FOR L TOPOLOGY NETWORKS DIMENSIONING

Table A.1 - Formulas for calculating the values of components in L-topology networks.

L topology type	Element values
Type 1	$L_1 = \frac{A}{2\pi f (G_L^2 + A^2)}$ $C_1 = \frac{A - B_L}{2\pi f}$
Type 2	$L_2 = \frac{1}{2\pi f (A + B_L)}$ $C_2 = \frac{G_L^2 + A^2}{2\pi f A}$
Type 3	$L_3 = \frac{B}{2\pi f}$ $C_3 = \frac{B - X_L}{2\pi f (R_L^2 + (B + X_L)^2)}$
Type 4	$L_4 = -\frac{(R_L^2 + (C + X_L)^2)}{2\pi f (C + X_L)}$ $C_4 = -\frac{1}{2\pi f C}$
Type 5	$C_{5a} = \frac{G_L^2 + A^2}{2\pi f A}$ $C_{5b} = -\frac{(A + B_L)}{2\pi f}$

Type 6	$L_{6a} = \frac{A}{2\pi f\left(G_L^2 + A^2\right)}$ $L_{6b} = -\frac{1}{2\pi f\left(A - B_L\right)}$
Type 7	$C_{7a} = -\frac{1}{2\pi fB}$ $C_{7b} = -\frac{B + X_L}{2\pi f\left(R_L^2 + (B + X_L)^2\right)}$
Type 8	$L_{8a} = \frac{C}{2\pi f}$ $L_{8b} = -\frac{(R_L^2 + (X_L + C)^2)}{2\pi f\left((X_L + C)\right)}$

In Table A.1 let assume admittance of the load as:

$$Y_L = G_L + jB_L = \frac{R_L}{R_L^2 + X_L^2} - j\frac{X_L}{R_L^2 + X_L^2} \tag{A.1}$$

and the variables of support as:

$$A = \sqrt{\frac{G_L}{R_s} - G_L^2}$$

$$B = \sqrt{R_L(R_s - R_L)} - X_L \tag{A.2}$$

$$C = -\sqrt{R_L(R_s - R_L)} - X_L$$

APPENDIX B – FORMULAS FOR L MATCHING NETWORKS IN CASCADE DIMENSIONING

The designs for different number of L network cascade are reported.

The schematic configuration of N+1 generic L networks cascade is reported (Fig.B.1).

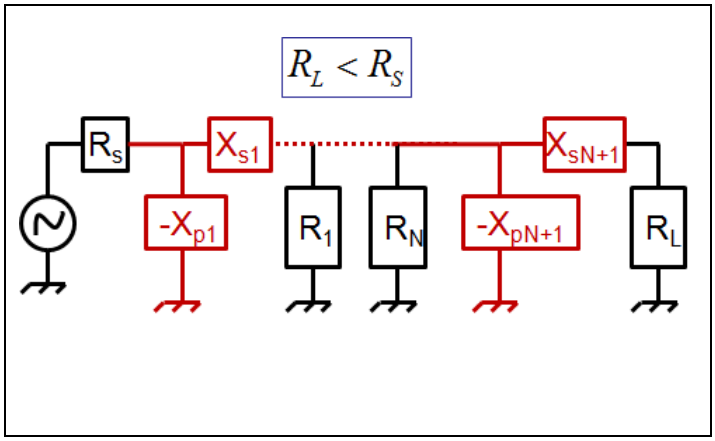

Figure B.1 – Cascade of N+1 L networks: $R_L<R_S$.

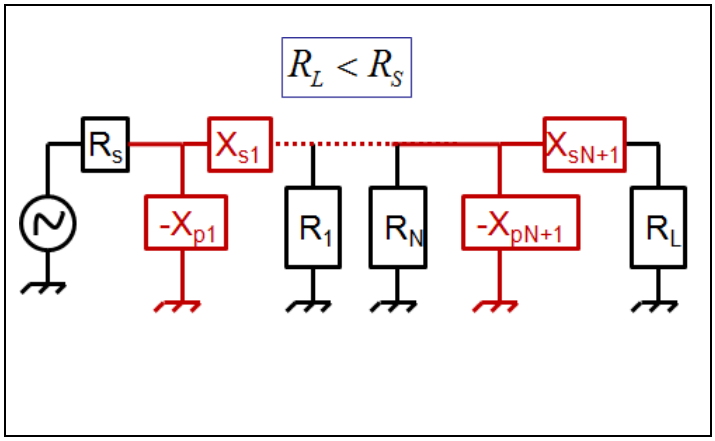

Figure B.2 – Cascade of N+1 L networks: $R_L>R_S$.

The two cases have to be distinguished in order to match the real part of the impedance of the load with the impedance of the source. The virtual resistances and the Q factor have to be realizing the equations described in Table B.1.

Table B.1 – Formulas for dimensioning the cascade of 3 L networks.

Case 1: $R_L > R_S$	Case 2: $R_L < R_S$
$\frac{R_1}{R_S} = \frac{R_2}{R_1} = \frac{R_L}{R_2} = 1+Q^2$	$\frac{R_1}{R_L} = \frac{R_2}{R_1} = \frac{R_S}{R_2} = 1+Q^2$
$\begin{cases} \frac{R_1}{R_S} = \frac{R_2}{R_1} \\ \frac{R_2}{R_1} = \frac{R_L}{R_2} \\ \frac{R_1}{R_S} = 1+Q^2 \end{cases}$	$\begin{cases} \frac{R_1}{R_L} = \frac{R_2}{R_1} \\ \frac{R_1}{R_L} = \frac{R_S}{R_2} \\ \frac{R_1}{R_L} = 1+Q^2 \end{cases}$
$R_1 = \sqrt[3]{R_S^2 R_L}, R_2 = \sqrt[3]{R_L^2 R_S}$ $Q = \sqrt{\frac{R_1}{R_S} - 1}$	$R_1 = \sqrt[3]{R_L^2 R_S}, R_2 = \sqrt[3]{R_S^2 R_L}$ $Q = \sqrt{\frac{R_1}{R_L} - 1}$
$X_{S1} = R_s Q, X_{p1} = \frac{R_1}{Q}$ $X_{S2} = R_1 Q, X_{p2} = \frac{R_2}{Q}$ $X_{S3} = R_2 Q, X_{p3} = \frac{R_L}{Q}$	$X_{p1} = \frac{R_S}{Q}, X_{S1} = R_1 Q$ $X_{p2} = \frac{R_1}{Q}, X_{S2} = R_2 Q$ $X_{p3} = \frac{R_2}{Q}, X_{S3} = R_L Q$

The dimensioning of a cascade of four L networks is reported in Table B.2.

Table B.2 - Formulas for dimensioning the cascade of 4 L networks.

Case 1: $R_L > R_S$	Case 2: $R_L < R_S$
$\frac{R_1}{R_S} = \frac{R_2}{R_1} = \frac{R_3}{R_2} = \frac{R_L}{R_3} = 1+Q^2$	$\frac{R_1}{R_L} = \frac{R_2}{R_1} = \frac{R_3}{R_2} = \frac{R_S}{R_3} = 1+Q^2$

$\begin{cases} \frac{R_1}{R_S}=\frac{R_2}{R_1} \\ \frac{R_1}{R_S}=\frac{R_3}{R_2} \\ \frac{R_1}{R_S}=\frac{R_L}{R_3} \\ \frac{R_1}{R_S}=1+Q^2 \end{cases}$	$\begin{cases} \frac{R_1}{R_L}=\frac{R_2}{R_1} \\ \frac{R_1}{R_L}=\frac{R_3}{R_2} \\ \frac{R_1}{R_L}=\frac{R_S}{R_3} \\ \frac{R_1}{R_L}=1+Q^2 \end{cases}$
$R_1=\sqrt[4]{R_S^3R_L}, R_2=\sqrt{R_LR_S}, R_3=\sqrt[4]{R_L^3R_S}$ $Q=\sqrt{\frac{R_1}{R_S}-1}$	$R_1=\sqrt[4]{R_L^3R_S}, R_2=\sqrt{R_LR_S}, R_3=\sqrt[4]{R_S^3R_L}$ $Q=\sqrt{\frac{R_1}{R_L}-1}$
$X_{S1}=R_sQ, X_{p1}=\frac{R_1}{Q}$ $X_{S2}=R_1Q, X_{p2}=\frac{R_2}{Q}$ $X_{S3}=R_2Q, X_{p3}=\frac{R_3}{Q}$ $X_{S4}=R_3Q, X_{p4}=\frac{R_L}{Q}$	$X_{p1}=\frac{R_S}{Q}, X_{S1}=R_1Q$ $X_{p2}=\frac{R_1}{Q}, X_{S2}=R_2Q$ $X_{p3}=\frac{R_2}{Q}, X_{S3}=R_3Q$ $X_{p4}=\frac{R_3}{Q}, X_{S4}=R_LQ$

The dimensioning of a cascade of five L networks is reported in Table B.3.

Table B.3 - Formulas for dimensioning the cascade of 5 L networks.

$R_L>R_S$	$R_L<R_S$
$\frac{R_1}{R_S}=\frac{R_2}{R_1}=\frac{R_3}{R_2}=\frac{R_4}{R_3}=\frac{R_L}{R_4}=1+Q^2$	$\frac{R_1}{R_L}=\frac{R_2}{R_1}=\frac{R_3}{R_2}=\frac{R_4}{R_3}=\frac{R_S}{R_4}=1+Q^2$

$\begin{cases} \frac{R_1}{R_S} = \frac{R_2}{R_1} \\ \frac{R_1}{R_S} = \frac{R_3}{R_2} \\ \frac{R_1}{R_S} = \frac{R_4}{R_3} \\ \frac{R_1}{R_S} = \frac{R_L}{R_4} \\ \frac{R_1}{R_S} = 1+Q^2 \end{cases}$	$\begin{cases} \frac{R_1}{R_L} = \frac{R_2}{R_1} \\ \frac{R_1}{R_L} = \frac{R_3}{R_2} \\ \frac{R_1}{R_L} = \frac{R_4}{R_3} \\ \frac{R_1}{R_L} = \frac{R_S}{R_4} \\ \frac{R_1}{R_L} = 1+Q^2 \end{cases}$
$R_1 = \sqrt[5]{R_S^4 R_L}, R_2 = \sqrt[5]{R_L^2 R_S^3}, R_3 = \sqrt[5]{R_L^3 R_S^2},$ $R_4 = \sqrt[5]{R_L^4 R_S}, Q = \sqrt{\frac{R_1}{R_S} - 1}$	$R_1 = \sqrt[5]{R_L^4 R_S}, R_2 = \sqrt[5]{R_S^2 R_L^3}, R_3 = \sqrt[5]{R_S^3 R_L^2},$ $R_4 = \sqrt[5]{R_S^4 R_L}, Q = \sqrt{\frac{R_1}{R_L} - 1}$
$X_{S1} = R_s Q, X_{p1} = \frac{R_1}{Q}$ $X_{S2} = R_1 Q, X_{p2} = \frac{R_2}{Q}$ $X_{S3} = R_2 Q, X_{p3} = \frac{R_3}{Q}$ $X_{S4} = R_3 Q, X_{p4} = \frac{R_4}{Q}$ $X_{S5} = R_4 Q, X_{p5} = \frac{R_L}{Q}$	$X_{p1} = \frac{R_S}{Q}, X_{S1} = R_1 Q$ $X_{p2} = \frac{R_1}{Q}, X_{S2} = R_2 Q$ $X_{p3} = \frac{R_2}{Q}, X_{S3} = R_3 Q$ $X_{p4} = \frac{R_3}{Q}, X_{S4} = R_4 Q$ $X_{p5} = \frac{R_4}{Q}, X_{S5} = R_L Q$